農研機構
NARO 国立研究開発法人 農業・食品産業技術総合研究機構

ラマン分光法によるトリアシルグリセロールの構造および相挙動解析

メタデータ	言語: English 出版者: 公開日: 2019-03-22 キーワード (Ja): キーワード (En): polymorphism, triacylglycerol multicomponent system, porcine fat, bovine fat, discrimination technique 作成者: 本山, 三知代 メールアドレス: 所属:
URL	https://doi.org/10.24514/00002250

Structure and Phase Characterization of Triacylglycerols by Raman Spectroscopy

Michiyo MOTOYAMA

Animal Products Research Division,
NARO Institute of Livestock and Grassland Science, Tsukuba, 305-0901 Japan

Abstract

Triacylglycerols (TAGs) are one of the main forms of energy storage in living organisms. Natural fats, which are nothing but the multicomponent TAG systems, are widely used in industrial products such as food, medicine and cosmetics. Industrial demands promote the studies on thermophysical properties of the multicomponent TAG systems for a long time; however, the whole picture of their phase behavior is yet to be drawn. With a view to understand the complicated phase behavior of natural fats, I have investigated on the physical mixtures of TAGs by Raman spectroscopy.

Firstly, the background of this study is introduced (Chapter 1). Raman spectroscopy is the appropriate method to characterize TAGs, particularly when they exist in multicomponent systems. The structure and phase behavior of TAGs are then summarized with emphasis on the recent developments (Chapter 2). The interesting phase properties of TAGs, polymorphism and "molecular compound" formations, are introduced. The factors affecting these phase properties, such as crystallization conditions, are also mentioned. Next, the spectral features of TAGs are described in relation to their phase specific structures (Chapter 3). On the basis of the accumulated spectroscopic data, Raman spectroscopy has contributed to reveal the detailed structure of TAG polymorphs. Based on the knowledge described in these chapters, two TAG systems are studied. They include a TAG binary system that is known to form a molecular compound (Chapter 4) and several natural fats that are widely used in industrial products (Chapter 5).

The results of the present study indicate that a third component, a molecular compound, is formed in the TAG binary system and its structure seems to be influenced decisively by crystallizing procedures. The molecular compound may be the phase dynamically formed by crystallization, rather than existing stationary in the liquid phase as previously considered (Chapter 4). In addition, the present study implies that the molecular compound may exist not only in a model binary system but also in real multicomponent systems. It is also shown that one can differentiate the origin of natural fats by detecting the difference in their polymorphic phases by using Raman spectroscopy (Chapter 5).

Finally, future prospects of Raman spectroscopic studies on TAG systems for deepening the present understanding are presented (Chapter 6). Recent developments on the spectrometer offer bright future prospects for Raman spectroscopic studies on multicomponent TAG systems. Raman spectroscopy helps us to draw the whole picture of the phase behavior of natural fats.

Key words: polymorphism, triacylglycerol multicomponent system, porcine fat, bovine fat, discrimination technique

Received 2011. 8. 1. Conferring University: The University of Tokyo

Chapter 1
Introduction

Triacylglycerols (TAGs) possess ideal properties for the energy storage in living organisms. They have high oxidation energy that is more than twice as high as those of sugars or proteins. Their hydrophobicity enables TAGs to self-assemble and exist without raising the osmotic pressure in a cell. They are one of the most important constituent of the life system. Despite these facts, TAGs have been put to the marginal area of biological studies, presumably because of their varying chemical structures and complex phase behaviors.

TAGs are familiar to anybody. They are used widely in many industrial products. Natural fats, which are nothing but the multicomponent TAG systems, are the major components of food as well as those of the matrices of cosmetics and medicine. [23] They are made up of more than 30 TAG species [32] with major constituent fatty acid generally being oleic acid. [78] Oleic acid is a representative unsaturated fatty acid that has one *cis* C = C double bond. Industrial demands, especially those for better chocolate production, have promoted the studies on thermophysical properties of TAGs in the past 100 years. [21,93] By the use of differential scanning calorimetry and pulse nuclear magnetic resonance, the crystallization and polymorphism of natural fats have been studied. [115] It is widely known today that TAG crystal polymorphism has considerable influence on the texture, fluidity and appearance of the final fat products. [28] However, the whole picture of polymorphic phase behavior of natural fats is yet to be drawn.

In order to study the polymorphic behavior of natural fats in more detail, TAG binary-systems as well as single-TAG systems are important as model systems. In fact, these systems have been investigated extensively by X-ray diffraction (XRD). XRD is powerful for TAG polymorph identification since each polymorph has its own wide angle and small angle XRD patterns derived from their particular subcell and layer structures. Furthermore, introduction of high flux X-ray beam by synchrotron radiation enables time resolved measurements (～10 s) [118] of polymorphic transformations of TAGs. This makes it possible to detect and measure transient phases which were often difficult to study because of their thermal instability. [34] Thanks to these XRD studies, a number of interesting phenomena occurring in TAG model systems have been elucidated.

The formation of "molecular compounds" is one of these interesting phenomena. [18,48] When two TAG species that have specific interactions with each other are mixed, they form a molecular compound at a fixed mixing ratio. A molecular compound behaves like a new, pure TAG species with unique phase behavior that differs from those of its component TAGs. All TAG species that have so far been reported to form molecular compounds have the oleic acyl moieties. The formation of molecular compounds is thought to mediated by the incompatible interaction between oleic and saturated acyl moieties and the compatible interactions between the oleic acyl moieties of the component TAGs. [33]

Another interesting phenomenon is the polymorphism. It has been suggested that the structure of the polymorph that appears first on crystallization determines the structure of the subsequently formed polymorphs and therefore the phase behavior. [24] The TAG species having both unsaturated and saturated acyl moieties shows this first-appearing polymorph whose structure can be distinguished from those of the other TAGs. [70] It is suggested that this may be one of the causes for the complicated polymorphic behavior of natural TAGs containing both saturated and unsaturated acyls.

Despite the above mentioned interesting indications, no precise structural data of the TAGs containing unsaturated acyls are available from single-crystal XRD analysis. The primary reason for this is the difficulty in obtaining the single crystals of TAGs. Crystals with adequate size for single-crystal XRD are difficult to be obtained. Even though they are obtained, the crystals are too soft to handle. Also, the crystal quality is often low especially for the TAGs which contain unsaturated acyls. Single-crystal XRD data have been reported so far only for three on TAGs and they are TAGs having saturated acyls only. [22,30,51]

Vibrational spectroscopies, namely Raman spectroscopy and infrared absorption spectroscopy, have contributed to reveal the detailed TAG structures on the basis of the accumulated spectroscopic data

of basic molecules such as polyethylene, [97-99,108,110-114] paraffins, [43,95,96] *n*-alkanes [42,101,103,105,130] and fatty acids. [40,41,47,54] The oleoyl acyl conformation, [16,106] the alkyl-chain-plane orientation [45] and the length of *trans* C-C chain [126] of TAG polymorphs have been studied in detail using these methods. The vibrational bands reflecting the alkyl-chain-plane orientation have been used to distinguish the TAG polymorphs. [4,12,13,90,127] Though it has not been fully appreciated, vibrational spectroscopy has a distinct advantage when one tries to deal with multicomponent TAG systems. A vibrational spectrum as a whole is often called "molecular finger print". By using this characteristic of vibrational spectra, one can extract information on the phases existing in complex TAG systems.

Within the context of "metabolic syndrome" in recent years, it can be said that Raman spectroscopy is a promised method to study TAGs. It has been used to study the status of TAGs in cells. [107] Raman spectroscopy is most suitable to study TAGs in the aqueous systems because it is not too sensitive to the presence of water. Even when the system contains more than 90w/w% of water, well resolved spectral features of lipids are obtainable. [54] The large polarizability of lipids gives strong Raman scattering; lipids are therefore tractable molecules for Raman spectroscopy. Their structural changes are reflected with high sensitivity in the spectra even though they are in aqueous systems. For example, Raman spectroscopy has been applied to monitor the breakdown of TAG complex in lipoprotein particles in an aqueous system. [9]

I have used Raman spectroscopy to study several selected binary/multi- component TAG systems, with a view to clarify the complicated phase behavior of natural fats. In the present thesis, the structure and phase behavior of TAGs are summarized with emphasis placed on recent developments (Chapter 2). The spectral features of TAGs are then described in relation to their phase specific structures (Chapter 3). On the basis of these, two TAG systems are studied. They include a TAG binary system that is known to form a molecular compound (Chapter 4) and several natural fats that are widely used in industrial products (Chapter 5). Future prospects of Raman spectroscopic studies on TAG systems for deepening the present understanding are also presented (Chapter 6).

Chapter 2
Structure and Phase Behavior of Triacylglycerols

Abstract

TAGs possess the basic structure of lipids: a glycerol backbone and acyl chains attached to it. They are the biological molecules, and oleoyls are the major constituent acyls of the TAGs observed in natural fats. TAGs form crystals with layer structure just like other long chain molecules, and exhibit a complex polymorphic phase behavior. Three polymorphs with different subcell structure, α, β' and β, are generally observed. Polymorphic transformation goes monotropically in this order in accord with thermal conditions. It is also known that TAGs form "molecular compound" in their binary systems. A molecular compound behaves like a new, pure TAG species with unique phase behavior that differs from those of its component TAGs. The formation of a molecular compound is thought to occur in terms of the specific intermolecular interactions between oleic acyl moieties of the component TAG molecules. In this chapter, the factors affecting TAG structures and phase behavior are summarized with emphasis on the recent developments.

Structure of TAGs

TAGs possess the basic structure of lipids: a glycerol backbone and acyl chains attached to it (Fig. 1). This basic structure is also conserved in the other important lipids, such as the main classes of phospholipids and glycolipids (Fig. 2).

In order to designate the stereochemistry of TAGs, the "*sn*" notation which stands for 'stereochemical numbering' is used in a manner similar to that used for the other glycerol containing lipids. When the glycerol molecule is drawn in a Fisher projection with the secondary hydroxyl group to the left of the central prochiral carbon atom, the carbons are numbered 1, 2 and 3 from top to bottom. Molecules that are stereospecifically numbered in this fashion have the prefix "*sn*" immediately preceding the term "glycerol" in the name

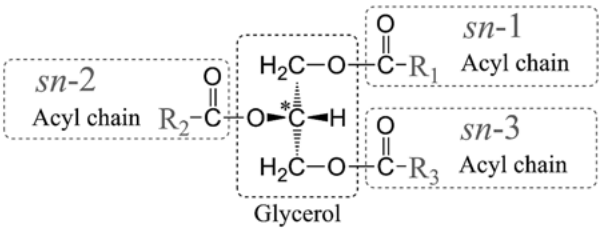

Fig. 1. Structure of a triacylglycerol (TAG). TAGs are esters of a glycerol (propane-1,2,3-triol) and three fatty acids.

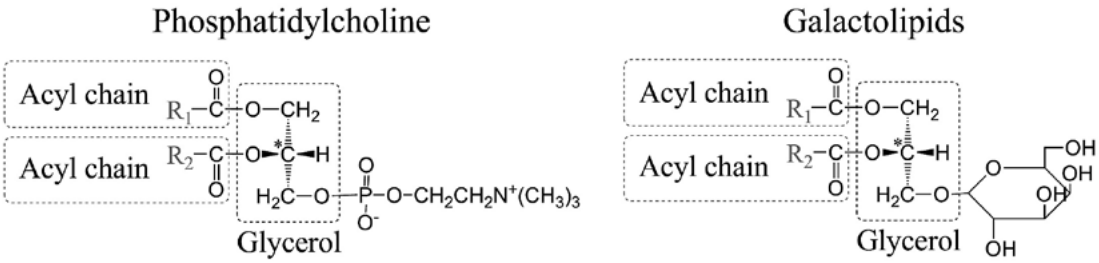

Fig. 2. A phospholipid and a glycolipid: The basic structure is widely observed in lipids

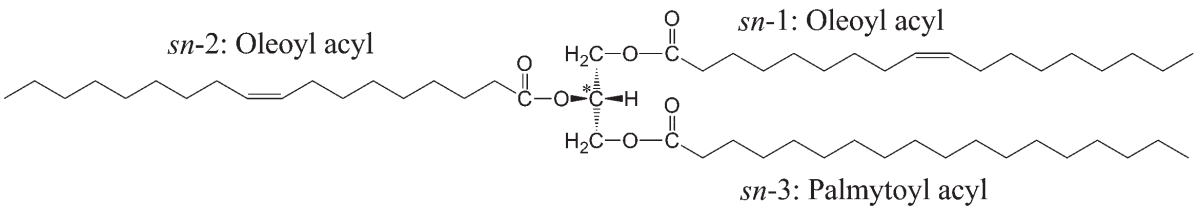

Fig. 3. 1,2-Dioleoyl-3-palmitoyl-*sn*-glycerol (OOP).

of the compound. The TAG molecule in Fig. 3 is therefore called "1, 2-dioleoyl-3-palmitoyl-*sn*-glycerol". This TAG molecule is also called "OOP" for short: "O" being the abbreviation for "oleic acyl" and "P" being for "palmitic acyl" wherein they are arranged in *sn* order.

The shape of a TAG molecule in solid phase is often compared to a "tuning fork" or the alphabet "h" (Fig. 4). To achieve these shapes, dihedral angles different from 180° which is normally expected are introduced along the skeletal bonds of the glycerol and of the acyl chains approximated to the glycerol. Generally, *sn*-1 and -3 acyl chains are oriented in one direction and *sn*-2 in the opposite direction as shown in Figs. 1 and 3. When the chain placed in *sn*-1 and -3 position are very different in their structure (*e.g.* short or unsaturated), this configuration (*sn*-1 and -3 opposed to -2) is not possible. There is an X-ray diffraction study which indicates that, in some crystal forms of PPO and SSO (S: stearic acyl), *sn*-1 and -2 chains point same direction. [92] Such a conformation is common in glycerophospholipids and glyceroglycolipids (Fig. 2).

The major factors that influence the physical properties of TAGs are the chemical structure of each acyl

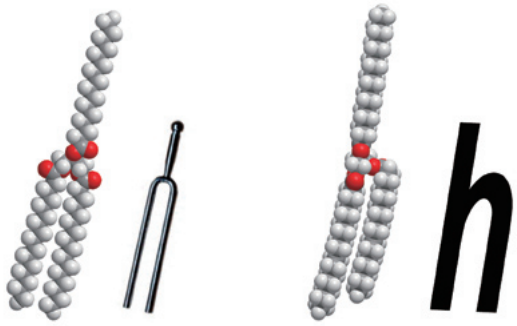

Fig. 4. Shapes of a triacylglycerol molecule

chain and its *sn* position. They are described in detail in the next section.

Mechanism deciding TAG composition

TAGs are the biological molecules and the major constituents of natural fats and oils. [87] All types of eukaryotes and a small group of prokaryotes accumulate TAGs as their energy source. [74,131]

Table 1 shows the fatty acid composition of natural fats. Oleic acid (C18:1), palmitic acid (C16:0), stearic acid (C18:0) and linoleic acid (C18:2) are the main constituents of TAGs. The fatty acid chains occurring in nature generally have even numbers of carbon atoms. This is because of the units of fatty acid synthesis. The *de novo* synthesis of fatty acids begins with introducing two carbons from malonil coenzyme A, and the fatty acid chain elongation proceeds with adopting also two carbons from malonil coenzyme A and acyl coenzyme A (Fig. 5).

The melting points of saturated fatty acids are shown in Fig. 6. The longer acids show the higher melting points. They show the odd-even-chain length effects: even numbered fatty acids have higher melting points than odd numbered ones. This trend is consistent with common knowledge of the odd-even-chain length effects on melting point observed in *n*-alkanes. [52]

Table 1. Fatty acid composition of a plant oil and an animal fat (w/w%) [78]

Fatty acid[a]		Olive oil	Porcine fat
C10:0		0.0	0.1
C12:0		0.0	0.1
C14:0		0.0	1.5
C14:1		0.0	0.1
C15:0		0.0	0.1
C16:0	Palmitic acid	9.9	24.7
C16:1		0.7	3.3
C17:0		0.7	0.3
C17:1		0.0	0.4
C18:0	Stearic acid	3.2	11.7
C18:1	Oleic acid	75.0	44.7
C18:2, n-6	Linoleic acid	10.4	10.9
C18:3, n-3		0.8	0.6
C20:0		0.0	0.2
C20:1		0.0	0.7
C20:2, n-6		0.0	0.5
C20:3, n-6		0.0	0.0
C20:4, n-6		0.0	0.2
C20:5, n-3		0.0	0.0

[a] Number of carbon atoms: number of C = C double bonds, position of C = C bonds

Fig. 7 shows the viscosities of stearic acid (C18:0) and oleic acid (C18:1). [91] Both fatty acids have the same number of carbons while oleic acid has one *cis* C = C bond. Oleic acid show lower viscosity than stearic acid due to the *cis* C = C which introduces a bent conformation to the molecule. This conformation prevents the fatty acids from packing tightly and alters the van der Waals force existing among the molecules.

The fatty acids are esterified to the glycerol *sn*-carbons in accord with enzyme substrate specificities. [89] The difference in *sn*-specific fatty acid composition is thus genetic in origin and it leads to the differences in physical properties (Table 2). These sets of fatty acids in Table 2, *e.g.* POP and PPO, have the same fatty acid composition, two palmitic acids and one oleic acid; however, there is a difference in their melting points which is derived from the difference in *sn* positions.

By using above mentioned mechanisms, living organisms control TAG physical properties in order to accommodate environmental temperature change. When the temperature becomes lower, the composition of TAGs becomes the one with higher unsaturated fatty acids in order to maintain the TAG fluidity. If TAGs are completely crystallized due to the low temperature, the cells are probably not able to use TAGs as the energy source. Homeoviscous adaptation, the term which is often used for cell membrane, can be also applied for TAGs in living organisms.

Table 2. Comparison of melting points between the TAGs consisting of same fatty acids [24]

TAG species[a]	Melting point(℃)[b]
POP	37
PPO	35
SOS	43
SSO	41
PSP	67
SPP	62
SPS	68
PSS	64

[a] P, palmitic acyl; O, oleic acyl; S, stearic acyl
[b] Average values of the experimental data shown in the reference

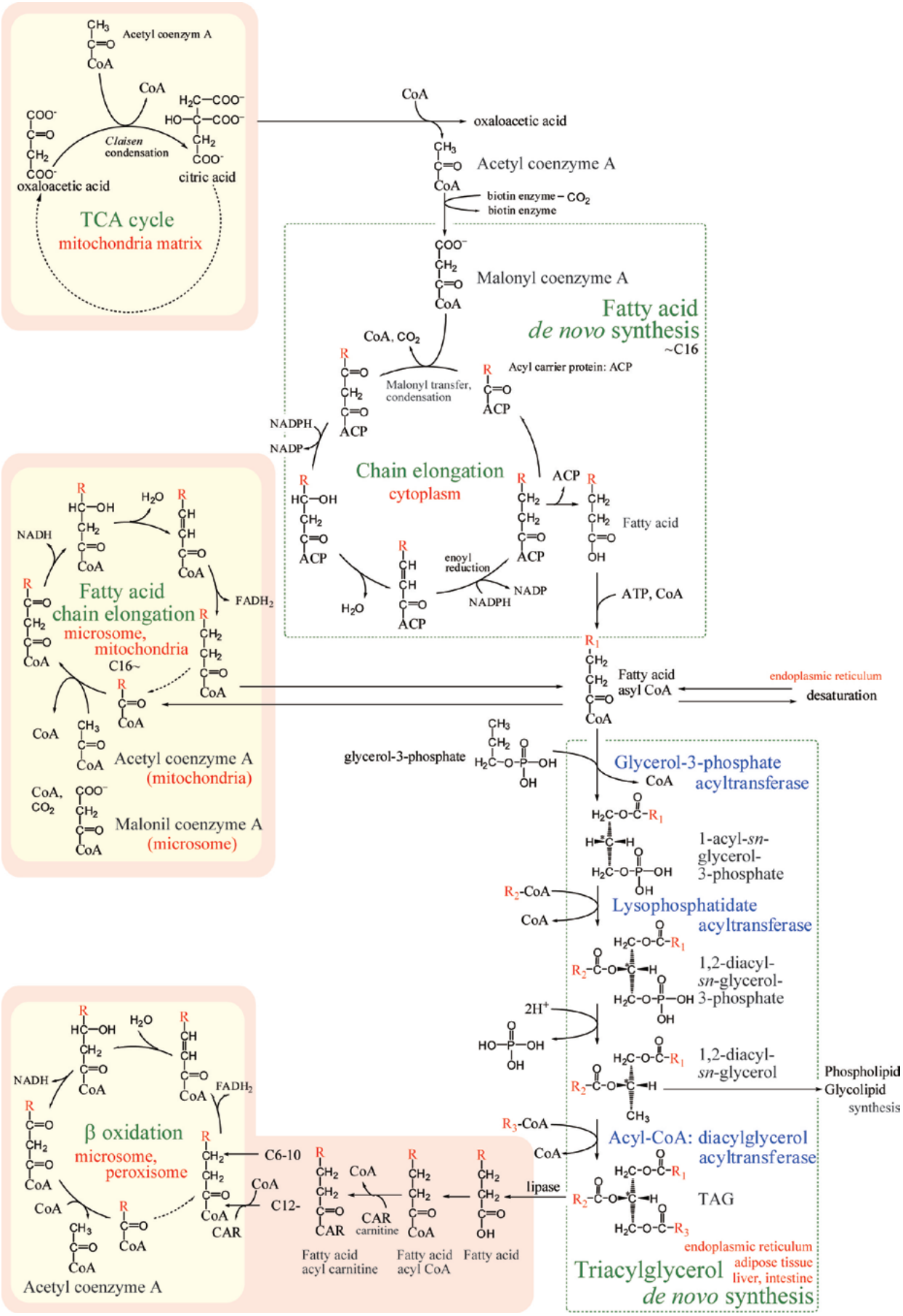

Fig. 5. TAG synthetic and metabolic pathways in a mammalian cell [29)]

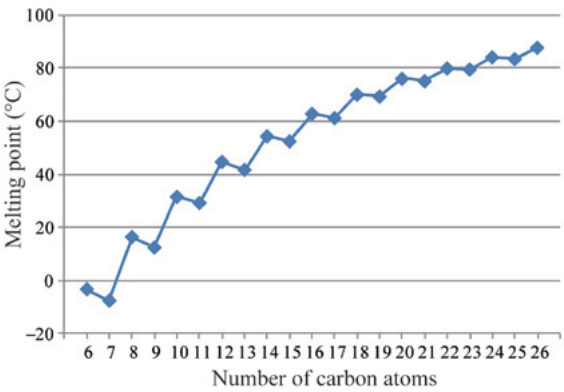

Fig. 6. Relationship between the carbon atom number of saturated fatty acids and their melting points [87]

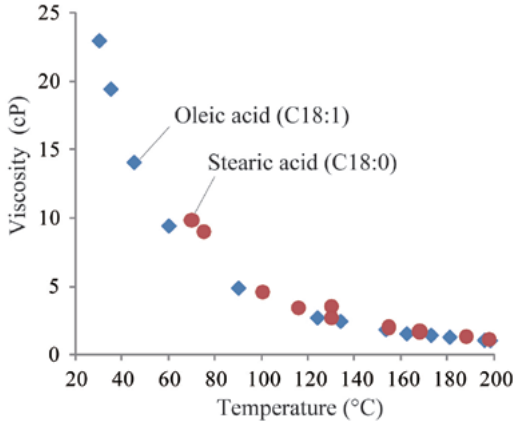

Fig. 7. Viscosities of two fatty acids. Stearic acid: Saturated acid with 18 carbon atoms. Oleic acid: Unsaturated 18-carbon fatty acid with one *cis* C=C [91]

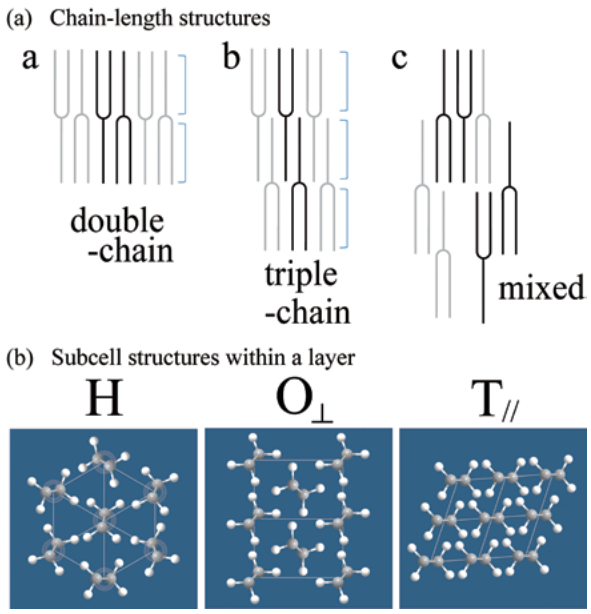

Fig. 8. Two kinds of Structure in TAG crystals. (a): Chain-length structure. [70] a, double-chains length structure; b, triple-chain lengths structure; c, mixed structure. (b) Subcell structure within a layer. H, hexagonal subcell structure; $O_{\perp}$, orthorhombic perpendicular subcell structure; $T_{//}$, triclinic parallel subcell structure

Polymorphic phase in TAG crystals

TAG crystals show polymorphism. Just like other long chain molecules, TAGs also form crystals with layer structures. These crystal structures of TAGs are usually classified by two distinctive features: the number of acyl-chain-length structures participating in a layer (Fig. 8a) and the type of subcell structure within the acyl-chain-length structures dictated by the inter-chain orientation (Fig. 8b). The stable crystal of TAGs has double-chain lengths or triple-chain lengths type of structure (Fig. 8a). The common subcell structure within a chain-length structure is known to be hexagonal with no ordered arrangement of the chain planes (H), orthorhombic with every second chain plane is perpendicular to the plane of the rest ($O_{\perp}$) or triclinic with all chain planes are parallel ($T_{//}$) (Fig. 8b).

The possible combination number of the chain-length structures and the subcell structures is large. A given TAG species has at least 36 possible packing manners in theory. In practice, however, only three structures called α, β' and β-polymorphs generally exist due to the packing preference which is brought by intermolecular interactions and thermodynamic conditions.

The polymorphic transformation goes monotropically in the order α, β' and β, indicated by the arrows in Fig. 9. For most of TAG species, the β polymorph is the most stable polymorph; however, β' is of the most stable one for some TAG species, *e.g.* PPO [81] and PPM, [46] M: Myristic acyl. For complex TAG mixtures, *i.e.* natural fats, β' polymorph is often the most stable polymorph. [115] The structure of the polymorphs and the structural changes associated with polymorphic phase transformation are described as follows (Fig. 9).

α-polymorph: Thermodynamically, this is the least stable phase with the lowest melting point. Its chain-length structure is generally double-chain and the subcell structure is H. The main part of the hydrocarbon chains are oscillating and hexagonally close packed. The methyl end group regions are somewhat more disordered, as in liquid crystals. [27]

β'-polymorph: This is the more stable phase showing the intermediate melting point. Its chain-length structure is double- or triple-chain and the $O_{\perp}$ subcell structure exists within all or part of the layer. The acyl chains are

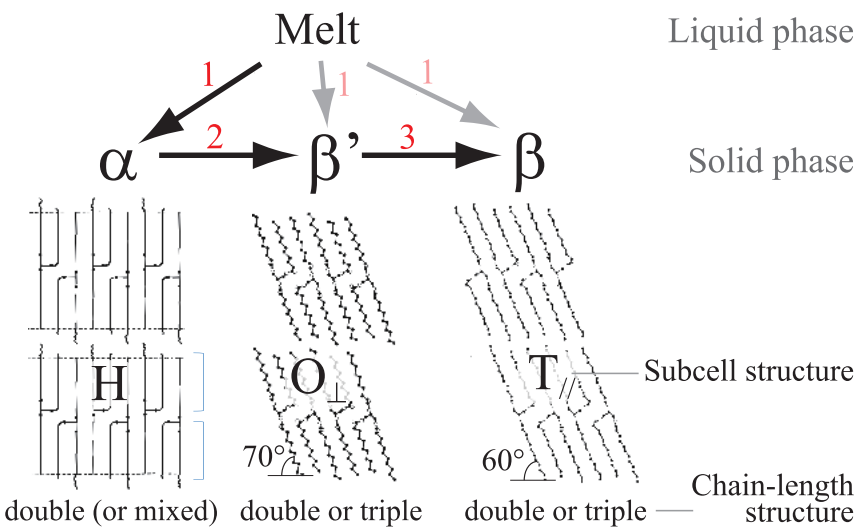

Fig. 9. Polymorphic transformation and structures of polymorphs [27]

tilted about 70° from the plane formed by methyl end groups.

β-polymorph: The most stable phase showing the highest melting point. Hydrocarbon chain planes are arranged in parallel and the subcell structure is generally $T_{//}$. The angle of tilt is about 60°.

These polymorphs are often described with subscripts, *e.g.* β_1, β_2. Only three terms, *i.e.* α, β' and β, are not enough to indicate the polymorphism of TAGs containing unsaturated acyls because of its complexity. [82] It is recommended that they are numbered in the order of decreasing melting points. [53] These nomenclatures with different subscript need not always indicate independent polymorphs. For example, Kellens *et al.* [36] reported that the melting point variation between [β'_1 and β'_2] and [β_1 and β_2] of a TAG seemed to be only due to crystal perfection and crystallinity. Mykhaylyk and Martin [70] also reported that α_2 phase formed in some TAGs species can be characterized as a transient structure. These polymorphs, however, are likely to be isolated and stabilized by cooling immediately after its formation. [46] To understand polymorphic transformations taking place in TAGs, especially in natural fats, the structure of various unstable phases have to be determined.

The lateral interaction among acyl chains, intermolecular glycerol interactions and the methyl ends interaction are the main driving force of the phase transformation. The associated structural changes can be explained as below.

Melt → solid phase (arrow 1 in Fig. 9): Cooling process. The C−C bonds within acyl chains become *trans* configuration. Crystallization is the least understood phase transition in terms of structural changes. The details are described in the next section.

α → β' (arrow 2): Hexagonal packing in α-polymorph likely to change always to the orthorhombic packing. [27] Which chain-length structure they form (double or triple) is depend on chain sorting which may be related to the conformational disordering of the α form. [25] The chains become tilt and the methyl ends become lined up. The methyl-groups overlap develops large intermolecular repulsion. To reduce this large repulsive energy, the perpendicular chain-plane arrangement (⊥) is likely to be introduced. [24]

β' → β (arrow 3): Parallel chain-plane arrangements (//) are introduced within all layers. The matching of the terminal methyl groups within the inter-layer space and the conformational order of unsaturated bonds, when such are present, is completed. [14,15,121]

The polymorph transformation to more stable phase can be melt-mediated process which enables the transformation finish in a shorter time compared to solid-to-solid transformations. [46,84] This difference can be explained by thermodynamics. [83]

Crystallization process

The cooling-down procedure from the TAG melt greatly influence the crystallization of fats. In fats industries, these procedures so-called "annealing" are the important part of the technology to control the polymorph formed. To understand the crystallization of TAG systems, general theories for crystal nucleation and crystal growth have been applied. [20] However, as been mentioned so far, polymorphism complicates the crystallization of TAGs. Herewith, a rough picture will be given for the crystallization of TAGs.

To describe the crystallization behavior of TAGs, Gibbs free energy (G) is the most important. Because crystallization, *i. e.*, phase transition, is the process which changes volume (V) and entropy (S) of the system; therefore, it is difficult to use the other thermodynamic potentials which have V and/or S as their variables:

$\Delta E = T\Delta S - P\Delta V$ (E : internal energy)

$\Delta H = T\Delta S + V\Delta P$ (H : enthalpy)

$\Delta F = -S\Delta T - P\Delta V$ (F : Helmholtz free energy)

where T is temperature and P is pressure.

For crystallization from the melt to occur, the activation energy barrier, $\Delta G^{\dagger\dagger}$, should be crossed over. The relative $\Delta G^{\dagger\dagger}$ values for TAG polymorphs were studied by Malkin [57] and they can be depicted as shown in Fig. 10. The larger $\Delta G^{\dagger\dagger}$ value indicates the greater difficulty of the formation of crystal nucleus. β-polymorph is most difficult to crystallize due to its largest $\Delta G^{\dagger\dagger}$. It is consistent with the observed crystallization rate which decreases in order of α, β' and β. [84]

ΔG is expressed by the function of temperature and pressure as:

$\Delta G = -S\Delta T + V\Delta P$

The Gibbs free energy of one particle is called chemical potential μ:

$\Delta\mu = -s\Delta T + v\Delta P$

μ is convenient to use especially when one wants to describe crystallization since some local equilibriums,

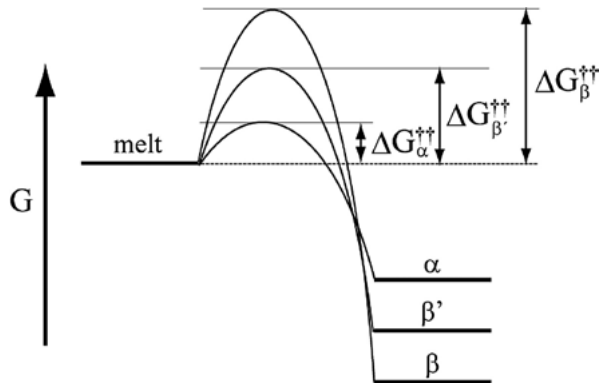

Fig.10. Diagram of the activation Gibbs free energy $\Delta G^{\dagger\dagger}$ [57,89] and those of each polymorph

i. e. liquid phase and solid phase, are coexisting within a system under crystallization process. The difference in μ between the local equilibrium systems (Δμ) is the driving force to cross over the activation energy barrier.

When Δμ is defined as:

$\Delta\mu \equiv \mu_{liquid} - \mu_{solid}$

μ_{liquid}: μ of the liquid phase exists at crystallization

μ_{solid}: μ of the solid phase exists at crystallization

it can be derived:

$\Delta\mu = -(s_{liquid} - s_{solid})\Delta T + (v_{liquid} - v_{solid})\Delta P$ — eq. 1

It can be supposed that the difference in volume is small between liquid and solid,

$v_{liquid} \approx v_{solid}$

Therefore, eq. 1 becomes:

$\Delta\mu = -(s_{liquid} - s_{solid})\Delta T$

where ΔT is called the supercooling:

$\Delta T = T_m - T$

T_m: melting temperature of the solid phase

T: actual temperature of the system

When larger ΔT is induced, the absolute value of Δμ becomes larger. The larger Δμ the larger the driving force for crystallization and the driving force cross the activation energy barrier $\Delta G^{\dagger\dagger}$, crystal nucleus is formed.

After the nucleation, crystals grow at a certain rate which is proportional to Δμ. Fig. 11 shows the Δμ of each polymorph at a temperature T. Δμ is larger in the order of $\Delta\mu_\alpha < \Delta\mu_{\beta'} < \Delta\mu_\beta$. This indicates that once the nucleus is formed, the more stable polymorph grows faster.

Structural changes of TAGs on crystallization are proposed by synchrotron radiation X-ray diffraction

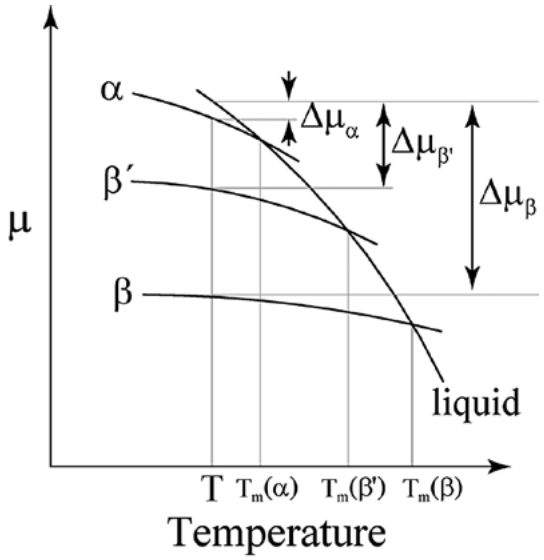

Fig.11. Relationship between chemical potential and temperature for liquid phase and three polymorphs of TAGs. Δμ, difference in chemical potential between liquid and solid; T, actual temperature; T_m, melting temperature [1,19,120,123]

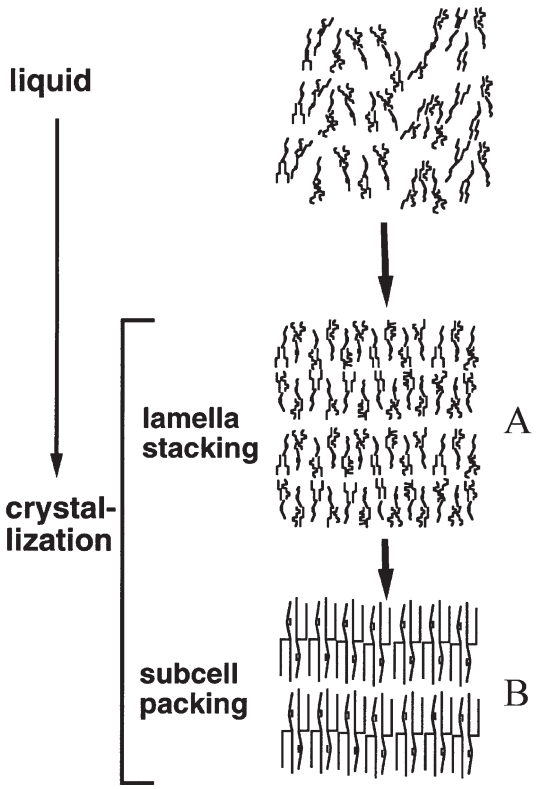

Fig.12. A model of crystallization of fats from neat liquid [80]

studies (Fig. 12). Lamella stacking is firstly occurred (A in Fig. 12), followed by the detailed subcell packing (B in Fig. 12). [118,119] It is estimated that the time required for the A to B transformation is of the order of several tens of second for SOS β'-polymorph and 500 second for SOS β_2-polymorph.

Regarding the formation of the lamella structure, Mykhaylyk *et al.* recently proposed the plausible model. [70,71] Two types of molecular dimmers possibly exist in a TAG liquid phase and the stability of these dimmers depends on thermal conditions and compatibilities between the TAG acyl moieties (see Fig. 46 on page 49). In a liquid state of TAGs containing solely saturated or unsaturated acyls, only one type of dimers with double-chain-length structure is formed and leading double-chain-length layer. In TAGs with both saturated and unsaturated acyls, a packing incompatibility between these acyls stabilizes both type of dimers and leading the formation of the lamella with random packing of the two dimers. The structural complexity of the latter lamella likely explains the complex phase behavior of TAGs with unsaturated acyls.

"Molecular compound" formation

It has been reported that a third component exists in some TAG binary systems. This third component is known as the "molecular compound".

It is generally accepted that the liquid phase of a TAG mixed system may be treated as a close approximation to an ideal mixture. [20] Once they are crystallized, they are separated and generally form solid solution (Fig. 13a). However, in some TAG binary systems which have "specific interactions", they form molecular compounds (Fig. 13b). A molecular compound behaves like a new, pure TAG species with unique phase behavior that differ from those of its component TAGs.

The first report on the molecular compound was made in 1963 by Moran. [66] He conducted DSC thermal analysis on several TAG binary systems and found unexpected melting behaviors in POP-OPO binary system. The observed phase diagram of POP-OPO system was likely to be made up of two binary systems, in juxtaposition, of POP-compound and compound-POP (Fig. 14). He thus proposed that the "molecular compound"

is formed in POP-OPO binary system and it would not be chemically bonded as in true compound, but merely a highly-favored crystal packing.

After this report, several studies have reported on the molecular compound formation in TAG binary systems using thermal analysis and powder X-ray diffraction. The formations of a molecular compound have also been observed in POP-PPO, [63,66] SOS-OSO [48] and SOS-SSO systems. [18,62] It must to note that oleoyl acyls (O) are present in both component TAGs of the above systems. Therefore, the intermolecular interactions at oleoc acyl moieties, including π-π interaction among olefinic groups, are thought to be the driving force for the molecular compound formation. It is quite interesting how such a van der Waals type interaction can enable the formation of the stable compound. However, the structure and the driving force for the compound formation are not well understood yet, despite numerous attempts.

With emphasis on the recent developments, the fundamental knowledge of polymorphism and molecular compound formation of TAG systems have been summarized in relation to the factor influencing these phenomena, such as TAG chemical structures and crystallization conditions. Since the phase behavior of a multicomponent TAG system is thought to be able to be obtained by summing all the behavior of the component TAGs, [20] it is important to understand these fundamentals of TAG structure and phase behavior.

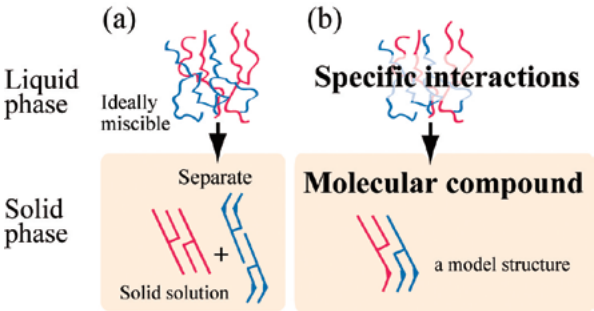

Fig.13. Illustration of "molecular compound" formation

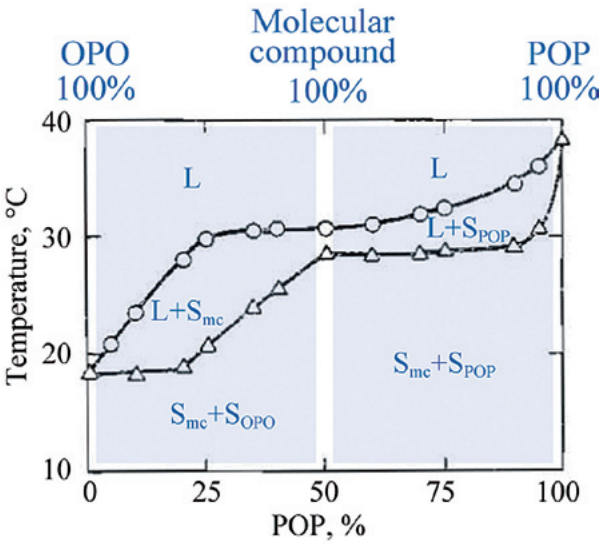

Fig.14. Melting behavior of POP-OPO binary systems. [66] Sample crystals were prepared as follows: Melts (100℃) were quenched to 0℃ and then incubated 2-4 weeks at as high a temperature as possible to induce most stable polymorphs. ○, melt point; △ thaw point; L, liquid; S_{mc}, solid of molecular compound; S_{OPO}, solid of OPO; S_{POP}, solid of POP.

Chapter 3
Raman Spectra of Triacylglycerols

Abstract

The total number of the atoms of a TAG molecule is about 170, hence it has approximately 500 normal modes. Some of them are selected to be observed as a vibrational spectrum, "a letter from the TAG molecule".

Vibrational spectroscopy is the suitable method to investigate TAG structural changes during phase transition because they can be applied not only the crystals but also the liquid phases. Since the conformational changes of TAGs are usually accompanied with large polarizability changes, their Raman spectra reflect these changes with high sensitivity and are particularly useful in this respect.

In this chapter, the Raman spectra of TAGs will be interpreted on the basis of the previous studies on polyethylene, paraffines, *n*-alkanes and fatty acids. Firstly, the vibrational modes of polyethylene will be briefly introduced because their spectra are understood well and they dominate the TAG composition. The assignments of Raman bands (1800 − 700cm^{-1}) observed in several TAG phases will be then illustrated with respect to each spectral region. Spectral differences among the phases will be explained in relation to their structures.

Introduction

TAGs are one of the well known molecules which give strong Raman scattering, since their acyl moieties that dominate the composition have large polarizability volumes. The structural changes during TAG phase transition are reflected with high sensitivity in the Raman spectra. In order to understand the complicated TAG spectra, the spectrum of polyethylene is the good reference. Polyethylene chains are the model compound of lipids, and their spectra are studied extensively for a long time.

A polyethylene chain, an infinite *trans* zigzag chain, is constructed by repeating $-CH_2-$ units which have nine proper vibrations: three atoms with three degree of freedom (*x*, *y* and *z*) for each. These vibrations are depicted in Fig. 15. Although the Bravais unit cell of polyethylene chains is $-CH_2-CH_2-$, the dispersion curve of polyethylene is often expressed taking $-CH_2-$ as the unit because of simplicity (Fig. 16). There are nine branches (ν_1, ν_2, $\cdots$ ν_i $\cdots$, ν_9) and the δ indicates the phase difference between two adjacent $-CH_2-$ units. Optical active vibrations have the value 0 or π for the δ; therefore, they can be expressed as $\nu_i(\delta=0)$ or $\nu_i(\delta=\pi)$. Among these modes, the Raman active modes are $\nu_1(\delta=0)$, $\nu_2(\delta=0)$, $\nu_3(\delta=\pi)$, $\nu_4(\delta=0)$, $\nu_4(\delta=\pi)$, $\nu_6(\delta=\pi)$, $\nu_7(\delta=0)$ and $\nu_7(\delta=\pi)$. [88]

In crystalline polyethylene, there are inter-chain interactions, which influence the above described vibrational modes. The dispersion curve for the crystal has been also acquired. [109,113] Polyethylene crystals have orthorhombic perpendicular ($O_\perp$) unit cell structure (Fig. 17a) and the Bravais unit contains two polyethylene chains (Fig. 17b). Therefore, every dispersion curve is split into two curves: One is for the vibration attributed to symmetric displacement of the adjacent-polyethylene chains; the other is for that of asymmetric (Fig. 18). This separation can be accounted for reasonably well using a model based on a short-range hydrogen atom-atom repulsive potential. [113] Because of the interaction between the two chains within a Bravais unit, the Raman spectra of the crystal become complicated. TAG polymorphs show similar types of crystal subcell structure; therefore, this effect should be kept in one's mind.

Another factor complicates TAG polymorph spectra is the band progression. Just as described above, the bands observed in polyethylene spectra are limited in the in-phase vibrations ($\delta=0$ or $\delta=\pi$). On the other hand, finite chains show a series of progression bands ($0\neq\delta\neq\pi$). [104] The spectral pattern of the progression bands reflects very sensitively the chain length of the *trans*-zigzag chain. TAGs consisting of the acyls with different chain length will have a few series of progression. [126]

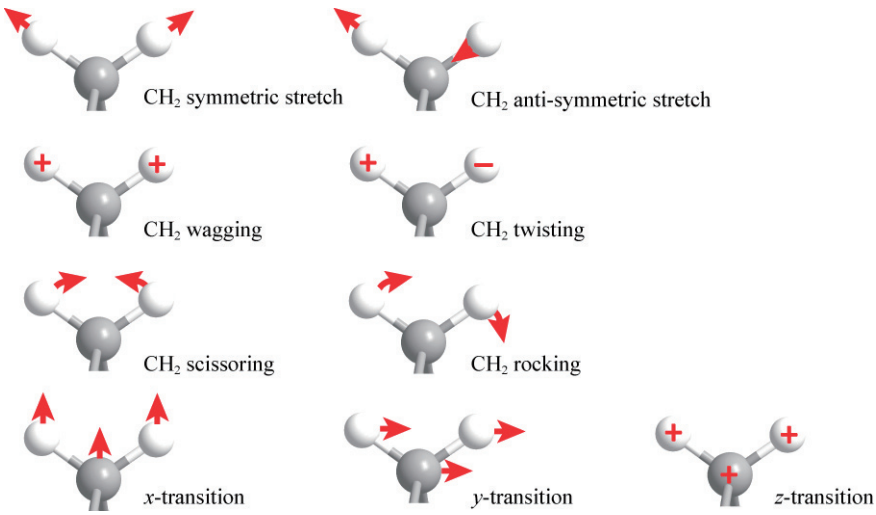

Fig.15. Nine normal modes of $-CH_2-$

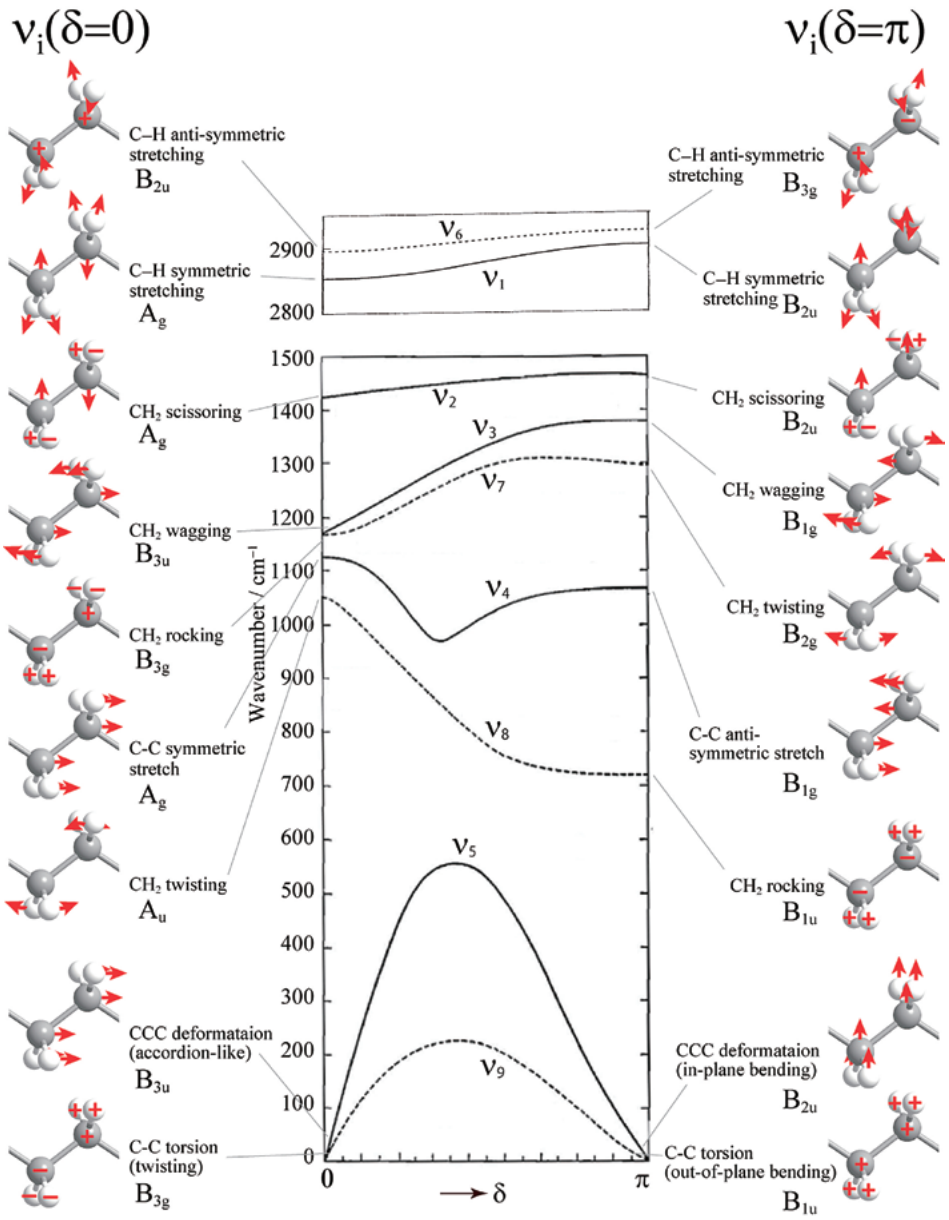

Fig.16. Dispersion curve of single polyethylene chain. [49,88,111,112] δ is the phase difference between two adjacent units (-CH_2-). Solid lines indicate in-plane vibrations, dashed lines indicate out-of-plane vibrations. CH_2 twisting and CH_2 rocking are coupled in ν_7 and ν_8.

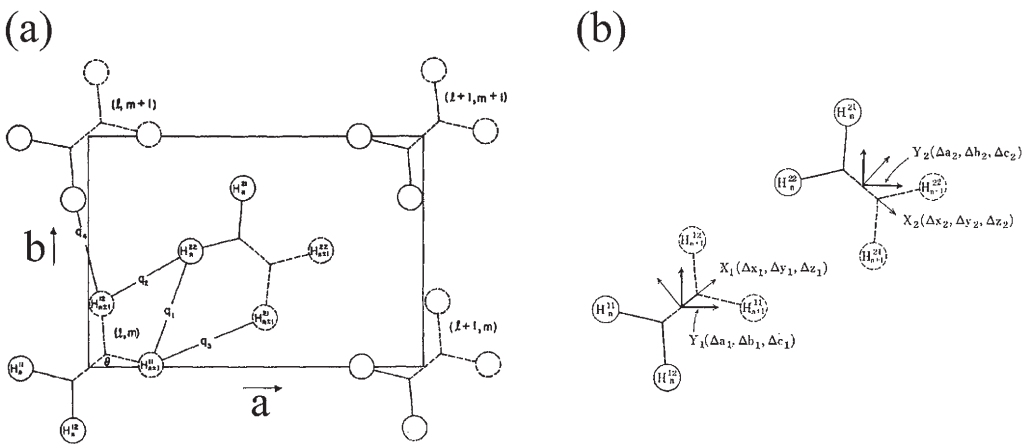

Fig.17. Crystal structure and the Bravais cell of crystal polyethylene. [113] (a), orthorhombic perpendicular ($O_\perp$) structure. [94] (b), Bravais unit cell and the coordinate system along the crystal axis

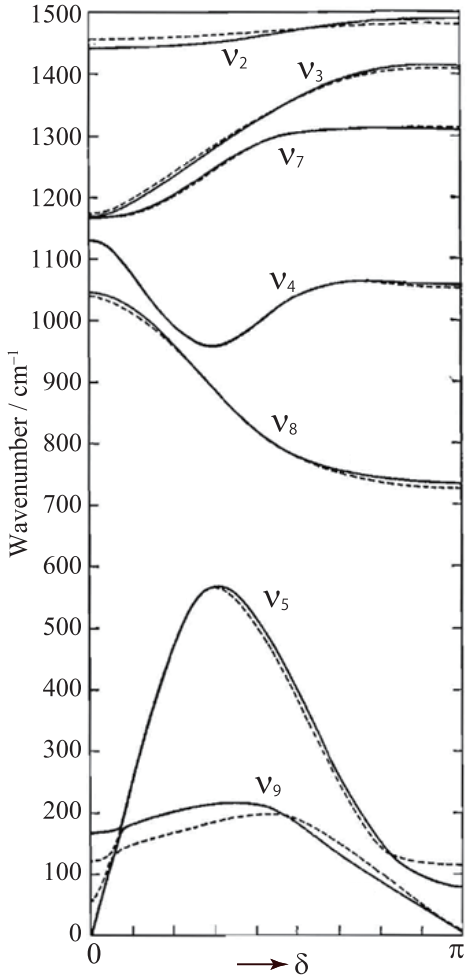

Fig.18. Dispersion curve of crystal phase of polyethylene. [109,113] δ is the phase difference between two adjacent units ($-CH_2-$). Solid lines indicate the vibrations attributed to symmetric displacement of the adjacent-polyethylene chains; dashed lines indicate those of asymmetric

During TAG phase transition, especially in solid to liquid transition, their spectra change drastically. For a random chain (not a *trans* zigzag), every normal mode would become more or less active due to the breakdown of selection rules. [114] Band progressions also affect the spectral changes during solid-liquid phase transition. In going from solid to liquid, *trans* zigzag chains introduce some *gauche* conformations into them and they are segmented into some shorter *trans* chains with a variety of length. The progressions reflecting their chain length are developed and layered as a consequence in the broad band features of liquid phase. Mizushima and Shimanouchi suggested that all-*trans* zigzag chain shorter than $C_{16}H_{34}$ are likely exist in liquid state of *n*-alkanes. [65] Long chain molecule acts as segments of *trans* zigzag chains in the liquid phase.

The introduction of *gauche* conformation has another effect. The spectrum of a all-*trans* chain, *e.g.* polyethylene, distributes all its intensity to the in-phase bands ($\delta = 0$ or $\delta = \pi$). For the liquid, however, the intensity distribution tends to be more even for all the modes in the progression. [100] The *gauche* conformations in the liquid affect the degree of coupling between adjoining oscillators which is determined by their relative orientation, and is reflected in the intensities of all the modes in the progression. [100] The progression bands which do not have intensities in all-*trans* conformation become apparent with some observable intensities in the liquid phase. Such 'density-of-states progression' explains the observed progression in liquid *n*-alkanes. [8]

It has not been explained explicitly; however, there is a general concept that a TAG spectrum is the superposition of that of each acyl-chain length structure (Fig. 19). This is probably based on the fact that the acyl chains are isolated by the glycerol moiety. It can be supposed that there is no vibrational coupling among the layers. This concept provides the basis for the vibrational spectroscopic studies on TAGs. Previous studies [64,125] have reveals acyl chain structures standing on this basis.

Experiment

Preparation of TAG samples

Three TAG species constituted of palmitic and oleic acyls were purchased from Sigma-Aldrich (St. Louis, MO, USA): tripalmitin (PPP, ≈ 99% purity), 1,3-dipalmitoy-2-oleoyl-*sn*-glycerol (POP, ≈ 99%) and 1,3-dioleoyl-2-palmitoyl-*sn*-glycerol (OPO, ≈ 99%). Their liquid- and polymorphic-phases were prepared as follows;

Approximately 2-mg PPP sample was put on a cover glass and kept >70℃ to acquire liquid phase. It was cooled down to 45℃ and crystallized to α-polymorph, and then heated up to 50℃ to transform α-polymorph to β'-polymorph. 3 μL of POP and OPO melts were put on cover glasses and kept at 50℃ to maintain in liquid phase. They were rapidly cooled down to 4℃ to acquire α-polymorph, then incubated at 20℃ for 11 days to transform the POP and OPO samples to more stable

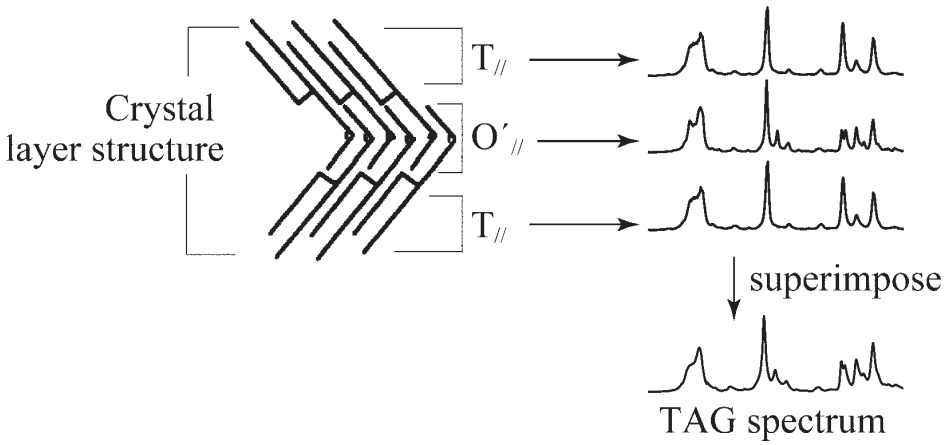

Fig.19. The concept to understand the spectra of TAGs which have acyl-chain length subcell structure.

polymorphs.

In addition to the TAG samples, polyethylene sheet (50- μm thickness) produced by blown-extrusion method was acquired at a retail market.

Raman spectroscopic measurement

For PPP samples, Raman scattering was excited with the 785-nm line of a Ti-sapphire laser (Spectra Physics 3900S, Newport, Santa Clara, CA, USA). The back-scattered Raman light from the sample was collected by an objective lens (LUCPlanFLN20x, Olympus, Tokyo, Japan) and measured with a spectrometer (Chromex 250i, Bruker Optik GmbH, Ettlingen, Germany) and a CCD detector (400×1340 pixels, Spec-10 400BR(LM), Roper, Sarasota, Florida, USA). The laser power was 17 mW at the sample point and the exposure time was 30 s. Spectral resolution was ~3 cm^{-1}.

For other samples, the 532-nm line of a Nd:YVO_4 laser (Verdi, Coherent, Santa Clara, CA, USA) was used as the excitation source. The back-scattered Raman light was collected by above mentioned objective lens and measured with a spectrometer (Shamrock, Andor, Belfast) and an EMCCD detector (Newton, Andor). The laser power was 3 mW at the sample point. Four measurements with 300 s exposure time were accumulated. Spectral resolution was ~2 cm^{-1}.

The integrated Raman intensities of almost all the polarization components were measured. During the measurement, sample temperatures were controlled by a cryostat (Linkam 10021, Tadworth, Surrey, UK) in order to maintain desired phases.

Result — Raman band assignments

The acquired Raman spectra were shown in Fig. 20. In this section, the assignments of bands observed in the TAG finger-print spectra will be described on the basis of the spectroscopic data of basic molecules such as polyethylene, paraffins, *n*-alkanes and fatty acids. They are summarized in Fig. 20 with comparison to a crystal polyethylene spectrum. As described in the introduction section, the bands observed in a TAG Raman spectrum are mostly related to those originating from polyethylene chain structures. For these bands, the notation of branch which the band belongs to (ν_i) has been added.

Region 1760 – 1720 cm^{-1}

The bands observed in this region originate from ester C=O stretching modes. [68] These bands contain information regarding the geometry of the ester region of TAGs. [4,5,128] TAGs have three ester linkages (Fig. 1); therefore, one can logically expect three vibrational bands in this region. Actually, the existence of three bands in the TAG liquid phase has been reported. [13]

The α-polymorph of TAGs does not show a clear feature with three bands. [1] This is likely to be due to its ambiguous configuration in the vicinity of the linkages.

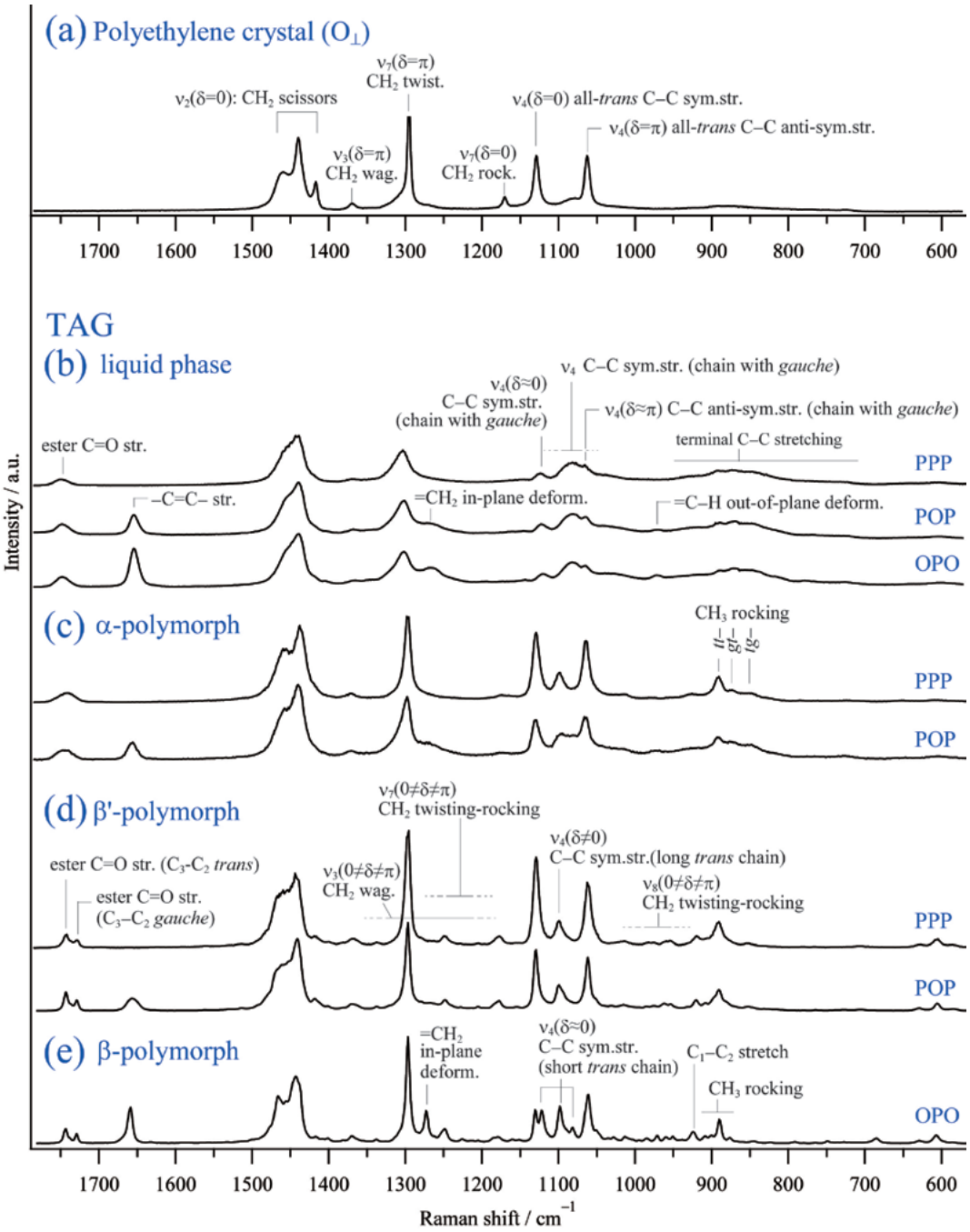

Fig.20. Assignments for TAG Raman bands

During the phase transition from α-polymorph to more stable phases, TAGs tend to configure 'h' conformer (see page 22) introducing a *gauche* configuration around C_2-C_3 bond in *sn*-3 acyl chain (Fig. 21). This change significantly affects in the frequency of the ester C=O stretching of the chain. From the previous studies, the band at ~1728 cm^{-1} corresponds this *sn*-3 C=O vibration, while the band at ~1743 cm^{-1} corresponds to *sn*-1 and -2 acyls' C=O with *trans* C_2-C_3 configuration. [1,69] Using these assignments, Sprunt *et al*. suggest the following approximate conformations for C_2-C_3 of three acyls of SOS in different polymorphic forms: β_1, two *trans*, one *gauche*; β_2 two *trans*, one *gauche*; β', three *gauche*; γ, one *trans*, two *gauche*; α, three disordered.

Between these two bands, a week band ~1737 cm^{-1} is observed. [13] Bicknell-Brown *et al*. reported that ester C=O stretching frequency is sensitive to rotation about the C_2-C_1 bond in some phospholipids. [2] It is likely the

reason for the existence of 1737 cm^{-1} band, and also for the band broadening of α-polymorph. On the other hand, da Silva and Rousseau speculated that the observation of three bands might be related to the presence of trace amounts of moisture in the samples that would interact with C=O bond of the esters, leading to a slightly altered conformation. [13]

Region 1680 – 1630 cm^{-1}

The band due to C=C stretching is seen at ~1655 cm^{-1} in the Raman spectra of TAGs which contain unsaturated acyl chains (Fig. 20). The frequencies of this vibrational mode depend sensitively on its conformation. The C=C bond existing in natural TAGs is normally in *cis* configuration. The conformation around *cis* C=C bond determines the overall shape of acyl chains and has a strong influence on the lateral packing and dynamic properties of the acyl chains, eventually affecting the overall TAG phase properties.

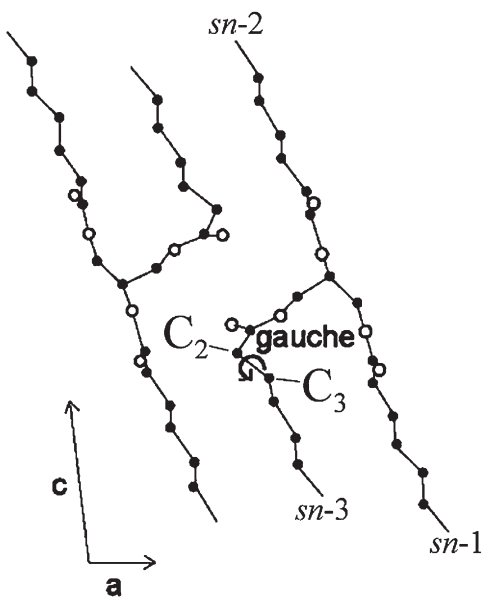

Fig.21. Molecular packing in the vicinity of the glycerol backbone in the β phase of TAGs [1,31,51]

Kobayashi *et al.* [40] reported in a study of oleic acid that the bands at 1661, 1657 and 1642 cm^{-1} are associated with the olefinic *skew-cis-skew'*, *skew-cis-trans*, *trans-cis-trans* conformations, respectively (Fig. 22). Koyama and Ikeda reported that ~1657 cm^{-1} is observed in amorphous forms of fatty acid with a *cis* olefin group. [47]

Additionally, a weak band at around 1633 cm^{-1} is observed (Fig. 20). This band can be found in some previous reports on TAGs, but the assignment of this band seems to be uncertain. This band is likely to be a mode other than $-CH_2-$ ones, since the vibrational modes from polyethylene moiety do not appear in this frequency region (Fig. 18). There are some possible origins of this band. Firstly, the carboxyl C=O stretching mode of impurities, such as diacylglycerols, monoacylglycerols and fatty acids, seems to be explainable. The purity of the commercially available TAG samples is less than 99%, >1% of impurities are therefore contained. Second, the C=C configuration other than shown in Fig. 22 is probably related. It has been reported that *skew-cis-skew* configuration exists in some fatty acids containing *cis* C=C bond. [85] The third possibility is the stabilization of π orbital of C=C bonds. In the spectra of TAGs having conjugated C=C bonds show such a low frequency band [107] because of the stabilization by π-π resonances. However, the TAGs shown in Fig. 20 do not have any C=C conjugation. Speculatively, it can be related to the intermolecular π-π stacking interaction because this band becomes clearer in the solid phase where the π-π stacking is expected to occur. Further investigation is needed for the conclusive assignment.

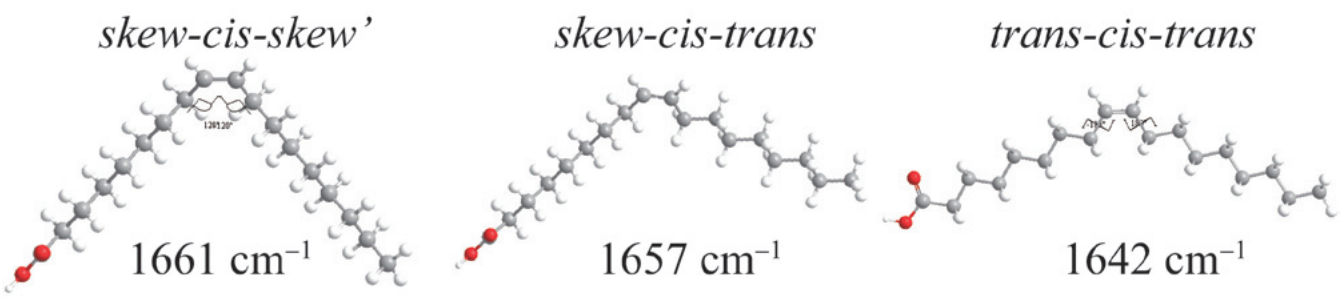

Fig.22. The configurations around *cis* C=C, overall shape of the oleic acid and their frequencies of Raman bands [40]

Region 1440 cm^{-1}

Interpretation of this CH_2 scissors mode region (ν_2) is complex for two main reasons. First, interactions between the vibrational modes whose symmetries are the same lead to Fermi resonances (Fig. 23a). [102] The Fermi resonances arise between the Raman active fundamental, $\nu_2(\delta=0)$ and the overtone of $\nu_8(\delta=\pi)$, and results in a doubling of the band in this region.

The second reason is that these modes are involved in strong inter-chain interactions within crystals. [102,113] For example the orthorhombic perpendicular structure ($O_\perp$) of polyethylene crystal, [113] which is the only case studied in any detail, the separation of the dispersion curve into a- and b-axis polarized components should be taken into account (Fig. 23b, also see page 31). In the Raman spectra of polyethylene, the band splitting originating from this polarization difference is observed only for $\nu_2(\delta=0)$ because the value of splitting for this mode is relatively large compared with other modes (Fig. 18). [113] The splitting of these two components is about 35 cm^{-1} at $\delta=0$ (Fig. 23b). As the result, the band ~1417 cm^{-1} is prominent in polyethylene $O_\perp$ crystals (Fig. 20a).

In TAGs, the band around 1460-1470 cm^{-1} shifts higher frequency region as the phase transforms into more stable one, *i. e.* liquid → α → β' → β (Fig. 20). It is likely due to the increase in inter-chain interaction which affects not only the frequency of $\nu_2(\delta=0)$ but also the one of $\nu_8(\delta=\pi)$. The frequency interval between $\nu_2(\delta=0)$ and the overtone of $\nu_8(\delta=\pi)$ reflects in the degree of Fermi resonance interaction.

The band splitting due to the crystal-field effect is distinctive at ~1417 cm^{-1} in β'-polymorph which has $O_\perp$ subcell structure (Fig. 20d). [38] It is, however, much weaker than that observed in polyethylene $O_\perp$ crystal (Fig. 20a). These are some possible reasons; namely crystal defects and imperfect perpendicular arrangements. In β'-polymorph of POP, the incomplete perpendicular arrangement occurs because their palmitoyl (extended) and oleoyl (bent) chains are packed in the same acyl-chain-length structure. [128] In the TAG β-polymorph having the $T_{//}$ subcell, in which polyethylene chains are parallel to each other, this band splitting is not apparent. [127]

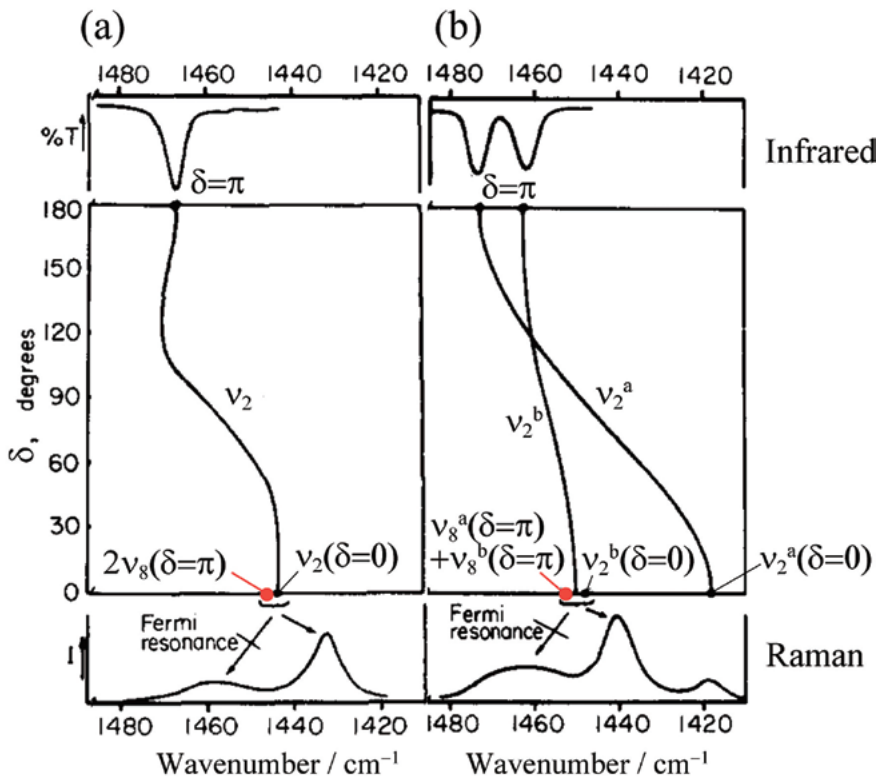

Fig.23. The CH_2 scissors mode frequencies dispersed in the perpendicular direction, plotted as a function of δ. [102] δ is the phase difference between two adjacent units -CH_2-. (a), the mode of extended isolated polyethylene chain. The doubling of Raman bands due to the Fermi resonance between ν_2 ($\delta=0$) and the overtone of ν_8 ($\delta=\pi$); (b), the modes of polyethylene orthorhombic crystals which are involved in strong intermolecular interactions.

In the melt and α-polymorph, the splitting can be detected although it is very weak. It may indicate that the acyl-chain planes are arranged not in the totally random way but in somehow biased one. To investigate the structure in TAG melt, it will be interesting to compare the strength of the band splitting between TAG melt and TAG molecules in solution where TAG acyl chains are arranged in the completely random distribution.

Region 1370 − 1180 cm^{-1}

The CH_2 wagging fundamental, $\nu_3(\delta = \pi)$, is prominent in this region. In the polyethylene crystal, this band appears at 1370 cm^{-1} (Fig. 20a). It originates from all-*trans* conformation of the extended chains.

In the TAG spectra, this band becomes broader as the chains become more and more conformationally disordered, *i. e.* β → β' → α → liquid (Fig. 20). However, the band intensity does not change much, in contrast to some other bands, *e. g.* 1180 cm^{-1} (see page 37) and ~1130 cm^{-1} (see page 38). Generally, band intensities may undergo drastic changes in going from a *trans* to a *gauche* bond. This intensity constancy is probably due to the orientation of the local polarizability derivative in the disordered chain. Cates, Strauss and Snyder (1994) reported that this band in liquid *n*-alkanes was assigned to the *gauche-trans-gauche'* configuration (Fig. 24). [8] This sequence has a local center of symmetry that allows this mode to appear in the Raman spectra. Therefore, the conformational change does not change the intensity very much.

The ν_3 mode shows its progressions in the region of 1370 − 1180 cm^{-1}. [95] They sensitively reflect the length and parity (odd/even) of the *trans* chain. The band observed at 1340 cm^{-1} in TAG β'- and β-polymorphs

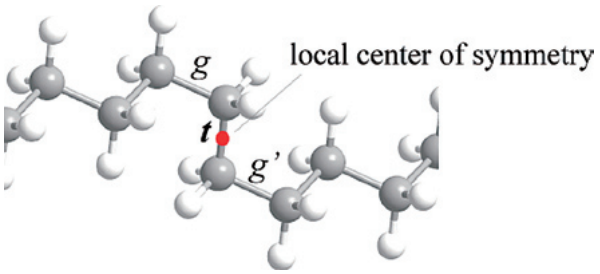

Fig.24. *Gauche-trans-gauche'* conformation observed in liquid phase

may be one of the progression bands (Fig. 20). This ν_3 progression bands are also appeared in infrared spectra, and Yano *et al.* used these bands as the reference to analyze the *trans* chain length of the acyls of TAGs. [126,127]

It should be noted that another type of ν_3 progressions has been reported in a study on *n*-alkanes. [8] These progressions can be observed also in the liquid phase. It is suggested that their origin lies in the density of vibrational states. For the liquid, the intensity distribution tends to be more even. The progression bands are much broader than those of the ordered chain and usually appear superimposed on a continuous background in the region 1370 − 1180 cm^{-1}. [8]

Region 1300 − 1180 cm^{-1}

The strong band at ~1300 cm^{-1} is the CH_2 twisting mode, $\nu_7(\delta = \pi)$. The most stable polymorph, β, shows a sharp band at 1296 cm^{-1}. On the other hand, liquid phase of TAGs give a strong but relatively broad band around 1305 cm^{-1}. Substantial conformational disorder in the liquid phase increases the frequency to around 1305 cm^{-1}. [122,129] The band observed in α or β' polymorphs is likely to be the superposition of these two bands.

At around 1170 cm^{-1}, the zone-center mode of the other side of ν_7 branch, $\nu_7(\delta = 0)$, appears in polyethylene crystal (Fig. 20a). This is the CH_2 rocking mode. In TAG spectra, this band appears ~1180 cm^{-1}. As shown in Fig. 20, this band intensity reflects the conformational disorder in crystals. The β'- and β-polymorphs have higher intensity of this band compare to α-polymorphs. In the liquid phase, this band smears out. It is known that the infrared rocking mode frequency of a CD_2 group substituted in a polyethylene chain is sensitive to *trans-gauche* rotational isomerization of the chain. [58] This sensitivity forms the basis of a commonly used infrared method for determining site-specific conformation in polyethylene systems, and applied to some model biological systems to investigate their conformational disorder. [60,61] Unlike these CD_2 rocking bands, the Raman CH_2 rocking band is not independent of other polyethylene bands; however, it is likely that this is a possible Raman probe for the degree of TAG crystal disorder.

In-between the two bands described above, ν_7 progression bands ($0 \neq \delta \neq \pi$, CH_2 twisting-rocking modes)

appear in 1300－1180 cm^{-1}. The band at ～1250 cm^{-1} is probably one of these bands because it broadens out in synchronization with 1180 cm^{-1} ($\nu_7(\delta=0)$) (Fig. 20). The band observed at 1275 cm^{-1} (Fig. 20e) has been assigned to the same origin; [106] however, it is more likely to have a different origin because this band does not appear in the spectra of β'-polymorph which show 1180 and 1250 cm^{-1} bands. The assignment of this 1275 cm^{-1} band is described in the next section. There are several other bands with relatively small intensity in this region. They can be assigned with high possibility to the ν_7 progression bands or the ν_3 progressions which overlap in this region.

Region 1280－1260 cm^{-1}

A broad band ～1265 cm^{-1} appears in the liquid phase of TAGs containing unsaturated acyl chains (Fig. 20b). The intensity of this band increase when the number of olefinic group increases. The origin of this band is the olefinic ＝CH in-plane deformation. [47] In the TAG crystals whose olefinic group are stacked (Fig. 25a), this band becomes narrower. From the study of fatty acid with *cis* olefinic group, this band is most intense for the *skew-cis-skew'* conformation of the －C＝C－ bond (Fig. 25b). [47] The observed bands in OPO β-polymorph could then be indicative of the *skew-cis-skew'* conformation. On the other hand, the β'-polymorph of POP does not show any distinctive band in this region. This observation supports the FT-IR study of Yano *et al.* (1993) where they reported the －C＝C－ conformation in β'-polymorph of POP should be deformed from *skew-cis-skew'*. [128]

Region 1140－1050 cm^{-1}

The bands derived from ν_4 branch, the C－C skeletal stretching modes are observed in this region. [112] They are one of the most important bands in the Raman spectroscopic study of polyethylene chain structure. Since the chain backbone is directly involved in these vibrations, substantial spectral changes are expected whenever the conformation of the backbone changes. Their band features are applied to investigate the conformational order of lipid bilayer [56,76,122] and TAGs [13,46,54,55,77].

In the Raman spectrum of polyethylene crystal where almost every C－C bond is in *trans* configuration, two sharp and strong bands are observed at 1130 and 1061 cm^{-1} in this region (Fig. 20a). They are the C－C symmetric stretching ($\nu_4(\delta=0)$) and the anti-symmetric stretching ($\nu_4(\delta=\pi)$) modes, respectively (Fig. 16). These two bands are prominent in the spectra of TAG solid phases (Fig. 20c, d and e) and indicating that they contain *trans* zigzag chains.

Between these two prominent bands, some sharp bands can be observed in TAG polymorphs. These bands have been assigned to the $\nu_4(\delta\approx 0)$ of *trans* zigzag chain. [40] The frequency of the band is affected by the chain length and chain boundary condition. A fundamental study was conducted by Kobayashi *et al.* using a number of mono-unsaturated fatty acids crystals. [40] The backbone of these mono-unsaturated fatty acids are separated into two *trans* C－C chains by the C＝C bond, one being the methyl-side chain and the other the carboxyl-side chain (Fig. 26). These two chains are different in their boundary

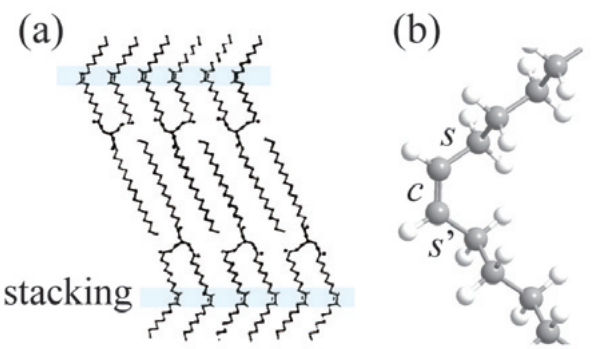

Fig.25. Structures around C＝C bonds observed in TAG crystals. (a), Crystal structure of β-polymorph of OSO. [44] C＝C bonds are stacked. (b), *skew-cis-skew'* conformation.

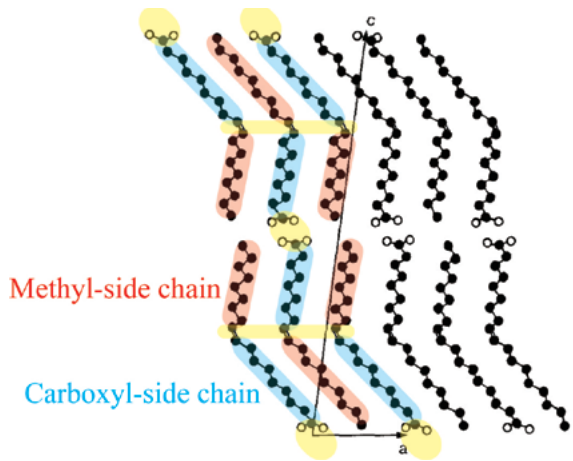

Fig.26. Crystal structure of oleic acid. [33] Yellow-shaded region indicate the parts where the intermolecular interaction is relatively strong.

condition. For methyl-side chain, one end is free and the other is fixed by inter-molecular interactions at C=C bond (Free-Fixed chain), whereas for the carboxyl-sided chain both ends are fixed because dimerization of the carboxyl groups (Fixed-Fixed chain).

Kobayashi *et al.* used the approximation of the simple coupled oscillators model for the chains with different carbon number (n), which for these two types of chain boundary conditions gives the following allowed phase angles (δ) :

$$\delta_k = (2k-1)\pi/2(n-1) \quad \text{(for Free-Fixed chain)} \text{ — eq.1}$$

$$\delta_k = k\pi/(n-1) \quad \text{(for Fixed-Fixed)} \text{ — eq.2}$$

where $k = 1, 2, \ldots, n-1$

As with polyethylene, the smallest k value ($k=1$, $\delta \approx 0$) corresponds to the C−C symmetric stretching vibration and the largest ($k=n-1$, $\delta \approx 0$) to the anti-symmetric stretching. Based on the above consideration, they have fitted experimental data of the mono-unsaturated fatty acids using the dispersion curve of the all-*trans* polyethylene ν_4 mode, leading to the assignment of Raman bands of oleic acid at 1125 and 1095 cm^{-1} to the C−C symmetric stretching mode of the methyl-side ($n=9$, Free-Fixed) and carboxyl-side chains ($n=9$, Fixed-Fixed) respectively (Fig. 27). [40]

It is shown that this assignment is maintained in a TAG, SOS. [106] The structural arrangement in the oleoyl chains of SOS may be seen as similar to the above, since in SOS the fixed-fixed part of the chain will be between the C=C bond and the polar ester groups of the glycerol backbone where intermolecular attraction is relatively strong. The free end of the free-fixed chain will be at the non-polar bilayer interface region.

In the spectrum of β-polymorph of OPO, there is an extra band at 1080 cm^{-1} in addition to the above mentioned 1125 and 1095 cm^{-1} bands (Fig. 20). This probably originates from the glycerol-side *trans* chain of *sn*-3 acyl of OPO which is the Fixed-Fixed chain with $n=7$ (Fig. 28). In TAG β-polymorph, it is known that the *sn*-3 chain is bent in the vicinity of glycerol (Fig. 21). As a consequence, that *trans* chain has a chain length shorter by two, compare to that of *sn*-1 (Fig. 28). Following eq.2, the $k=1$ mode of Fixed-Fixed chain with $n=7$ should have $\delta = 30°$, and likely to have a frequency around 1080 cm^{-1} (Fig. 27).

In the spectrum of solid phase of PPP, a band exists ~1100 cm^{-1} (Fig. 20c and d). This band origin must be a different from $k=1$ mode. PPP does not have any C=C bond; therefore, it contains only long *trans* chains. For larger n, the value of δ for $k=1$ becomes smaller near to 0 (eq. 1). Such small δ does not explain the frequency of ~1100 cm^{-1}. Vogel and Jahnig assigned this band to a ν_4 progression mode with $k=3$ of *trans* C−C chain. [122] PPP contain $n=16$, Free-Fixed *trans* chains. The δ of $k=3$ mode for the chain can be calculated from eq. 1, and it is

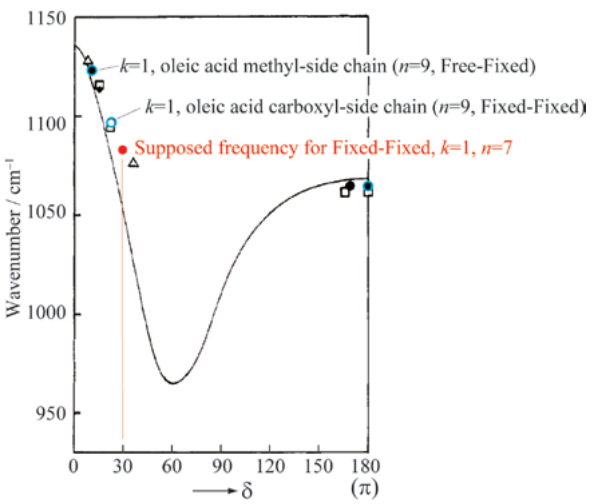

Fig.27. Frequencies of C−C stretching modes for mono-unsaturated fatty acids. [40] ○, oleic acid; □, palmitic acid; △, petroselinic acid, and ●, erucic acid.

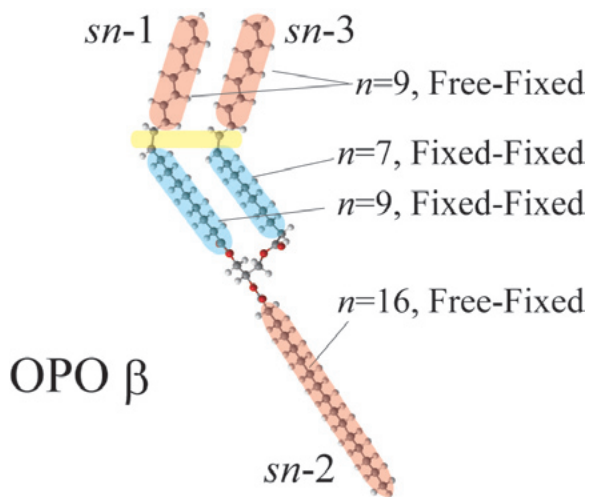

Fig.28. Structure of OPO β-polymorph with indicating each *trans* chain length and its boundary condition

30°. This δ value is reasonable to explain this band origin.

The Raman spectra of TAG liquid phase show a characteristic broad band at ～1080 cm^{-1} (Fig. 20b). This is related to the increased number of *gauche* configuration in the liquid; [13,26,27] however, this band is not directly attributable to *gauche* bond stretching. [98] The broad band shape is probably due to the *trans* chain segmentation and the density-of-states progressions induced by the increased *gauche* configurations (see also page 32).

Region 980 – 960 cm^{-1}

The band due to *cis* = C – H out-of-plane deformation [56] is seen at ～970 cm^{-1} in the Raman spectra of liquid TAGs containing unsaturated acyl chains (Fig. 20b).

In the spectra of TAG β'- and β-polymorphs, a series of small bands can be observed. These are likely to be ν_8 progression bands. [95] In crystals, the ν_8 branch splits into two components which are polarized along crystal a- and b-axis (Fig. 18). Therefore, each of the progression bands tend to split into two components in the crystals.

Region 930 – 700 cm^{-1}

The bands observed in 900 – 875 cm^{-1} region originate from the CH_3 terminal rocking mode of hydrocarbon chains. [86] This mode is consist of several vibrational modes, principally of in-plane methyl rocking, $C_{\omega-1} - C_{\omega}$ (the bond between the terminal methyl C atom and the next C) stretching, and CCC deformation which is localized in the end of chains. For a chain longer than about ten carbon atoms, their in-phase and out-of-phase frequencies differ by only a few cm^{-1} (Fig. 29). For a chain shorter than ten, these vibrations which are essentially degenerate in long chains, interact and lead to separated bands as shown in Fig. 29.

The bands observed in OPO β-polymorph spectrum in this region (Fig. 20), *i. e.* 909, 900, 890 and 877 cm^{-1}, are satisfactorily explained by Fig. 29. However, less stable polymorphs show other bands whose frequencies differ from those in Fig. 29. These bands can be explained by the acyl chain packing imperfections at the crystal layer surface (Fig. 30). [130] TAGs need not always consisting of the set of acyl chains with the best packing compatibility; therefore, it is likely to have some surplus part as shown in Fig. 30. These surplus parts tend to introduce *gauche* rotational configuration, and this change influences on the CH_3 rocking frequency. The *gauche – trans* configuration from the methyl ends (*gt –*) results in the frequency of

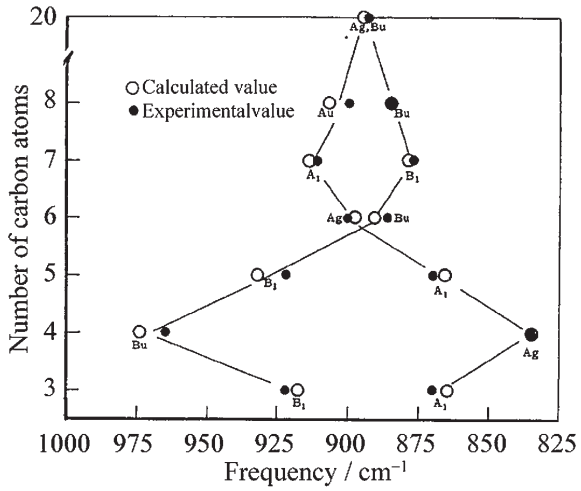

Fig.29. The frequencies of the in-plane methyl rocking mode of *n*-alkanes [86]

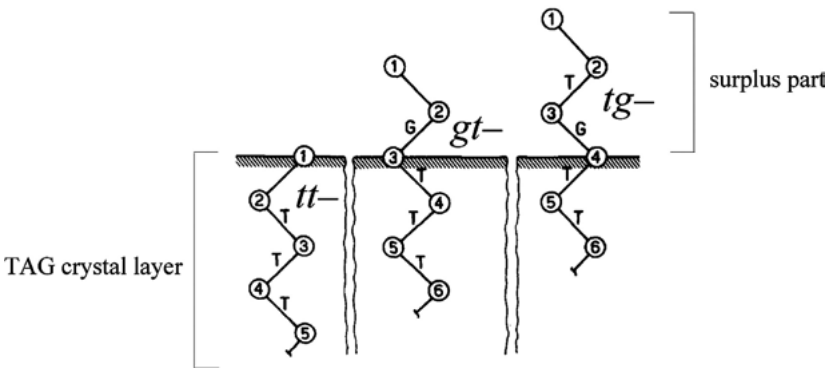

Fig.30. Depiction of the chain packing imperfection at the crystal layer surface. [130] *t*, *trans*; *g*, *gauche*.

879 cm^{-1}.[37,130] Likewise, *gg*− and *tg*− result in 862 and 850 cm^{-1}, respectively. These end-*gauche* configurations explain the weak bands in this region (Fig. 20).

It should also be noted here that there are also the bands of C_1-C_2 (the bond between the ester C atom and the next C) stretching mode in the region 920−850 cm^{-1}.[3,72] The band at around 920 cm^{-1} is probably assigned to this mode.[83] Also, the broad band that contribute the background in the 950−700 cm^{-1} region which is remarkable in TAG liquid phase spectra (Fig. 20a) is probably due to the delocalized C−C stretching modes at a chain terminal.[98]

On the basis of the accumulated spectroscopic data, Raman spectroscopy has contributed to reveal the detailed structure of TAG polymorphs. The spectral regions other than described in this chapter, *i. e.* low-frequency and ~3000 cm^{-1} regions, are also very informative. Raman spectroscopy is really instrumental in elucidating the structure and phase behavior of TAG systems.

Chapter 4
Investigation of Molecular Compound Formation in a TAG Binary System

Abstract

Raman spectroscopy has been applied to characterize physical mixtures of TAGs. Solid phase and liquid phase of the 1,3-dipalmitoyl-2-oleoyl-*sn*-glycerol (POP) and 1,3-dioleoyl-2-palmitoyl-*sn*-glycerol (OPO) binary system, which is thought to be a molecular compound forming system, were investigated. The obtained Raman spectra were subjected to singular value decomposition (SVD) for extracting the spectrum and the concentration profile for each phase existing in the system. As the result, the existence of the POP-OPO molecular compound is shown spectrometrically in the crystal sample set. The compound is apparently formed at the molar ratio of POP:OPO = 1:2 with deformed C = C configuration, and it is inconsistent with the previous reports. This inconsistency may be due to the difference in thermal treatment of crystal preparation. In the liquid samples, no evidence relating to the compound formation is observed. It is likely that the molecular compound does not exist in the liquid phase and it is the dynamically formed phase being influenced by crystallizing procedure. The factors affecting the structure of molecular compound are discussed.

Introduction

It has been reported that a third component exists in some TAG binary systems. This third component is known as the "molecular compound" and behaves like a new, pure TAG species with unique phase behavior that differs from those of its component TAGs (see also page 28). Specific molecular interactions are thought to be operating between the component TAGs leading to the compound formation. Minato *et al.* (1997) investigated on POP-OPO system by thermal analysis and have clearly shown the formation of molecular compound at POP:OPO = 1:1 ratio.[63] The molecular compound has a stable phase, β-polymorph, with a distinct melting point which is different from that of either of POP or OPO.

The structure model for the POP-OPO molecular compound is proposed by powder X-ray analysis and polarized-infrared spectroscopy.[63,64] Because of the bent geometrical structure of oleoyl chains, it is assumed that compact packing of oleoyl and palmitoyl chains in the same leaflet may arouse serious steric hindrance. Consequently, the structure model with a double chain length structure shown in Fig. 31a is most plausible.[63] This structure is in contrast to the triple chain length structure of corresponding polymorph of each component TAG, β-polymorphs of POP and OSO (Fig. 31b).[44,128] These results indicate that the intermolecular interaction at olefinic groups play a key factor in the formation of a molecular compound.

Despite these quite interesting indications, no precise structural data from single crystal X-ray diffraction techniques on molecular compounds are available. The major reason for this lack of data can be ascribed to difficulties in obtaining single crystals of TAGs containing unsaturated fatty acyls. The crystallinity is often not adequate for crystal X-ray diffraction study.

It is believed that the POP-OPO molecular compound is formed immediately after mixing POP and OPO in their liquid phase.[117] It is based on the readily constructed model structure with supposed of the stacking of olefinic groups (Fig. 31a). If this supposition is correct, oleoyl chain interactions can additionally arise in the liquid

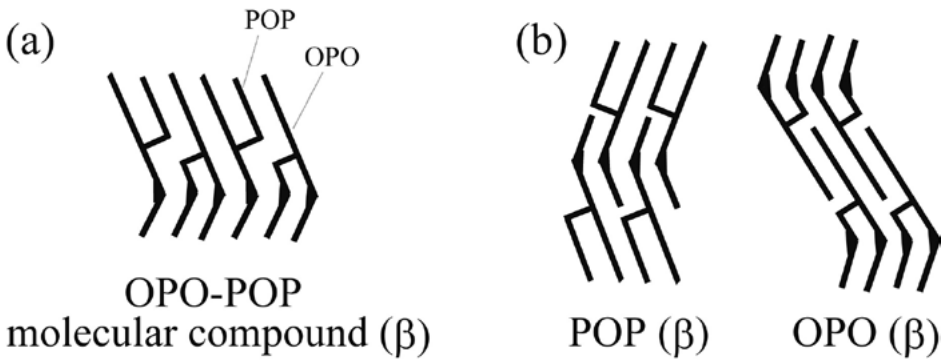

Fig.31. Structure model of the β-polymorph of POP–OPO compound (a), [63] and the structures of its component TAGs (b). [44,128]

phase when mixing the component TAGs. To investigate such interaction, Raman spectroscopy is the suitable method. In contrast to X-ray diffraction analysis, Raman spectroscopy can be applied to the liquid phase to study its structure, and indeed, it has revealed the structure formed on TAG crystal nucleation. [26]

In this chapter, the combination of Raman spectroscopy and singular value decomposition analysis (SVD) has been applied to address the problem of molecular compound formation in the TAG binary system. SVD is useful for extracting physically meaningful components from two-dimensional data dependent on a physical variable. It is obvious that this technique helps to extract the qualitative (spectrum) and quantitative (concentration) information on the molecular compound from a set of Raman spectra of POP-OPO mixture with different concentration of the component TAGs. By using this technique, the structure and the mechanism of the compound formation have been studied.

Experiment

Samples

POP and OPO were purchased from Sigma-Aldrich (St. Louis, MO, USA). The purity of the samples was verified by the following gas chromatography and it was about 99%. Both samples were used without further purification. They were completely melted at 50 ℃ and mixed with a vortex mixer to prepare the eleven samples with different molar ratio of POP and OPO in 10% increments. The concentration of each TAG molecule in the binary mixture was confirmed by gas chromatography. 0.5 mg of the sample was dissolved into ～50 μL of *n*-heptane to make ～10 mg/ml sample solution. 0.5-μL solution was injected into a gas chromatograph (Shimadzu GC-17A, Kyoto, Japan) with an auto-injector (Shimadzu AOC-17). Split injection mode was selected and the ratio was 1:10. Helium was used as the carrier gas with 30-cm/s linear gas rate. The injector and detector temperatures were 320 and 370℃, respectively, the oven temperature was raised from 250 to 365℃ at a rate of 5℃/min and hold 365℃ for 5 min. The gas-chromatography-capillary column was a Rtx-65TG (15-m length, 0.32-mm i.d. and 0.1-μm film thickness) (Restek, Bellefonte, PA, USA). Signals were detected with a flame-ionization detector. The reference material IRMM-801 (IRMM, Geel, Belgium) was used for peak identification and determination the calibration factor of each triacylglycerol. The chromatographic peaks detected after 14-min injection, which corresponded to the TAGs with acyls' -carbon-atoms number >40, were integrated to calculate the total TAG amount. Each TAG quantity was expressed as the ratio to the total. All samples were analyzed in duplicate.

Two sample sets were prepared: One is crystals and the other is melts. Crystal samples were prepared as follows: The samples were heated at 50℃ to be completely melted and cooled down to 4℃ to crystallize the metastable polymorph. They were then placed in an incubator (IJ201, Yamato Scientific, Tokyo) held at 20℃ for 11 days to transform the crystals into more stable forms. Nitrogen atmosphere was provided in order to avoid the autoxidation of TAGs. Melt samples were prepared by heating the sample to 50℃ and gradually cooling down to 40℃ by a cryostat (Linkam 10021, Tadworth, Surrey, UK).

Differential scanning calorimetry (DSC)

The polymorph of the sample crystals was checked by DSC using a DSC-60 (Shimadzu, Kyoto, Japan). Approximately 1.5 mg of each sample melt was set in an aluminum pan. The pans were incubated with the same thermal condition described in the sample section. The DSC was set to 10℃ and analysis was performed from this temperature up to 60℃ at a heating rate of 5℃/min. An empty pan was used as a reference sample.

Raman spectroscopic measurement

The samples were kept at 15 and 40℃ for the crystal and melt samples, respectively, by a cryostat during the measurement (Fig. 32). Dry nitrogen atmosphere was provided in order to keep free of sample autoxidation and condensed moisture. Raman scattering was excited with the 532-nm line of a Nd:YVO_4 laser (Verdi, Coherent, Santa Clara, CA, USA). The back-scattered Raman light from the sample was collected by an objective lens (LUCPlanFLN20x, Olympus, Tokyo) and measured with a spectrometer (Shamrock, Andor, Belfast) and an EMCCD detector (Newton, Andor). The integrated Raman intensities of all the polarization components were measured. The laser power was 3 mW at the sample point. Four measurements with 300 s exposure time were accumulated. Spectral resolution was ~2.1 cm^{-1}.

Extraction of the components in the system using singular value decomposition (SVD)

The Raman spectra were analyzed with SVD for extracting the concentration profile and spectrum for each independent spectral component (Fig. 33). Details are described as follows.

Firstly, Raman spectra were subjected baseline correction using a line fitting and then normalized with the CH_2-scissors bands in order to eliminate the effect of laser power fluctuation.

The Raman spectra were assembled to form the matrix M (Fig. 33). The rows and columns of the matrix were the Raman spectra (λ) and the sample number (11 in the present study), respectively. Then, SVD was applied to the matrix. SVD is a mathematical treatment to decompose a given matrix M into a product of three matrices U, W and V (Fig. 33 eq. 1). U and V are orthonormal matrices and W is a diagonal matrix. Each diagonal element of the matrix W is a positive real number and is called singular value. The magnitude of singular value w_{ii} indicates the contribution of the product of row vector u_i and column vector v_i to the matrix M (eq. 2). The w_{ii} are ordered according to their contribution to the total variance in the observations. Hence, the first few elements, $w_{1\cdot1}\cdots w_{n\cdot n}$, are associated with the physically significant information in the system, and the remaining elements are primarily associated with the random instrumental and experimental error. The n is therefore the number of significant components in the data set.

Then, by using the acquired number n, the spectrum and the concentration profile of each component were isolated under constraints in order to minimize ambiguities. The constraints were as follows:

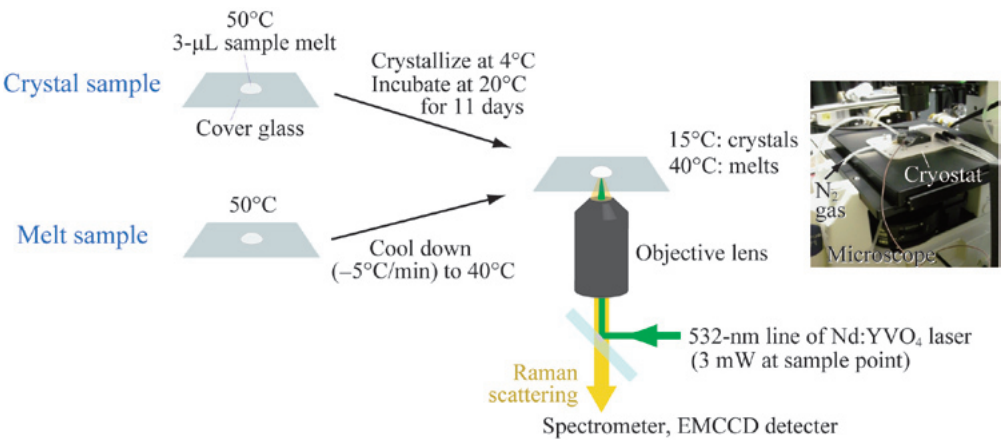

Fig.32. Sample preparation and Raman spectroscopic measurement

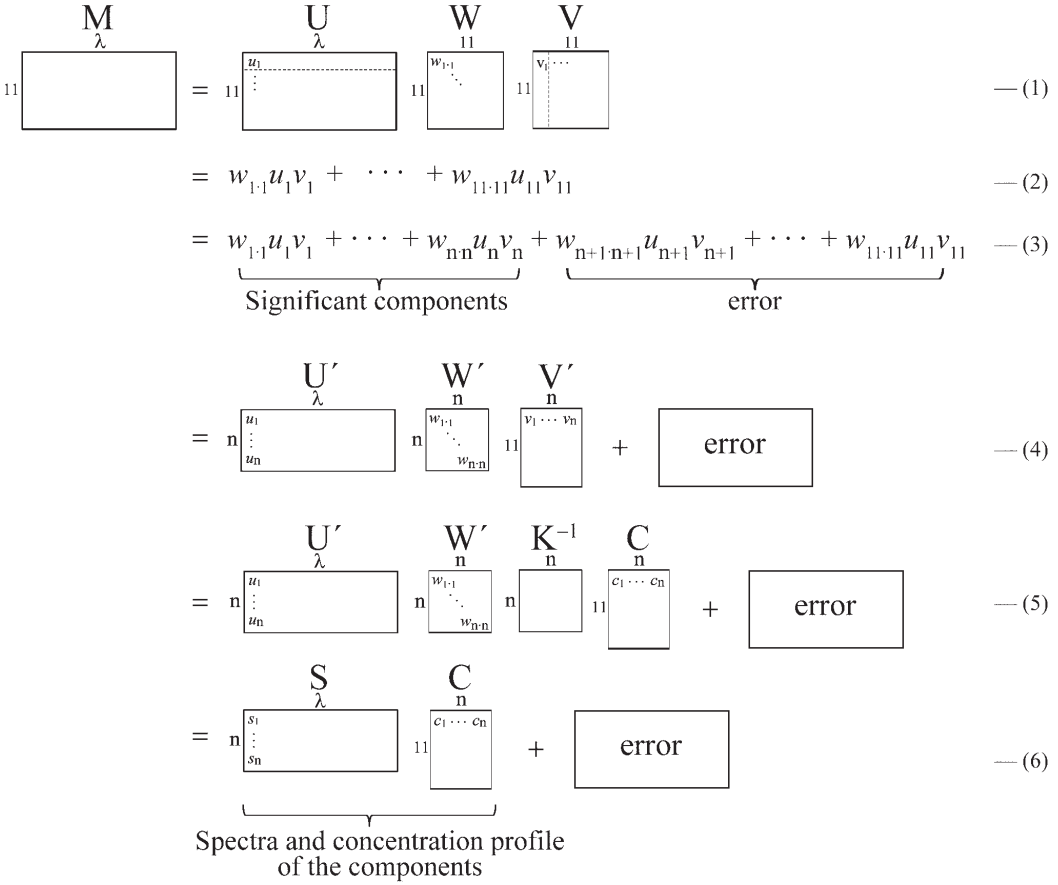

Fig.33. The scheme of the extraction of the spectra and concentration profiles of the significant components in the data.

1) authentic POP and OPO spectra and non-negativity for spectra, and
2) non-negativity, unimodality and closure for concentration profiles.

Results and discussion

Properties of the samples

The concentrations of POP and OPO of the samples were shown in Fig. 34. It is confirmed that the sample set of the present study is composed of the samples with the desired molar ratios of component TAGs in 10% increments.

The DSC heating curves of the samples are shown in Fig. 35. 100%-POP sample shows the endothermic peak at 30.4℃ and this corresponds to POP β'_2-polymorph (Table 3). Likewise, 100%-OPO sample shows the peak at 21.1℃, it is due to the OPO β_1-polymorph. The samples with any other composition than that of the pure components show an endothermic peak between these two temperatures. The previous study reported that the melting temperature of POP-OPO molecular compound were 16℃ and 32℃ for α - and β-polymorph respectively. [63] From the DSC curves, it is likely that these polymorphs of the POP-OPO molecular compound are not formed in the present study.

Raman spectra and concentration profiles of the components in the crystal samples

The Raman spectra of the polycrystals of eleven samples are shown in Fig. 36. Every spectrum shows the sharp conformational-sensitive bands at ～1745, 1296, 1130, ～1100 and 1060 cm^{-1} which are characteristic to solid phase of TAGs.

These spectral data are assembled into a matrix and subjected to SVD. The result is shown in Fig. 37. From the first to the third elements have relatively high singular values, while after the fourth elements have small values. This indicates that three distinctive phases exist in the sample set.

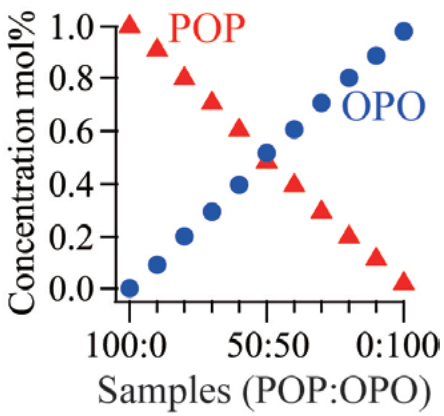

Fig.34. The concentration profiles of POP and OPO of the samples

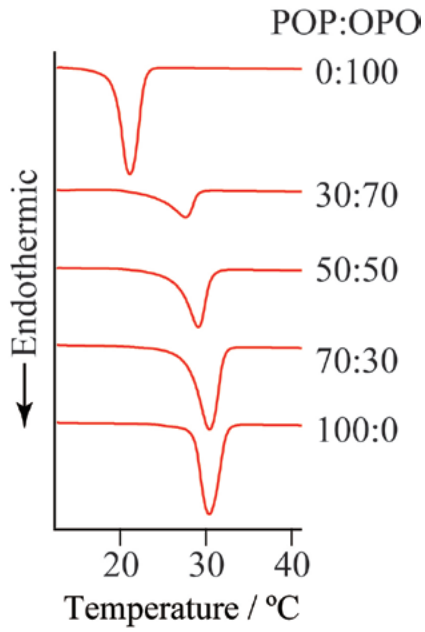

Fig.35. DSC heating thermograms of the crystal samples

Table 3. Melting points of polymorphs of POP [82] and OPO [63]

Triacylglycerol	Polymorph	Melting point (℃)
POP	α	15.2
	γ	27.0
	δ	29.2
	β'_2 (pseudo-β'_2)	30.3
	β'_1 (pseudo-β'_1)	33.5
	β_2	35.1
	β_1	36.7
OPO	α	−18.3
	β'	11.7
	β_2	15.8
	β_1	21.9

Then, the concentration profiles and Raman spectra of these three phases are reconstructed. It is confirmed that two spectral components are not enough to explain the data set. The concentration profiles and spectra show unreasonable features (data not shown). On the other hand, three components successfully explain the data set. The reconstructed concentration profiles and spectra of the three components are shown in Fig. 38 and Fig. 39. When the sample is 100%-POP, concentration index of the component 1 is 1 (Fig. 38), therefore, the component 1 is POP. The reconstructed Raman spectrum for the component 1 successfully reproduces the spectrum of 100%-POP sample (Fig. 39). Likewise, the component 2 is identified as pure OPO. The spectrum for the component 2 also successfully corresponds to that of 100%-OPO sample. The component 3 is likely to be a phase formed by mixing POP and OPO. It shows a meaningful concentration profile. Also, its reconstructed Raman spectrum shows a natural spectral feature which is composed of Lorentzian curves. From these results, the existence of the third component in the binary system is shown spectrometrically, and its concentration profile and Raman spectrum are successfully determined.

Structure of the third component

From the acquired concentration profiles (Fig. 38), it is observed that the component 3 is apparently formed at a molar ratio which is different from the previous studies. [63,66] Fig. 40 shows the model-concentration profile with supposing the third component is formed at POP:OPO = 1:1 or at 1:2 molar ratio. The latter profile is more similar to the acquired profile (Fig. 38). Therefore, the component 3 is thought to be formed at POP:OPO = 1:2 molar ratio.

One plausible reason for this discrepancy is that the component 3 is a polymorph of the OPO other than β and not a molecular compound. The rationale for this is that the sum of the concentration of component 2 (OPO β-polymorph) and component 3 (Fig. 41) almost reproduce the total amount of OPO shown in Fig. 34. However, the melting point of POP:OPO = 30:70 sample, where component 3 accounts for 80% amount (Fig. 38), is about 27.5℃ (Fig. 35). This melting temperature is higher than any polymorph of OPO; therefore, it is difficult to assign

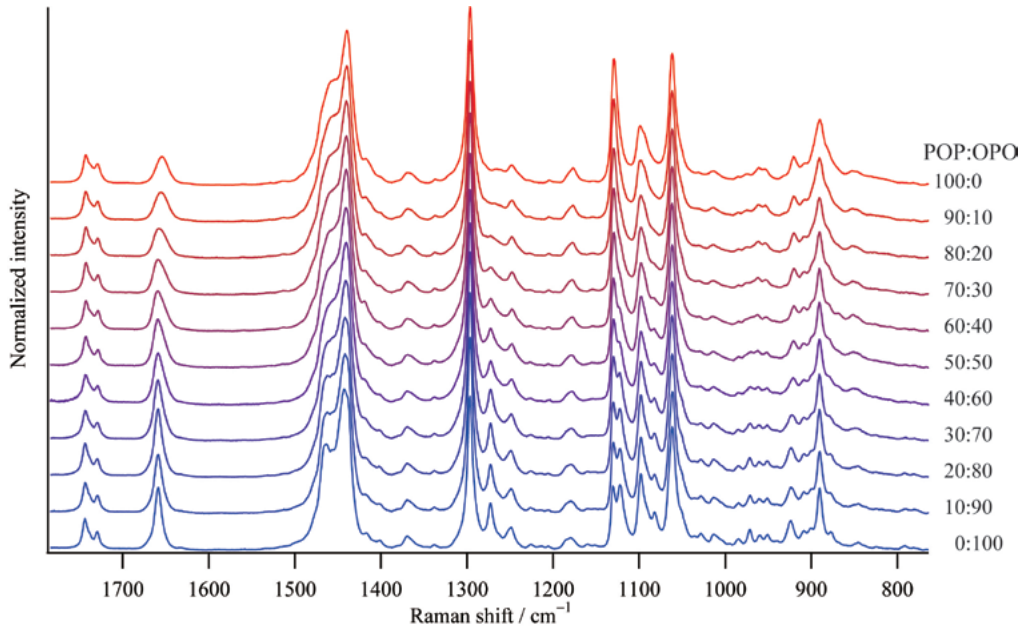

Fig.36. Raman spectra of the polycrystal of eleven POP-OPO binary mixtures

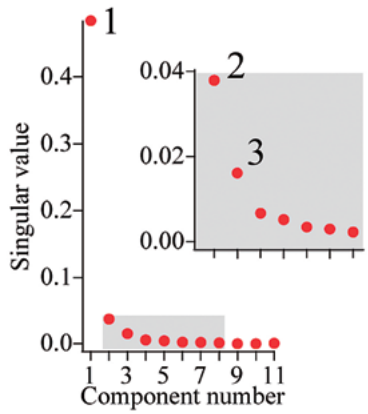

Fig.37. Result of SVD. Three elements are detected as the major ones

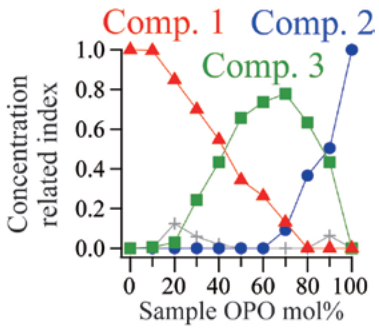

Fig.38. Reconstructed concentration profiles of the three components. ▲, component 1; ●, component 2; ■, component 3; +, residuals.

component 3 to an OPO polymorph. Also, supposing the component 3 as a polymorph of POP is unreasonable in terms of the sum concentration of components 1 and 3. Therefore, the component 3 is more likely to be a phase composed of both TAGs.

To acquire the structural information on the POP: OPO = 1:2 compound, its Raman spectrum is compared to the averaged spectrum of one part of POP β'-polymorph and two parts of OPO β-polymorph (1 × (POP β') + 2 × (OPO β), Fig. 42). They are both normalized with the CH_2 scissoring band area (~1440 cm^{-1}) and their difference spectrum is also shown. The difference spectrum has continuous positive intensities at 1370 − 1230, 1100 − 1000 and 880 − 800 cm^{-1}. They are corresponding to the background increases which are characteristic in the spectrum of the less stable polymorphic phase of TAG molecules (see Chapter 3) and indicate the existence of disorder in the crystal especially at the methyl end region of the acyl chains.

The difference spectrum (Fig. 42) shows the ~1745 cm^{-1} band broadening to the higher frequency region and the increasing ~1737 cm^{-1} band intensity. They are corresponding to the deformations introduced to the vicinity of ester linkages (see Chapter 3). The 1:2 compounds likely to have the conformational ambiguities also at glycerol moieties.

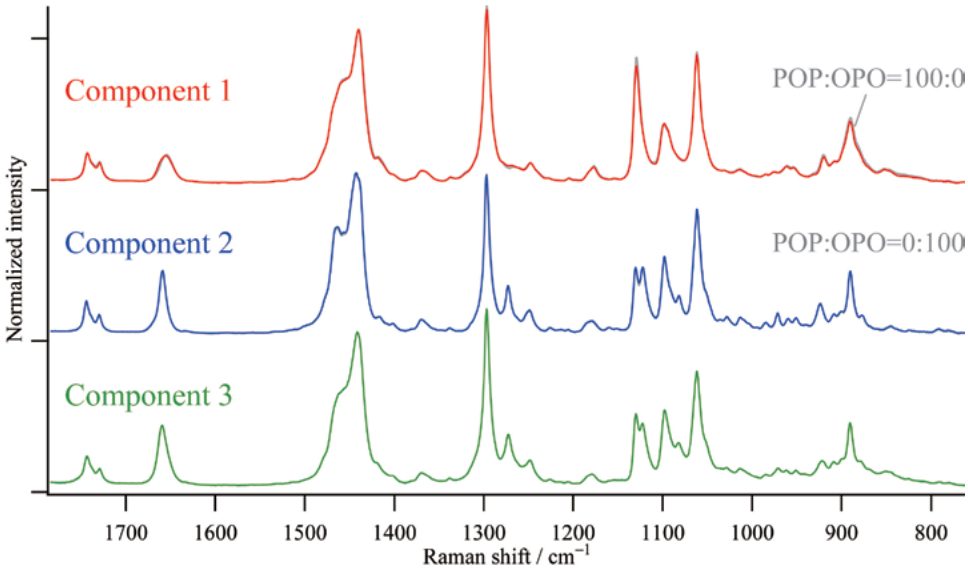

Fig.39. Reconstructed Raman spectra. The spectra of components 1 and 2 almost overlap the spectra of POP-100% and OPO-100% (gray lines), respectively.

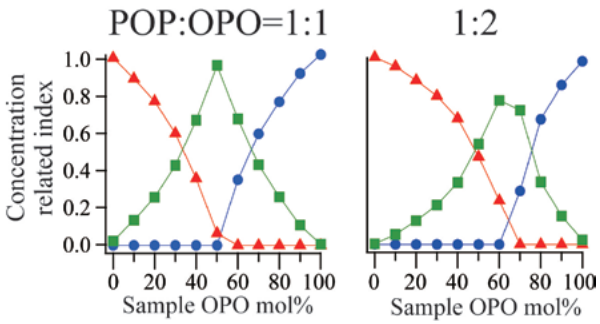

Fig.40. The calculated model concentration profiles with supposing the third component is formed at POP: OPO=1:1 (left) and with supposing 1:2 (right). ▲, component 1; ●, component 2; ■, component 3.

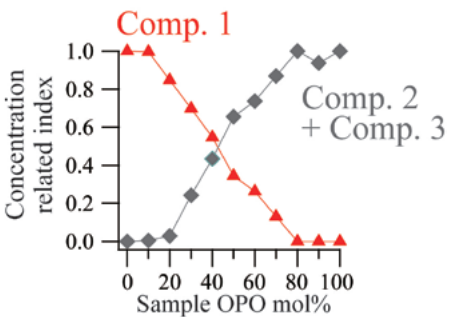

Fig.41. Concentration profiles. ▲, component 1; ◆,component 2 plus component 3.

The sharp feature of 1272 cm^{-1} band of the 1:2 compound indicates that the compound contains *slew-cis-skew'* configuration at C=C bond (see Chapter 3). However, some other configurations are likely to be also existed since its band intensity and width are smaller and broader than those of OPO β-polymorph (Fig. 39). Fig. 43 shows the C=C stretching band region and the results of the curve fitting by Lorentzian functions. Two bands can be detected at ~1660 and ~1654 cm^{-1} in the 1:2 compound spectrum. The former band is prominent in the OPO β-polymorph and its C=C configuration is assigned to *skew-cis-skew'*. [40] This C=C configuration leads to a low-angle bend in the oleic acyl and is likely to play a important role on the intra- and inter-molecular acyl chain stacking as shown in Fig. 44a. The latter band, ~1654 cm^{-1}, which is observed in POP β'-polymorph corresponds to deformed *slew-cis-skew'* configuration. [128] Oleoyl and palmitoyl acyls are packed in the same leaflet in POP β'-polymorph (Fig. 44b) and this incomplete stacking of oleoyl acyls deforms the *skew-cis-skew'* configuration. In the 1:2 compound, the existence of 1654 cm^{-1} band indicates that a significant amount of the deformed configuration exists and the C=C packing is not perfect, it is different from the model proposed by Minato *et al.* (Fig. 31a). [64]

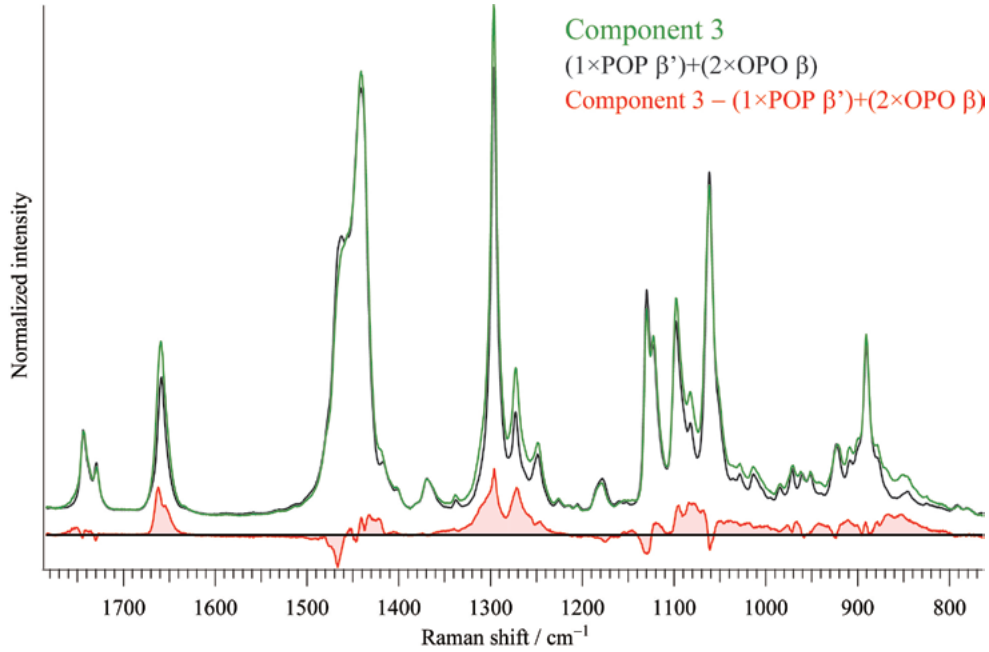

Fig.42. Comparison between the spectra of component 3 and the averaged spectrum of one part of POP β' and two parts of OPO β((1 × POP β')+(2 × OPO β)). The difference spectrum is also shown.

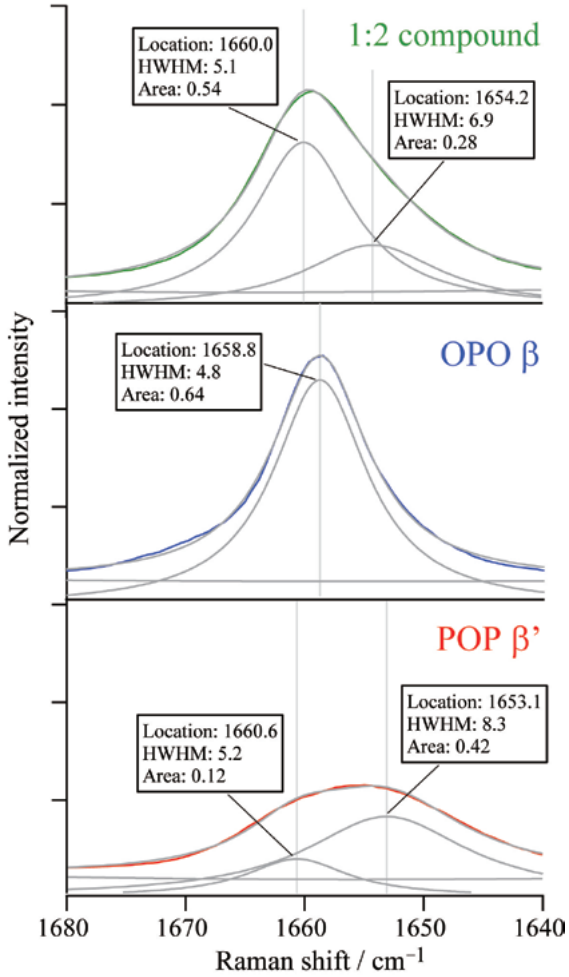

Fig.43. C=C stretching region of the Raman spectra of POP, OPO and 1:2 compound and their curve fitting results.

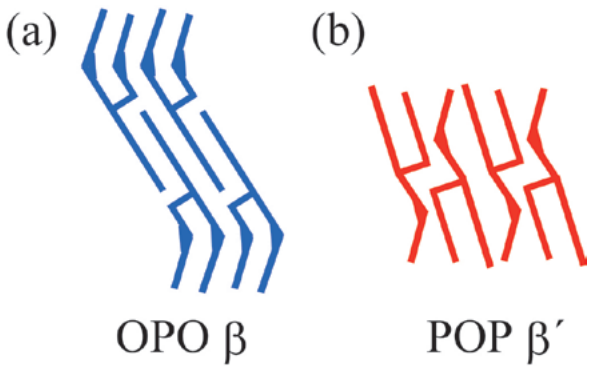

Fig.44. Crystal structures of OPO β-polymorph and POP β' -polymorph [44,128]

Investigation of the compound formation in melt

Regarding the compound formation in liquid phase, Raman spectra of the sample melt were measured at 40℃ are analyzed by SVD (Fig. 45). Only two components are detected, corresponding POP and OPO. It indicates that mixing these two TAG species in liquid phase does not give rise to the intermolecular interaction between POP and OPO similar to that observed in the crystal phase.

In TAG melt, two variants of molecular dimers are considered as stable units (Fig. 46). [70] They represent different chain length structures with different locations

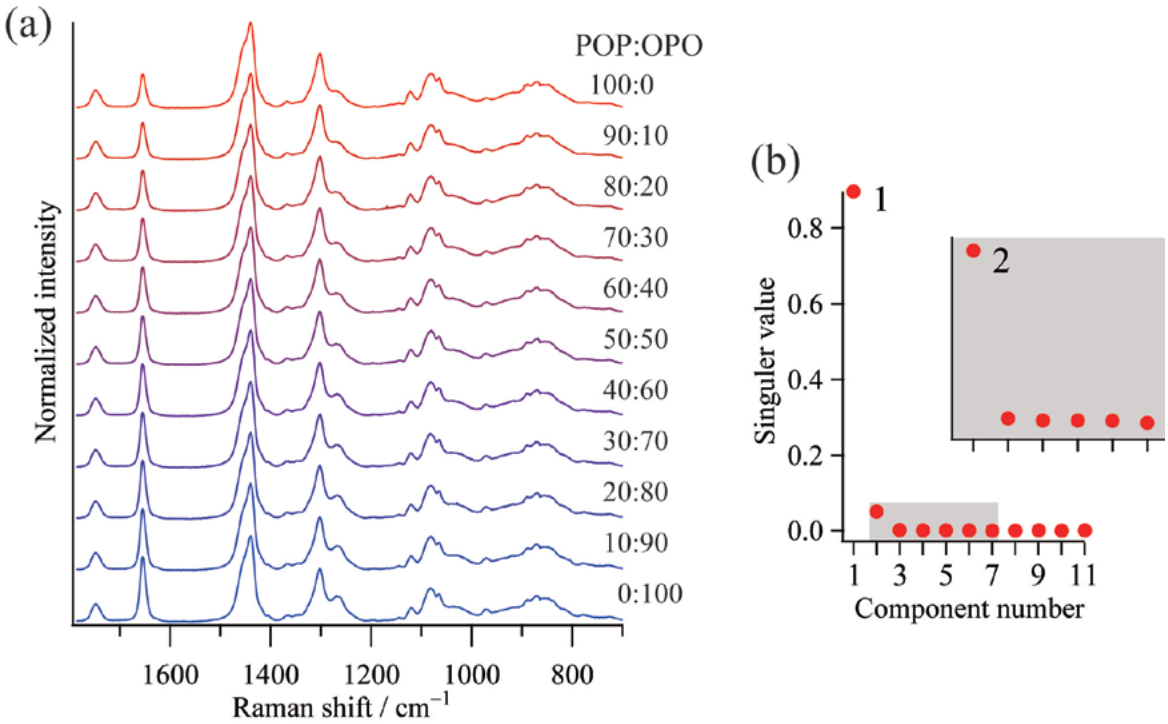

Fig.45. Raman spectra of the melt samples (a) and its SVD result (b)

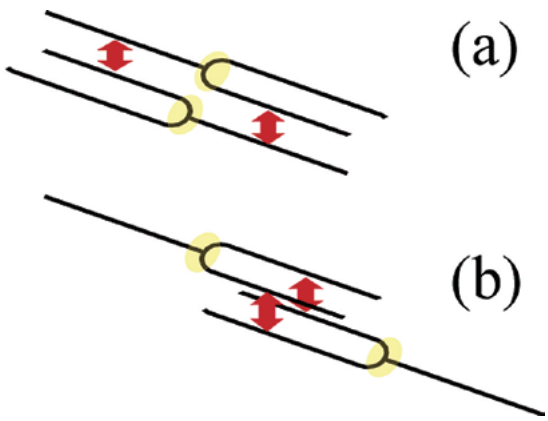

Fig.46. A schematic 3D representation of possible molecular dimers in TAG melts. [70] (a), glycerol moieties of the adjacent molecules are close to each other and form a dimeric units; (b), glycerol moieties are spaced and form a three-chain length structure.

of the glycerol moieties of adjacent molecules. Both dimers can involve four acyl chain interactions between the two molecules, and the stability of these dimers should be dependent on both the structure of the acyls and the thermodynamic conditions. Regarding the two-chain length structure of the POP-OPO compound model (Fig. 31a), the dimer with the close glycerol moieties (Fig. 46a) should be more stable in POP-OPO melt. However, any spectral changes ascribed to the increase of this dimer can be detected. It is reported that a packing incompatibility between saturated and unsaturated acyls leads to stabilize both type of dimers in the liquid phase of a TAG consisting of these acyls. [70] Therefore, both dimers presumably coexist in 100%-POP and 100%-OPO melt, as well as in their mixtures. This is the plausible reason for the any spectral changes observed by mixing.

Factors affecting the structure of molecular compound

In the present study, the molecular compound is formed at POP:OPO = 1:2 molar ratio which is inconsistent with the previous studies. There are two possible reasons: the difference in the crystal incubation duration and the cooling procedure.

In the study of Minato *et al.*, the binary mixtures of POP and OPO were incubating over one month while the incubation period was eleven days in the present study. Shorter incubation time may generate a metastable structure of the molecular compound other than β-polymorph. This may explain the DSC melting results of this study. However, it is unlikely that the 1:2 compound

will be broken and reconstructed into 1:1 compound after some incubation period.

Regarding the latter possibility, Koyama and Ikeda conducted an interesting study on fatty acids and phospholipids containing C=C bonds. [47] They reported that the *skew-cis-skew'* configuration dominates in the sample with annealing treatment (slow cooling) while little exists in the samples with rapid cooling. The POP: OPO=1:2 molecular compound have significant amount of the configuration different from *skew-cis-skew'*. This indicates that the crystallizing condition in the present study is somehow faster than those in the previous studies. It was an annealing treatment in the previous study (crystallizing at 20 or 29℃). [63] More recently, Mykhaylyk and Martin observed a transient mesophase, α_2-polymorph, after a rapid cooling from melt. [71] The α_2-polymorph is specifically observed for TAGs consisting of both saturated and unsaturated acyls. They suggest that the structural incompatibility between saturated and unsaturated acyl chains equalizes the stability of the two molecular pairs in melt (Fig. 46), and results in the α_2-polymorph where the two pairs coexist. [70] This is likely to be the reason for the formation of the 1:2 compound, since α-polymorphs are considered to have large influence on the polymorph which will be formed next. Fig. 47 summarizes the putative mechanism for the formation of

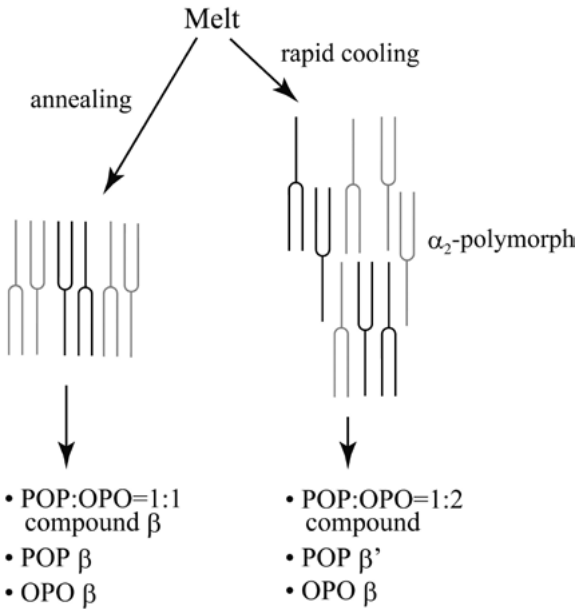

Fig.47. Illustration of the relation between the cooling treatments and the resulting phases

1:1 and 1:2 compounds. An annealing treatment induces the molecular pair with two-chain length structure in the melt, and it will readily form 1:1 compound. On the other hand, a rapid cooling introduces the α_2-polymorph in the binary system, and its structure provides the decisive difference between the two compound structures. The crystallizing procedure has also modified the POP polymorph. While it is β in the previous study (annealing), it is β' in the present one (rapid cooling).

Conclusion

The formation of the molecular compound in POP-OPO binary system has been shown spectrometrically. This compound is likely to form at POP:OPO=1:2 molar ratio, which is different from the previous reports. Since it has been believed that the POP-OPO molecular compound is formed just after mixing the component TAGs in their liquid phase, this observation raises interesting questions. The 1:2 compound shows the deformed C=C configuration which indicates that the compound is formed by a rapid cooling process. The rapid cooling probably introduces the specific phase, α_2-polymorph, in the POP-OPO system and its structure provides the fundamental difference in the molecular compound structure (1:1 or 1:2). It is likely that the molecular compound does not exist in the liquid phase, it is the dynamically formed phase being influenced by crystallizing procedure.

It is quite interesting how the van der Waals type interaction among the acyl moieties can enable the formation of the stable compound. The ratio of POP:OPO =1:2 appears plausible, because it also corresponds the number of oleoyl acyls they have. Oleoyls have been thought the key factor forming the compound. The conclusion from the present study is in accordance with this empirical evidence.

Chapter 5
TAG Phase Behaviors in Multicomponent Systems

Abstract

Naturally occurring TAGs are present in multicomponent systems which consist of more than 30

TAG species. It is empirically known that the mixing of these multicomponent systems, accompanied by a large TAG compositional change, would indicate a transition to a completely different fat with different phase behavior. However, because of the complexity, the underlying causes are not known so far.

Adopting bovine and porcine fats as the instance of TAG multicomponent systems, the influence of the difference in TAG composition on their phase behavior and phase behavior of their mixture are investigated. From their Raman spectra, it is shown that porcine fats contain β'-polymorphs, while bovine fats do not contain them. The difference arises due to the TAG compositional difference between the two fats. The major TAG species in porcine fats (OSatO) is likely to form β'-polymorphs in the present experimental condition. In bovine-porcine mixture systems, however, β'-polymorphs scarcely exist even in the presence of porcine fat upto 50%. The SatOSat-OSatO type "molecular compound" formation is the most likely reason why the addition of the bovine fat disturbs the β'-polymorph formation. The empirically known drastic changes of phase behavior which are caused by mixing multicomponent systems seem to be due to "molecular compound" formation.

The feasibility of Raman spectroscopy to differentiate the origin of animal fats is also discussed.

Introduction

The most familiar multicomponent TAG system is probably cocoa butter which chocolates are made of (Fig. 48). This system has been studied extensively for a long time (*e.g.* Peschar *et al.*) [75] because of its importance in food industry. However, its phase behavior and the underlaid mechanisms have still many secrets.

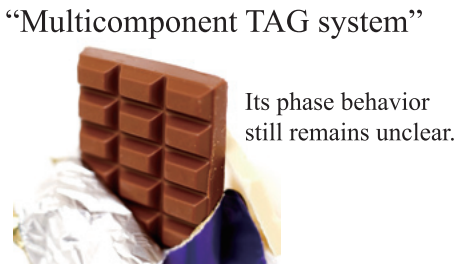

Fig.48. The most familiar multicomponent TAG system

Natural fats are generally made up of TAGs. [6,87] They contain about more than 30 TAG species [32] and it is known that these multicomponent TAG systems also exhibit polymorphism. [20,79,115] The phase behavior varies depending on the TAG composition.

The TAG composition of biological systems is genetically determined. Even though their fatty-acid compositions of the systems do not have much difference (Table 4), their TAG compositions are diverged. This diversity is due to the substrate specificity of the enzymes involved in the TAG biosynthesis (Fig. 5). [89] This specificity difference is appearing as the difference in *sn*-specific fatty acid composition, *i.e.* TAG composition (Table 5).

As shown in Table 5, bovine fat and porcine fat, which are both widely used in food industry, have different TAG composition. Bovine fats have high concentration of TAGs with oleoyl acyls in their *sn*-2 position. On the other hand, porcine fats have ones with oleoyls in their *sn*-1 and *sn*-3 positions. Saturated fatty acyl chains (*e.g.* palmitic and stearic acyls) occupy the positions other than those mentioned above. They can be depicted as Fig. 49. Such difference in TAG composition may bring about polymorphic difference between these two fats.

It is said that small TAG compositional changes could be explained as the natural variations in the properties of the fats, however, large compositional changes of multicomponent TAG systems would indicate a transition to a completely different fat with different phase behavior. [116] For example, mixing of porcine fat and palm oil at 1:1 ratio produces the fat containing relatively more solid phase (Fig. 50). [66] It is suggested that the compound formation is the reason for the change in phase behavior; however, no evidence for the molecular

Table 4. Fatty-acid composition of bovine and porcine fats [124]

Fatty acid	Bovine	Porcine
Myristic acid (C14:0)	3.7	1.6
Palmitic acid (C16:0)	26.1	23.9
Palmitoleic acid (C16:1)	6.2	2.4
Stearic acid (C18:0)	12.2	12.8
Oleic acid (C18:1)	35.3	35.8
Linoleic acid (C18:2)	1.1	14.3
Linolenic acid (C18:3)	0.5	1.4

Table 5. *Sn*-specific fatty acid composition of bovine [11] and porcine fats [10]

Fatty acid	Bovine fat			Porcine fat		
	sn-1	*sn*-2	*sn*-3	*sn*-1	*sn*-2	*sn*-3
Myristic acid (C14:0)	2.9	1.5	5.7	0.7	3.5	0.6
Palmitic acid (C16:0)	42.0	24.6	21.9	9.8	72.1	5.4
Palmitoleic acid (C16:1)	2.1	0.8	2.9	1.7	3.7	2.1
Stearic acid (C18:0)	34.4	11.3	32.4	38.8	3.8	11.3
Oleic acid (C18:1)	14.9	**55.3**	34.6	**42.7**	14.0	**65.4**
Linoleic acid (C18:2)	0.2	3.9	0.3	6.3	2.9	15.2
Saturated-acid total	**79.3**	37.4	**60.0**	49.3	**79.4**	17.3
Total	96.5	97.4	97.8	100.0	100.0	100.0

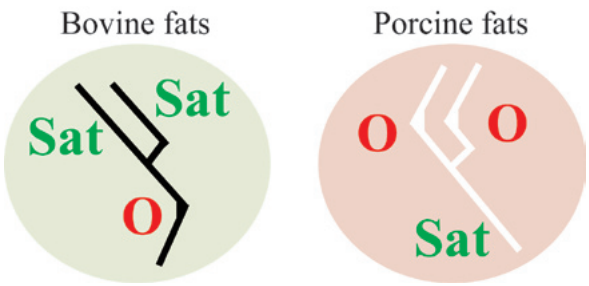

Fig.49. Illustration of the major TAGs of bovine and porcine fats. Sat: Saturated acyl chain. O: Oleoyl chain

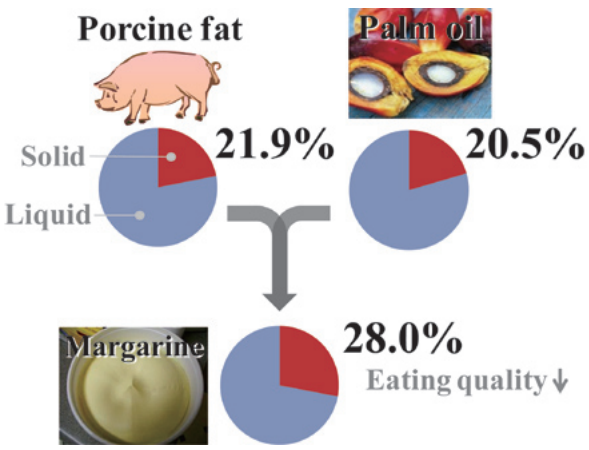

Fig.50. After crystallizing at 4℃ for 1.5 hours and then incubating at 20℃ for 1 week, porcine fat and palm oil contain 21.9% and 20.5% solid phase, respectively. After mixing these two fats, it becomes to contain more solid phase (28.0%). Such a high solid content often deteriorates eating quality. [66]

compound formation in the mixed multicomponent system has been shown so far.

The objective of this chapter is to investigate the phase behavior of TAG multicomponent systems, adopting bovine and porcine fats as the instances of such systems. Especially, the influence of the difference in TAG composition on their phase behavior and the phase behavior of their mixture fats are focused. The feasibility of Raman spectroscopy to differentiate the origin of fats is also discussed.

Experiment

Samples and TAG profile analysis

Seven bovine fats (Bovine tallow A-G) and nine porcine fats (Porcine fat A-I) were used (Table 6). All fats were unfractionated and commercially available. They were used without further purifications. The TAG profiles of the 16 sample fats were analyzed by gas-chromatography (see the experimental section of Chapter 4, page 42).

Raman spectroscopic measurement and analysis

The samples were thoroughly melted at 50℃ and 5-μL melt was put on a CaF_2-slide glass (0.3-mm thickness). The slide glass was set in a cryostat (Linkam 10021, Tadworth, Surrey, UK) and nitrogen atmosphere was provided in order to avoid autoxidation. Firstly, the sample was heated at 80℃ for 1 min to erase any crystal memories. Then crystals were prepared by cooling down to incubation temperatures (10, 0, −10 and −20℃) at a rate of −20℃/min and hold for 5 min. Raman spectra were measured after the incubation and the samples were kept at the incubation temperature in a cryostat during the measurements.

Raman scattering was excited with the 785-nm line

of a Ti-sapphire laser (Spectra Physics 3900S, Newport, Santa Clara, CA, USA) (Fig. 51). The back-scattered Raman light from the sample was collected by an objective lens (LUCPlanFLN20x, Olympus, Tokyo, Japan) and measured with a spectrometer (Chromex 250i, Bruker Optik GmbH, Ettlingen, Germany) and a CCD detector (400×1340 pixels, Spec-10 400BR(LM), Roper, Sarasota, Florida, USA). The laser power, measured by a power meter with a photodiode sensor (PD300, Ophir Optronics, Jerusalem, Israel), was 30 mW at the sample point. Three measurements with 60 s exposure time were accumulated. Spectral resolution was 3.8 cm^{-1}. The laser focal point was about 11 μm in diameter with 60-μm spatial resolution in the horizontal direction.

Raman measurements were made in duplicate. The spectra were averaged, baseline subtracted and deconvoluted with the slit function of the spectrometer (a Gaussian function, the half width at half maximum was 1.9 cm^{-1}) with the use of a triangular apodizing function. The deconvoluted spectra were normalized with the CH_2-scissors bands (1410−1480 cm^{-1}) in order to eliminate the effect of laser power fluctuation. The intensity of

Table 6. Samples and their detailed information

Sample name		Product name	Identity
Bovine fat	A	"Beef tallow"	Sigma-Aldrich, 03-0660
	B	"Edible beef tallow"	Manufacturer 1, product A, lot. A
	C	"Edible beef tallow"	Manufacturer 1, product A, lot. B
	D	"Refined beef tallow"	Manufacturer 2, product A
	E	"Edible refined beef tallow", JAS*	Manufacturer 3, product A, lot. A
	F	"Edible refined beef tallow", JAS	Manufacturer 3, product A, lot. B
	G	"Hett"	Manufacturer 4, product A
Porcine fat	A	"Pork fat"	ERM†-BB444
	B	"Pork fat"	ERM-BB446
	C	"Pork fat"	BCR‡-430
	D	"Refined lard", JAS	Manufacturer 1, product B, lot. A
	E	"Refined lard", JAS	Manufacturer 1, product B, lot. B
	F	"Refined better lard", JAS	Manufacturer 3, product B, lot. A
	G	"Refined better lard", JAS	Manufacturer 3, product B, lot. B
	H	"Refined lard"	Manufacturer 4, product D, lot. A
	I	"Refined lard"	Manufacturer 4, product D, lot. B

*JAS: Japanese Agricultural Standard
† ERM: Europian Reference Material
‡ BCR: Community Bureau of Reference

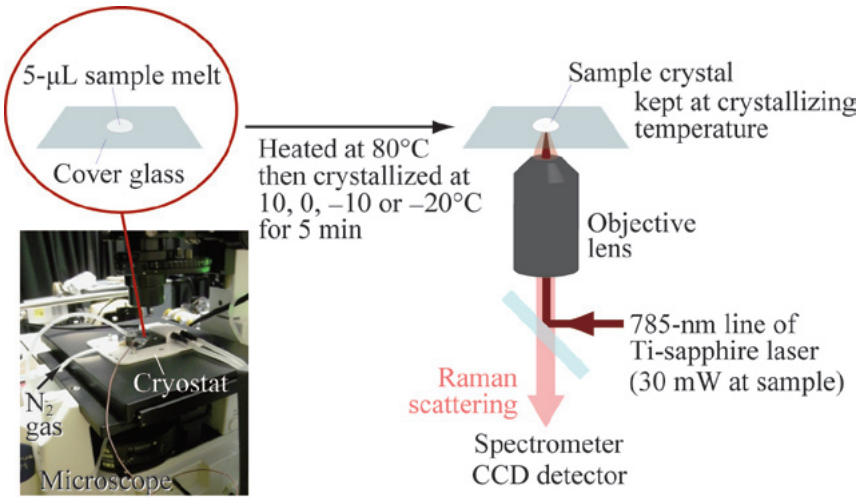

Fig.51. Sample preparation and Raman spectroscopic measurement

the 1417 cm^{-1} band was acquired by band fitting using a Lorentzian function and the data were assessed with Welch's analysis of variance and the *t*-test.

Results and discussion

Fatty acyls are abbreviated: Myristic acyl, M; palmitic acyl, P; oleic acyl, O; stearic acyl, S; linoleic acyl, L; arachidic acyl, A. TAG molecular species are expressed with three-letters notation using the abbreviated letters, *e.g.* POS. "POS" can include six TAG species: *Sn*-POS, *sn*-PSO, *sn*-OPS, *sn*-OSP, *sn*-SPO and *sn*-SOP, while "*sn*-POS" means the specific TAG species: *Sn*-1-palmitoyl-2-oleoyl-3- stearoylglycerol.

TAG profile of the samples

The TAG profiles of tested samples are presented in Table 7. Though variances among previous studies exist, the overall tendency of the profile of the present study is in agreement with these reports. [17,32] In reference to these studies, *sn*-OPO is the most abundant TAG species in the present-sample set of porcine fats. Its concentration is estimated to be approximately 22% (w/w) of the total TAG; *sn*-OPO accounts for more than 95% of POO in porcine fats [32] and the POO concentration of the present study is about 23%. This POO concentration (23%) has been derived by using its relative amount (77%, Dugo *et al.*, 2006) to POO+PLS (30.1% of the total TAG, Table 7). On the other hand, *sn*-POO/OOP is the major component in the bovine fats. Its concentration is estimated to be approximately 22% (w/w) of the total TAG; *sn*-POO/OOP accounts for ~86% of POO [32] that corresponds to 25.1% of POO+PLS in bovine fats. [17] The second major TAG in the bovine fats is *sn*-POS/SOP whose concentration is estimated to be ～7% (w/w) of the total TAG; *sn*-POS/SOP accounts for 61% [32] of POS (11.3% of the total TAG, Table 7).

Raman spectra of fat crystals

On cooling, melts of bovine- and porcine-fats begin to crystallize when the temperature becomes approximately 20℃. Both fats show granular morphologies composed of a large number of small crystals. It is difficult to identify polymorphic forms only by microscopic images because a polymorphic form could appear in different crystal sizes and different crystal shapes. [35]

Fig. 52 shows the optical image of bovine and porcine fats. They show polycrystalline morphology. By the use of an objective lens with a small numerical aperture (N.A. = 0.45), the size of focal point (11 μm in diameter with 60 μm in depth) is set enough larger than those of crystals. This helps in acquiring the Raman spectra of a polycrystal with more randomized arrangement.

The Raman spectra of bovine fat A and porcine fat A, which have moderate compositions within each fat group (Table 7), at different incubation temperatures are compared in Fig. 53a. Though these Raman spectra largely resemble one another, the porcine fat shows a shoulder at 1417 cm^{-1} (Fig. 53b), while the bovine fat does not exhibit this band at the incubation temperature of ≥ 0℃. This band is assigned to the CH_2-scissors mode characteristic of the orthorhombic perpendicular ($O_{\perp}$) subcell structure.

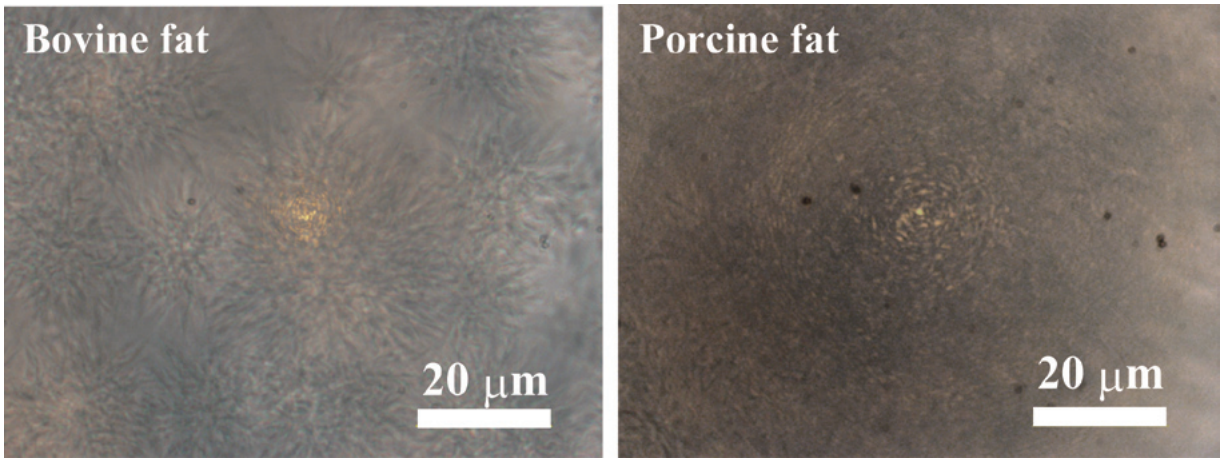

Fig.52. Crystals of bovine and porcine fats at 5℃

Table 7. TAG profiles of the samples. Unit: g/100-g total TAG.

		TAG molecule*							
		PPP	MOP	PPS	POP	PLP	PSS	POS	POO (OPO) +PLS
Bovine fat	A	2.0 ± 0.0†	4.2 ± 0.1	2.5 ± 0.0	9.4 ± 0.1	0.9 ± 0.1	1.6 ± 0.0	12.3 ± 0.0	25.9 ± 0.1
	B	3.6 ± 0.0	4.1 ± 0.0	2.4 ± 0.0	10.7 ± 0.0	1.1 ± 0.2	1.4 ± 0.0	10.1 ± 0.1	23.3 ± 0.1
	C	3.8 ± 0.0	4.4 ± 0.0	2.6 ± 0.0	11.6 ± 0.0	1.3 ± 0.2	1.5 ± 0.0	10.6 ± 0.0	25.1 ± 0.0
	D	6.1 ± 0.0	4.4 ± 0.0	2.8 ± 0.1	12.4 ± 0.2	1.2 ± 0.2	1.3 ± 0.0	10.2 ± 0.1	23.4 ± 0.1
	E	2.5 ± 0.0	4.5 ± 0.0	2.9 ± 0.0	9.8 ± 0.0	1.1 ± 0.1	2.2 ± 0.0	12.1 ± 0.0	25.2 ± 0.1
	F	2.1 ± 0.0	4.8 ± 0.1	2.6 ± 0.1	9.4 ± 0.1	1.1 ± 0.0	1.9 ± 0.0	11.3 ± 0.2	24.9 ± 0.4
	G	1.6 ± 0.0	3.7 ± 0.1	2.3 ± 0.0	8.8 ± 0.0	1.0 ± 0.2	1.7 ± 0.0	13.1 ± 0.2	26.8 ± 0.2
	Median	2.5	4.4	2.6	9.8	1.1	1.6	11.3	25.1
Porcine fat	A	0.7 ± 0.0	1.7 ± 0.1	2.1 ± 0.1	9.0 ± 0.1	1.2 ± 0.1	1.9 ± 0.0	20.3 ± 0.0	30.5 ± 0.0
	B	0.7 ± 0.0	1.8 ± 0.0	2.1 ± 0.0	9.2 ± 0.0	1.2 ± 0.2	1.9 ± 0.0	20.2 ± 0.0	30.6 ± 0.1
	C	0.5 ± 0.0	1.7 ± 0.1	1.6 ± 0.1	7.5 ± 0.1	1.8 ± 0.1	1.5 ± 0.0	18.6 ± 0.0	30.1 ± 0.1
	D	1.0 ± 0.0	2.2 ± 0.0	2.4 ± 0.0	8.9 ± 0.1	2.0 ± 0.2	2.2 ± 0.0	19.8 ± 0.1	29.0 ± 0.0
	E	1.0 ± 0.0	2.2 ± 0.0	2.4 ± 0.0	8.9 ± 0.1	1.8 ± 0.1	2.2 ± 0.0	19.5 ± 0.0	28.7 ± 0.2
	F	0.9 ± 0.0	2.1 ± 0.1	2.4 ± 0.0	9.1 ± 0.1	1.6 ± 0.1	2.1 ± 0.0	20.1 ± 0.1	29.3 ± 0.1
	G	0.9 ± 0.0	2.2 ± 0.0	2.4 ± 0.0	9.1 ± 0.1	2.0 ± 0.2	2.1 ± 0.0	19.6 ± 0.1	29.2 ± 0.1
	H	0.7 ± 0.0	1.9 ± 0.0	1.9 ± 0.0	8.4 ± 0.0	1.0 ± 0.2	1.6 ± 0.0	18.9 ± 0.1	30.9 ± 0.1
	I	0.8 ± 0.0	1.8 ± 0.0	2.3 ± 0.0	8.5 ± 0.0	1.3 ± 0.0	2.3 ± 0.0	19.9 ± 0.1	30.1 ± 0.1
	Median	0.8	1.9	2.3	8.9	1.6	2.1	19.8	30.1

continued

		TAG molecule*							
		PLO	SSS	SOS	SOO	OOO+SLS	SLO	SOA	AOO
Bovine fat	A	4.0 ± 0.1	1.0 ± 0.0	3.8 ± 0.1	8.3 ± 0.1	4.9 ± 0.3	1.0 ± 0.2	0.1 ± 0.0	–
	B	4.4 ± 0.1	0.8 ± 0.0	2.6 ± 0.1	6.0 ± 0.1	4.4 ± 0.2	0.9 ± 0.2	6.2 ± 0.1	0.1 ± 0.0
	C	4.7 ± 0.0	0.9 ± 0.0	2.8 ± 0.0	6.5 ± 0.0	4.5 ± 0.2	1.0 ± 0.1	0.1 ± 0.1	–
	D	4.5 ± 0.1	0.8 ± 0.0	2.6 ± 0.0	5.9 ± 0.0	4.7 ± 0.1	0.9 ± 0.1	–	–
	E	4.7 ± 0.1	1.2 ± 0.0	2.9 ± 0.0	6.6 ± 0.1	4.3 ± 0.0	1.2 ± 0.1	–	–
	F	4.4 ± 0.1	1.1 ± 0.0	3.2 ± 0.1	7.2 ± 0.1	4.5 ± 0.1	1.2 ± 0.0	–	–
	G	4.2 ± 0.0	1.0 ± 0.0	4.0 ± 0.1	8.8 ± 0.0	5.1 ± 0.0	1.0 ± 0.1	0.1 ± 0.0	–
	Median	4.4	1.0	2.9	6.6	4.7	1.0	0.1	–
Porcine fat	A	8.8 ± 0.0	0.5 ± 0.0	1.2 ± 0.0	3.7 ± 0.1	3.3 ± 0.0	1.9 ± 0.0	–	–
	B	8.9 ± 0.0	0.5 ± 0.0	1.2 ± 0.0	3.5 ± 0.0	3.3 ± 0.0	2.0 ± 0.1	–	–
	C	11.1 ± 0.1	0.5 ± 0.0	1.1 ± 0.0	3.5 ± 0.0	3.2 ± 0.0	2.2 ± 0.0	0.1 ± 0.0	–
	D	8.5 ± 0.1	0.5 ± 0.0	1.5 ± 0.1	4.1 ± 0.1	3.3 ± 0.0	1.9 ± 0.1	–	–
	E	8.3 ± 0.1	0.5 ± 0.0	1.6 ± 0.0	4.1 ± 0.0	3.6 ± 0.1	1.9 ± 0.0	–	–
	F	8.5 ± 0.1	0.4 ± 0.1	1.4 ± 0.0	3.9 ± 0.1	3.4 ± 0.2	1.9 ± 0.1	–	–
	G	8.3 ± 0.1	0.5 ± 0.0	1.4 ± 0.0	3.7 ± 0.1	3.5 ± 0.0	1.9 ± 0.2	–	0.1 ± 0.0
	H	8.8 ± 0.1	0.5 ± 0.1	1.5 ± 0.0	4.4 ± 0.0	3.9 ± 0.1	2.2 ± 0.0	–	–
	I	8.9 ± 0.1	0.5 ± 0.0	1.5 ± 0.0	4.1 ± 0.0	3.5 ± 0.0	2.2 ± 0.1	–	–
	Median	8.8	0.5	1.4	3.9	3.4	1.9	–	–

* TAGs shown are the identifiable major species present
† Values represent the mean value of two replicates with standard deviation

[39] In terms of TAG, it is the β'-polymorph that has the $O_{\perp}$ subcell structure to give rise to this band. [82] It is therefore shown that the porcine fat contains the β'-polymorph under the present experimental conditions. It is widely known that porcine fats tend to be crystallized in β-form. [20,115] Due to the highly-biased distribution of palmitic acyl at *sn*-2 position in porcine fats, they are easy to pack and reorder to the most orderly and stable polymorphic form, β. The metastable β'-polymorph formation in the present study is most likely to be caused by the rapid cooling rate and short incubation time. Campos and co-workers also reported that a rapid cooling induced β' in a porcine fat. [7] Nucleation and growth of the metastable form normally predominate in fat crystallization and reformation to the

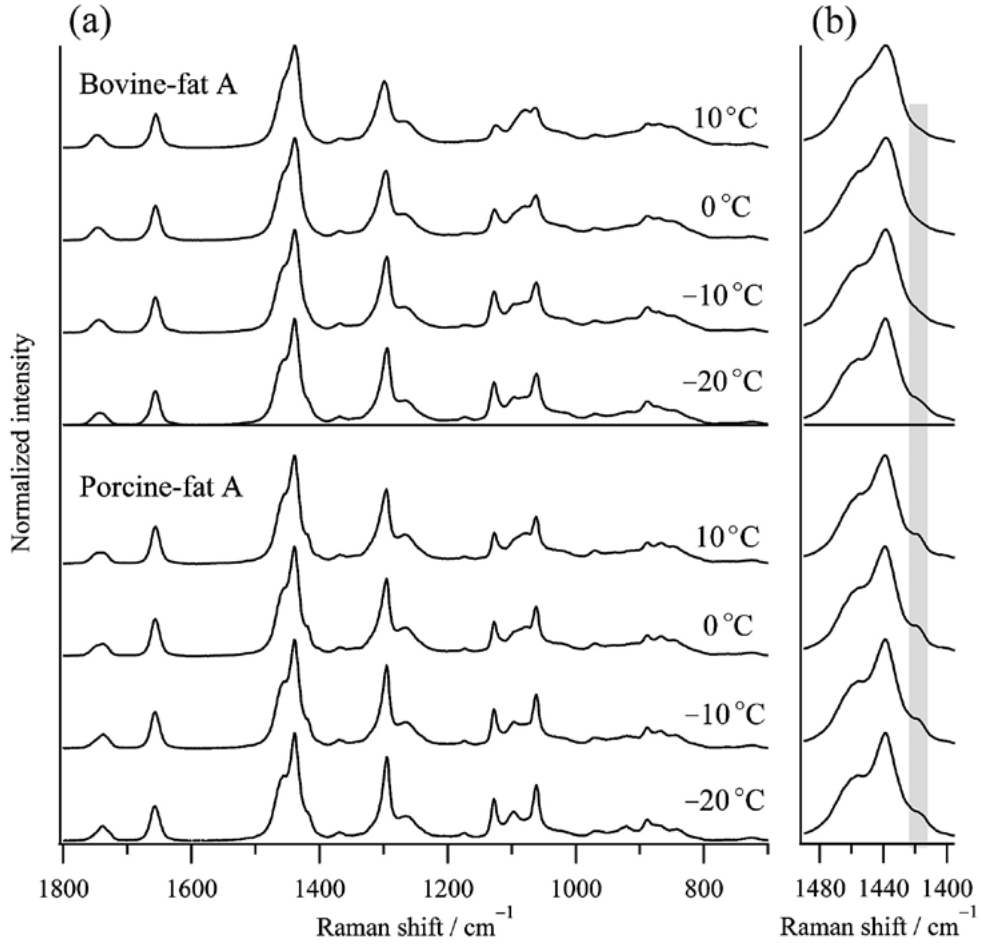

Fig.53. Raman spectra of bovine- and porcine-fats at each incubation temperature. (a) Spectra of bovine-fat A and porcine-fat A. These two fats have the medium TAG composition within each animal-fat group (see Table 2). (b) Enlarged spectra of the CH_2-scissors region corresponding to each left-hand-side spectrum. Shaded region indicates the position ～1417 cm^{-1}. [67]

most stable polymorph is the kinetic process that takes time. The reformation seems to be uncompleted within the 5-min incubation period in the present study.

In the bovine fat, cooling to −20℃ produces the β'-polymorph (Fig. 53b). This observation is in accordance with the previous study that has reported the rapid cooling to −25℃ produces the β'-polymorph in bovine fat. [79] On the contrary the incubation temperatures of 10, 0 and −10℃ induce small amount of β'-polymorph formation even though the melting point of β'-polymorph in bovine fats is higher than these temperatures. [79] It might be because the cooling to above −20℃ provided insufficient supercooling for the bovine fat to crystallize in the β' form. For TAG crystallization, it is known that melts should be cooled well below the melting point because of the free energy penalty associated with crystal formation. [59] More stable polymorphs have higher free energy penalty and therefore they need more supercooling to crystallize. The incubation temperatures above −20℃ are likely to form less stable α-polymorph in the bovine fat and this is confirmed by the Raman spectra.

This difference in crystallization is due to the difference in $\Delta G^{\dagger\dagger}$ (see Chapter 2, page 27). The values of $\Delta G^{\dagger\dagger}$ for bovine and porcine fats are almost impossible to measure because these fats do not express distinctive melting points. They melt over a wide range of temperature rather than at a distinctive temperature as would be the case for pure TAGs. However, the melting points (T_m) of SatOSat and OSatO TAGs have been studied in details (Fig. 54). [14] OSatO type TAGs, which are the major components in porcine fats, have relatively low melting temperature than SatOSat. It means that

OSatO has higher Gibbs free energy, therefore, $\Delta G^{\dagger\dagger}$ is smaller in OSatO. The difference in free energy is likely to be the reason for the formation of more stable polymorph (β') in porcine fats (Fig. 55).

The differences, other than the 1417 cm^{-1} band between the spectra of the bovine fat and those of the porcine fat, are not sensitive to the polymorphic difference. Relatively large differences are observed in the C−C stretch- (1140−1040 cm^{-1}) and the C=O stretch-region (1770−1720 cm^{-1}). The intensities of these conformation-sensitive bands have been employed as a measure of conformational order of TAG. [5,128] However, the significant amount of liquid TAG (*i. e.* TAG in random form) within the sample masks the band features due to the crystal polymorphs. At the temperature range of the present experiment, bovine fats and porcine fats are in the form of crystalline suspensions in liquid-form TAG.

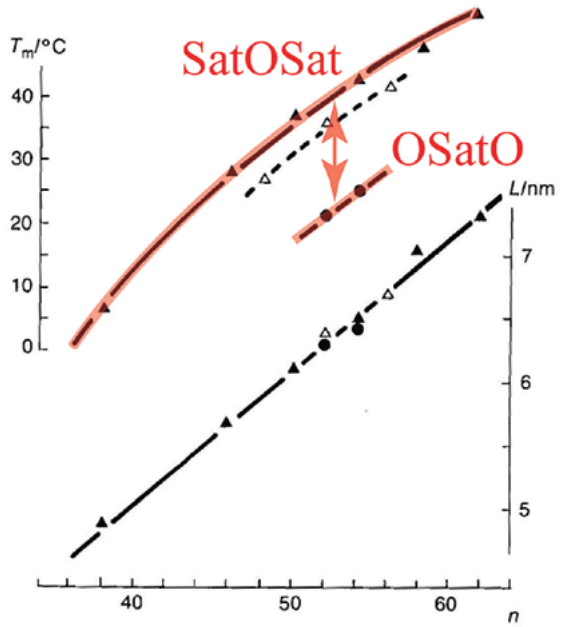

Fig.54. Difference in melting point (T_m) of β-polymorphs of SatOSat and OSatO type TAGs. n: the number of acyl chain carbon atoms. ▲, SatOSat; ●, OSatO; △, SatO(Sat+2). [14]

The 1417 cm^{-1}-band intensities ($A_{1417\,cm^{-1}}$) of both fats are acquired by band fitting (Fig. 56a) and their dependence on incubation temperatures is shown (Fig. 56b). The difference in $A_{1417\,cm^{-1}}$ between the porcine and bovine fats is most remarkable when the incubation temperature is −10～0℃.

Fig. 57a shows the Raman spectra of the seven bovine fats and the nine porcine fats measured at the incubation temperature of 0℃. The 1417 cm^{-1} band is easily detected in all porcine fats, while it is very weak in bovine fats. The $A_{1417\,cm^{-1}}$ value of each sample is acquired by the band fitting and plotted for each fat group in Fig. 57b. The variances of the $A_{1417\,cm^{-1}}$ values of these two groups are unequal; therefore, Welch's *t*-test is conducted to find whether the averages are significantly different. The average $A_{1417\,cm^{-1}}$ value of porcine fats is statistically higher than that of bovine fats at a significance level of $P<0.0001$ (Fig. 57b). It is therefore shown that this Raman band discriminates the origins of the present sample sets. The difference in polymorphic features enables Raman spectroscopy to distinguish these two fats by a single band.

In the next step, the crystallization behaviors of

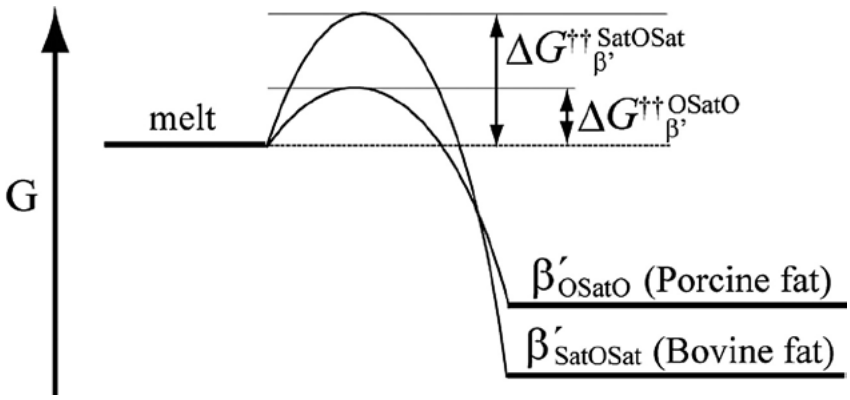

Fig.55. Schematic diagram for the $\Delta G^{\dagger\dagger}$ of β'-polymorph of SatOSat and OSatO TAGs

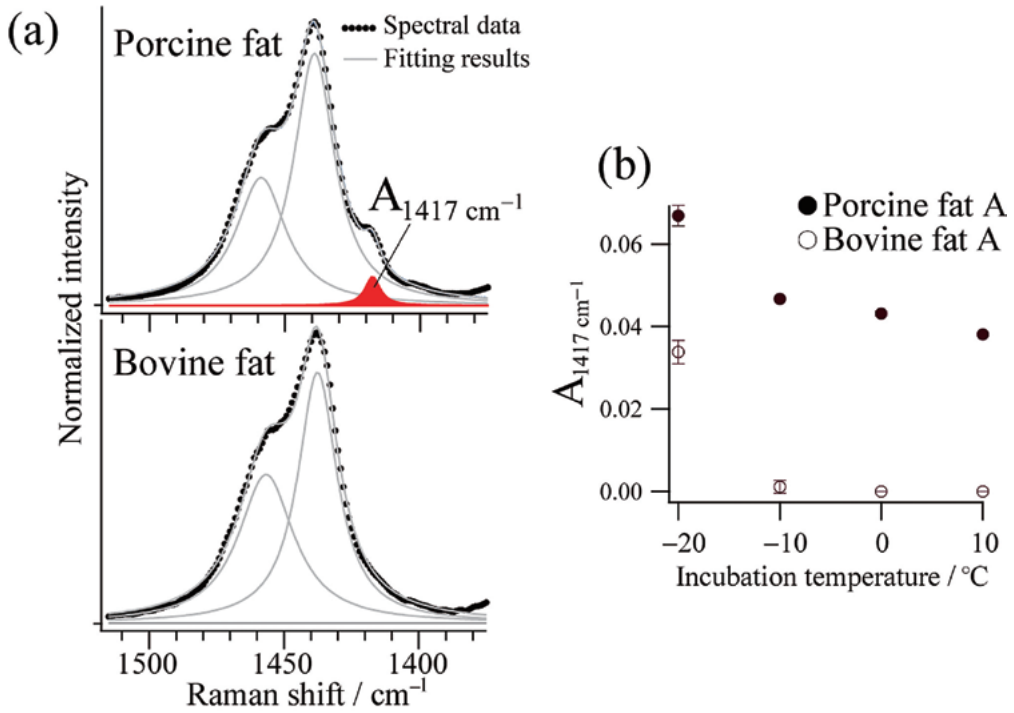

Fig.56. The 1417 cm^{-1}-band intensities ($A_{1417\ cm^{-1}}$) of both fats. (a) Intensities are acquired by Lorentzian-band fitting. (b) Relation between $A_{1417\ cm^{-1}}$ and incubation temperatures. [67)]

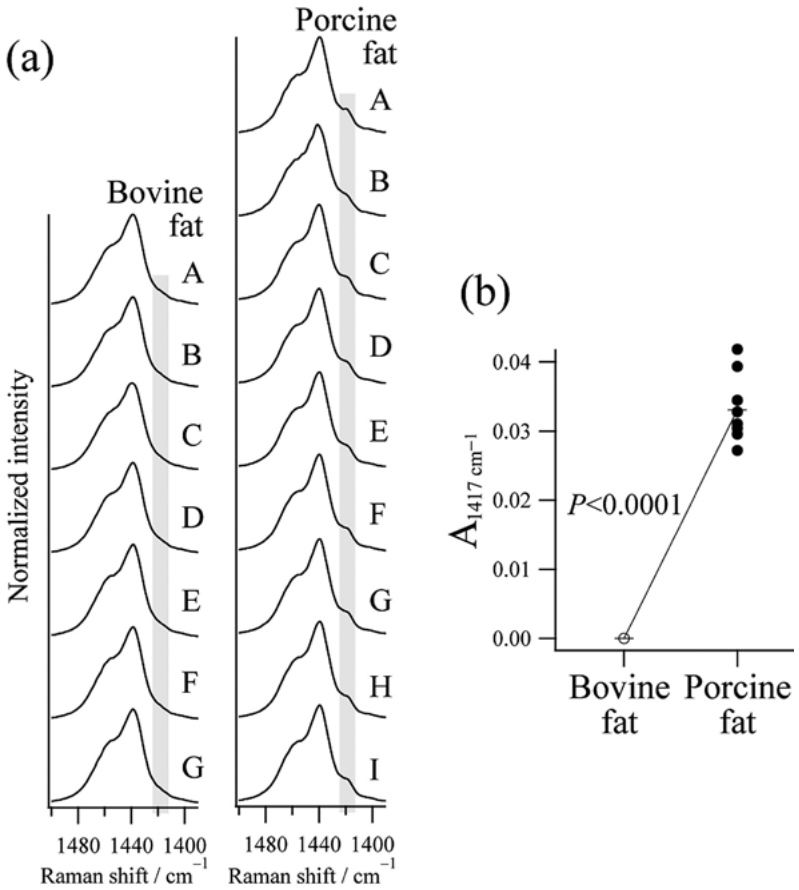

Fig.57. Raman spectra of the CH_2-scissors region of all samples after rapid cooling down to and incubation at 0℃ (a). The 1417 cm^{-1}-band intensity ($A_{1417\ cm^{-1}}$) of each sample is plotted for each fat group (b). The average $A_{1417\ cm^{-1}}$ value of each fat group (indicated by ―) is also plotted. The porcine fats have statistically higher $A_{1417\ cm^{-1}}$ values than the bovine fats at a significance level of P<0.0001. [67)]

bovine-porcine-mixture fats are investigated. Bovine-fat A and porcine-fat A were thoroughly melted and mixed using a vortex mixer to prepare the mixture fats with different porcine-fat concentrations. The 1417 cm^{-1} band intensities measured for 15-different-mixing ratios are plotted in Fig. 58. When porcine fat concentrations are below 50%, the band intensities at 1417 cm^{-1} are too small to be detected. It is indicated that the β'-polymorph scarcely exists even in the presence of porcine fat upto 50%. The approximated-straight line of the band intensity ratio does not intersect the point of origin (solid line in Fig. 58). Considering the fact that the porcine fat contains a large amount of β' forming TAGs (*i. e.* OSatO), this line should intersect the point of origin (dashed line in Fig. 58). The addition of the bovine fat markedly disturbs the β'-polymorph formation of these TAGs.

The "molecular compound" formation is the most likely reason why the addition of the bovine fat disturbs the β' formation in the porcine fat (Fig. 59). The porcine fat TAGs (OSatO) are likely to produce "molecular compounds" with the TAGs in added bovine fats (SatOSat). The OSatO/SatOSat-type molecular compound forms α and β polymorphs but does not form β'. [48,63] "Molecular compounds" are likely to be formed also in multicomponent systems.

Conclusion

It has been shown that bovine and porcine fats have different crystallization properties. In the present experimental condition, porcine fats contain β'-polymorph, on the other hand, bovine fats contain α but not β'-polymorph. It is due to their TAG compositional differences: OSatO-type TAG, the major TAG in porcine fats, has smaller $\Delta G^{\dagger\dagger}$ than SatOSat-type, the major TAG in bovine fats. This difference in crystallization properties is reflected in their Raman spectra. Porcine fats exhibit the band at 1417 cm^{-1} which is derived from the $O_{\perp}$ subcell structure of β'-polymorph.

Using above described difference, Raman spectroscopy can differentiate bovine fats and porcine fats by the single band at 1417 cm^{-1}. In bovine-porcine fat mixture, however, this band is not detected even in the presence of porcine fat upto 50%; an addition of bovine fat to porcine fat is likely to produce SatOSat-OSatO type molecular compound in the mixture, and they do not form polymorph.

Food safety requires the development of reliable techniques that ensure the origin of animal fats. In 2007, a food processing company added porcine fats to its bovine products, such as minced beef, for getting unfair profit. [50] The detection sensitivity of the present method will be higher in bovine-porcine adipose tissue mixture than in extracted fat mixture; because the porcine fat tends to exist within cells and avoid complete mixing with the bovine fat. Also, Raman spectroscopy is not too sensitive to water which is contained in biological tissues. This is the advantage of this method. The possibility of application of this Raman spectroscopic method to adipose tissues will be investigated.

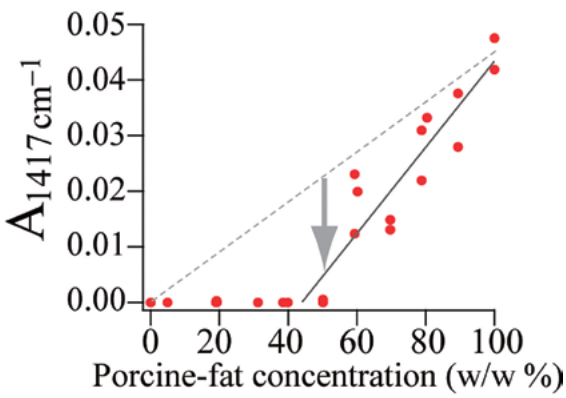

Fig.58. Relation between $A_{1417\ cm^{-1}}$ and porcine-fat concentration. The dashed line is the approximated-straight line fitted with the data of 60–100% porcine-fat concentrations. The arrow indicates the hindrance of β'-polymorph formation by mixing the fats.

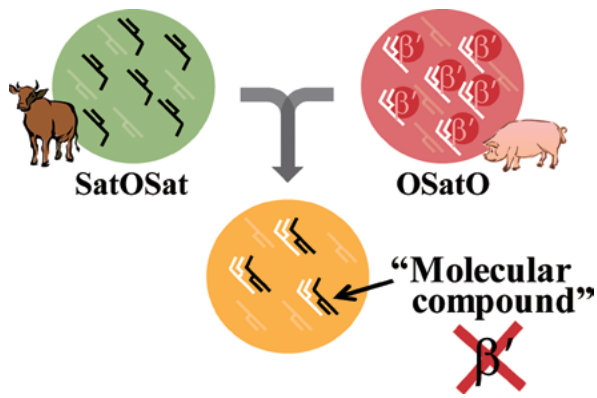

Fig.59. Description for the reduction in β'-polymorph in the mixture fats

The thermal history is the key factor that makes this method feasible. If an appropriate incubation temperature is found, other fats can also be discriminated by their polymorphic features. This new idea of using polymorphic features to discriminate the fat origin will contribute to refine the existing spectroscopic methods. IR spectroscopy can also employ this idea: IR absorption bands of the CH_2-rock and CH_2-scissors modes also show distinctive bands derived from orthorhombic-subcell structure of the β'-polymorph. [39] Raman spectroscopy which is sensitive to fats crystal structure has high potential as the powerful tool for the quality control of fats.

Chapter 6
Conclusion

With a view to understand the complicated phase behavior of natural fats, I have investigated on the physical mixtures of TAGs by Raman spectroscopy. The results indicate that a third component, the molecular compound, is formed in a model binary TAG system and its structure seems to be influenced decisively by crystallizing procedures. The molecular compound may be the phase dynamically formed by crystallization rather than existing stationary in the liquid phase as previously considered. In addition, the present study implies that the molecular compound may exist not only in a model binary system but also in multicomponent systems. It is also shown that one can differentiate the origin of natural fats by detecting the difference in their polymorphic phases by using Raman spectroscopy.

For a deeper understanding on TAG structures and phase behaviors, Raman spectroscopy is a promising method which can contribute to solutions of the remaining issues described below:

1. Structures formed during initial stages of TAG crystallization.

It has been suggested that the structure of the polymorph that appears first on crystallization works decisively to influence the overall phase behavior. Revealing the mechanism of formation of this first-appearing polymorph is important from the application point-of-view, since it has a potential to program TAG phase behavior for producing better industrial products. The polymorph which appears first on crystallization is an unstable phase; therefore, the fast methods which can trace the phase transition are required. Raman spectroscopy has already fulfilled this requirement. Most recently, Raman spectrum of low-frequency region that is sensitive to crystal structures can be obtained less than one second. [73] It is, thus, fast enough to trace the TAG phase transition.

2. Conformation of glycerol moieties

Glycerols are the backbone of TAGs and also of other lipids, and influence the overall structure of these molecules. It has been suggested that the glycerol moieties adopt specific configurations in each TAG polymorphs. However, there is little information on the conformation of the glycerol moieties. It is not only due to the lack of precise structural data from single-crystal XRD but probably also due to the lack of the information of the vibrational spectrum of glycerol moieties. Raman spectroscopy can provide the fundamental information on this backbone structure.

3. Characteristics of TAGs in a living system

TAGs are the form of energy storage of a living system. Therefore, their characteristics such as content, unsaturation degree, acyl chain length and turnover speed should reflect the condition of a cell. Since Raman spectroscopy can measure such quantities of TAGs *in situ*, it has a potential to dynamically monitor the condition of a living cell based on its lipid profile.

On the basis of the accumulated spectroscopic data, Raman spectroscopy has contributed to reveal the structure and the phase behavior of TAG model systems. The three Raman spectroscopic studies described above will provide the new insights of TAG systems. Recent developments on the spectrometer enable to acquire the spectra with high sensitivity. They offer bright future prospects for the Raman spectroscopic studies on multicomponent TAG systems. Raman spectroscopy helps us to draw the whole picture of the phase behavior of natural fats.

References

1) Akita, C., Kawaguchi, T. and Kaneko, F. (2006). Structural study on polymorphism of *cis*-unsaturated triacylglycerol: Triolein, Journal of Physical Chemistry B, 110(9), 4346-4353.
2) Bicknell-Brown, E., Brown, K.G. and Person, W.B. (1980). Configuration-dependent Raman bands of phospholipid surfaces. 1. Carbonyl stretching modes at the bilayer interface, Journal of the American Chemical Society, 102(17), 5486-5491.
3) Bicknell-Brown, E., Brown, K.G. and Person, W.B. (1981). Configuration-dependent Raman bands of phospholipid surfaces. 2. Head group and acyl stretching modes in the 800 − 900 cm^{-1} region, Journal of Raman Spectroscopy, 11(5), 356-362.
4) Bresson, S., El Marssi, A. and Khelifa, B. (2005). Raman spectroscopy investigation of various saturated monoacid triglycerides, Chemistry and Physics of Lipids, 134(2), 119-129.
5) Bresson, S., El Marssi, M. and Khelifa, B. (2006). Conformational influences of the polymorphic forms on the C = O and C − H stretching modes of five saturated monoacid triglycerides studied by Raman spectroscopy at various temperatures, Vibrational Spectroscopy, 40(2), 263-269.
6) Buchgraber, M., Ullberth, F., Emons, H. and Anklam, E. (2004). Triacylglycerol profiling by using chromatographic techniques, European Journal of Lipid Science and Technology, 106(9), 621-648.
7) Campos, R., Narine, S.S. and Marangoni, A.G. (2002). Effect of cooling rate on the structure and mechanical properties of milk fat and lard, Food Research International, 35(10), 971-981.
8) Cates, D.A., Strauss, H.L. and Snyder, R.G. (1994). Vibrational modes of liquid *n*-alkanes: Simulated isotropic Raman spectra and band progressions for C_5H_{12}-$C_{20}H_{42}$ and $C_{16}D_{34}$, Journal of Physical Chemistry, 98(16), 4482-4488.
9) Chan, J.W., Motton, D., Rutledge, J.C., Keim, N.L. and Huser, T. (2005). Raman spectroscopic analysis of biochemical changes in individual triglyceride-rich lipoproteins in the pre- and postprandial state, Analytical Chemistry, 77(18), 5870-5876.
10) Christie, W.W. and Moore, J.H. (1970). A comparison of structures of triglycerides from various pig tissues, Biochimica et Biophysica Acta-Lipids and Lipid Metabolism, 210(1), 46-56.
11) Christie, W.W., Nikolovadamyanova, B., Laakso, P. and Herslof, B. (1991). Stereospecific analysis of triacyl-*sn*-glycerols via resolution of diastereometric diacylglycerol derivatives by high performance liquid chromatography on silica. Journal of the American Oil Chemists' Society, 68(10), 695-701.
12) Da Silva, E., Bresson, S. and Rousseau, D. (2009). Characterization of the three major polymorphic forms and liquid state of tristearin by Raman spectroscopy, Chemistry and Physics of Lipids, 157(2), 113-119.
13) Da Silva, E. and Rousseau, D. (2008). Molecular order and thermodynamics of the solid-liquid transition in triglycerides *via* Raman spectroscopy, Physical Chemistry Chemical Physics, 10(31), 4606-4613.
14) De Jong, S., Van Soest, T.C. and Van Schaick, M.A. (1991). Crystal structures and melting points of unsaturated triacylglycerols in the β phase, Journal of the American Oil Chemists' Society, 68(6), 371-378.
15) De Jong, S.D. and Van Soest, T.C. (1978). Crystal structures and melting points of saturated triglycerides in the β-2 phase, Acta Crystallographica Section B-Structural Science, 34, 1570-1583.
16) Dohi, K., Kaneko, F. and Kawaguchi, T. (2002). X-ray and vibrational spectroscopic study on polymorphism of trielaidin, Journal of Crystal Growth, 237, 2227-2232.
17) Dugo, P., Kumm, T., Fazio, A., Dugo, G. and Mondello, L. (2006). Determination of beef tallow in lard through a multidimensional off-line non-aqueous reversed phase-argentation LC method coupled to mass spectrometry, Journal of Separation Science, 29(4), 567-575.
18) Engstrom, L. (1992). Triglyceride systems forming molecular-compounds, Fett Wissenschaft Technologie-Fat Science Technology, 94(5), 173-181.
19) Ferguson, R.H. and Lutton, E.S. (1947). The

polymorphism of triolein, Journal of the American Chemical Society, 69(6), 1445-1448.

20) Foubert, I., Dewettinck, D., Van de Walle, D., Dijkstra, A.J. and Quinn, P.J. (2007). Section 7, Physical properties: Structural and physical characteristics, In The Lipid Handbook with CD-ROM (Gunstone, F.D., Harwood, J.L. and Dijkstra, A.J., eds.), 3rd edition, 471-534, CRC Press, Boca Raton.

21) Garti, N. and Sato, K., eds. (1988). Crystallization and polymorphism of fats and fatty acids, Surfactant science series, Vol. 31, 450p, Marcell Dekker Inc., New York.

22) Goto, M., Kodali, D.R., Small, D.M., Honda, K., Kozawa, K. and Uchida, T. (1992). Single crystal structure of a mixed-chain triacylglycerol: 1,2-dipalmitoyl-3-acetyl-*sn*-glycerol. Proceedings of the National Academy of Sciences of the United States of America, 89(17), 8083-8086.

23) Gunstone, F.D. and Padley, F.B., eds. (1997). Lipid Technologies and Applications, 834p, Marcel Dekker. Inc., New York.

24) Hagemann, J.W. (1988). Thermal behavior and polymorphism of acylglycerides, In Crystallization and polymorphism of fats and fatty acids (Garti N and Sato, K., eds.), 9-95, Marcel Dekker Inc., New York.

25) Hagemann, J.W. and Rothfus, J.A. (1992). Computer modeling of packing arrangements and transitions in saturated-*cis*-unsaturated mixed triglycerides, Journal of the American Oil Chemists' Society, 69(5), 429-437.

26) Hernqvist, L. (1984). On the structure of triglycerides in the liquid-state and fat crystallization, Fette Seifen Anstrichmittel, 86(8), 297-300.

27) Hernqvist, L. and Larsson, K. (1982). On the crystal-structure of the β'-form of triglycerides and structural-changes at the phase-transitions LIQ.→α →β'←β, Fette Seifen Anstrichmittel, 84(9), 349-354.

28) Hoerr, C.W. (1964). X-ray diffraction of fats. Journal of the American Oil Chemists' Society, 41(7), 4.

29) Ishimoto, S. (1996). Shuyou taisha keirozu, in Seibutsugaku jiten (Yasugi, R., Ozeki, H., Furuya, M. and Hidaka, T., eds.), 4th edition, Iwanami shoten, Tokyo, 1620.

30) Jensen, L.H. and Mabis, A.J. (1963). Crystal structure of β-tricaprin, Nature, 197(486), 681-682.

31) Jensen, L.H. and Mabis, A.J. (1966). Refinement of structure of β-tricaplin, Acta Crystallographica, 21, 770-781.

32) Kallio, H., Yli-Jokipii, K., Kurvinen, J.P., Sjovall, O. and Tahvonen, R. (2001). Regioisomerism of triacylglycerols in lard, tallow, yolk, chicken skin, palm oil, palm olein, palm stearin, and a transesterified blend of palm stearin and coconut oil analyzed by tandem mass spectrometry, Journal of Agricultural and Food Chemistry, 49(7), 3363-3369.

33) Kaneko, F., Yano, J. and Sato, K. (1998). Diversity in the fatty-acid conformation and chain packing of *cis*-unsaturated lipids, Current Opinion in Structural Biology, 8(4), 417-425.

34) Kellens, M., Meeussen, W. and Reynaers, H. (1990). Crystallization and phase-transition studies of tripalmitin, Chemistry and Physics of Lipids, 55(2), 163-178.

35) Kellens, M., Meeussen, W. and Reynaers, H. (1992). Study of the polymorphism and the crystallization kinetics of tripalmitin - A microscopic approach, Journal of the American Oil Chemists' Society, 69(9), 906-911.

36) Kellens, M., Meeussen, W., Riekel, C. and Reynaers, H. (1990). Time resolved X-ray diffraction studies of the polymorphic behavior of tripalmitin using synchrotron radiation, Chemistry and Physics of Lipids, 52(2), 79-98.

37) Kim, Y.S., Strauss, H.L. and Snyder, R.G. (1989). Conformational disorder in the binary mixture $n\text{-}C_{50}H_{102}/n\text{-}C_{46}H_{94}$: A vibrational spectroscopic study, Journal of Physical Chemistry, 93(1), 485-490.

38) Kobayashi, M. (1988). Vibrational spectroscopic aspects of polymorphism and phase transition of fats and fatty acids, In Crystallization and polymorphism of fats and fatty acids (Garti, N. and Sato, K., eds.), 139-187, Marcel Dekker Inc., New York.

39) Kobayashi, M. and Kaneko, F. (1989). Molecular and crystal-structures of lipids and related-compounds, Journal of Dispersion Science and Technology, 10(4-5), 319-350.

40) Kobayashi, M., Kaneko, F., Sato, K. and Suzuki, M. (1986). Vibrational spectroscopic study on polymorphism and order-disorder phase-transition in oleic-acid, Journal of Physical Chemistry, 90(23), 6371-6378.

41) Kobayashi, M., Kobayashi, T., Itoh, Y. and Sato, K. (1984). Polytypism in normal-fatty acids and low-frequency Raman-spectra: stearic-acid *B*-form, Journal of Chemical Physics, 80(6), 2897-2903.

42) Kobayashi, M., Sakagami, K. and Tadokoro, H. (1983). Effects of interlamellar forces on longitudinal acoustic modes of *n*-alkanes, Journal of Chemical Physics, 78(11), 6391-6398.

43) Kobayashi, M., Uesaka, T. and Tadokoro, H. (1976). Polarized Raman-spectra of single-crystal *n*-$C_{36}H_{74}$, Chemical Physics Letters, 37(3), 577-581.

44) Kodali, D.R., Atkinson, D., Redgrave, T.G. and Small, D.M. (1987). Structure and polymorphism of carbon-18 fatty acyl triacylglycerols — Effect of unsaturation and substitution in the 2-position, Journal of Lipid Research, 28(4), 403-413.

45) Kodali, D.R., Atkinson, D. and Small, D.M. (1989). Molecular packing of 1,2-dipalmitoyl-3-decanoyl-*sn*-glycerol (PP10): Bilayer, trilayer, and hexalayer structures, Journal of Physical Chemistry, 93(11), 4683-4691.

46) Kodali, D.R., Atkinson, D. and Small, D.M. (1990). Polymorphic behavior of 1,2-dipalmitoyl-3-lauroyl(PP12)- and 3-myristoyl(PP14)-*sn*-glycerols, Journal of Lipid Research, 31(10), 1853-1864.

47) Koyama, Y. and Ikeda, K.I. (1980). Raman-spectra and conformations of the *cis*-unsaturated fatty-acid chains, Chemistry and Physics of Lipids, 26(2), 149-172.

48) Koyano, T., Hachiya, I. and Sato, K. (1992). Phase-behavior of mixed systems of SOS and OSO, Journal of Physical Chemistry, 96(25), 10514-10520.

49) Krimm, S., Liang, C.Y. and Sutherland, G. (1956). Infrared spectra of high polymers. 2. Polyethylene, Journal of Chemical Physics, 25(3), 549-562.

50) Kyodo news (2007), Meat Hope chief admits pork was disguised as ground beef, The Japan Times, June 21, p. 2.

51) Larsson, K. (1965). The crystal structure of β-form of trilaurin. Arkiv fur Kemi, 23(1), 1-15.

52) Larsson, K. (1966). Alternation of melting points in homologous series of long-chain compounds. Journal of the American Oil Chemists' Society, 43(10), 559-562.

53) Larsson, K. (1966). Classification of glyceride crystal forms, Acta Chemica Scandinavica, 20(8), 2255-2260.

54) Larsson, K. (1973). Conformation-dependent features in Raman-spectra of simple lipids, Chemistry and Physics of Lipids, 10(2), 165-176.

55) Larsson, K. and Rand, R.P. (1973). Detection of changes in environment of hydrocarbon chains by Raman-spectroscopy and its application to lipid-protein systems. Biochimica et Biophysica Acta-Lipids and Lipid Metabolism, 326(2), 245-255.

56) Lippert, J.L. and Peticola,W.L. (1972). Raman active vibrations in long-chain fatty-acids and phospholipid sonicates, Biochimica et Biophysica Acta -Biomembranes, 282, 8-17.

57) Malkin, T. (1954). The polymorphism of glycerides, Progress in the Chemistry of Fats and other Lipids, 2, 2-14.

58) Maroncelli, M., Strauss, H.L. and Snyder, R.G. (1985). On the CD_2 probe infrared method for determining polymethylene chain conformation, Journal of Physical Chemistry, 89(20), 4390-4395.

59) McClements, D.J. and Decker, E.A. (2007). Lipids, In Fennema's food chemistry (Damodaran, S., Parkin, K.L. and Fennema, O.R., eds.), 4th edition, 155-216, CRC press, Boca Raton.

60) Mendelsohn, R. and Davies, M.A. (1991). CD_2 rocking modes as quantitative fourier-transform infrared spectroscopic probes of conformatinal disorder in phospholipid bilayers, In Fourier Transform Infrared Spectroscopy in Colloid and Interface Science (Scheuing, D.R., ed.), 24-43, American Chemical Society.

61) Mendelsohn, R., Davies, M.A., Schuster, H.F., Xu, Z.C. and Bittman, R. (1991). CD_2 rocking modes as quantitative infrared probes of one-, two-, and three-bond conformational disorder in dipalmitoylphosphatidylcholine and dipalmitoylphosphatidylcholine / cholesterol mixtures, Biochemistry, 30(35), 8558-8563.

62) Minato, A., Ueno, S., Smith, K., Amemiya, Y. and Sato, K. (1997). Thermodynamic and kinetic study on phase behavior of binary mixtures of POP and PPO forming molecular compound systems, Journal of Physical Chemistry B, 101(18), 3498-3505.

63) Minato, A., Ueno, S., Yano, J., Smith, K., Seto, H., Amemiya, Y. and Sato, K. (1997). Thermal and structural properties of *sn*-1,3-dipalmitoyl-2-oleoylglycerol and *sn*-1,3-dioleoyl-2-palmitoylglycerol binary mixtures examined with synchrotron radiation X-ray diffraction, Journal of the American Oil Chemists' Society, 74(10), 1213-1220.

64) Minato, A., Yano, J., Ueno, S., Smith, K. and Sato, K. (1997). FT-IR study on microscopic structures and conformations of POP-PPO and POP-OPO molecular compounds, Chemistry and Physics of Lipids, 88(1), 63-71.

65) Mizushima, S.I. and Simanouti, T. (1949). Raman frequencies of *n*-paraffin molecules. Journal of the American Chemical Society, 71(4), 1320-1324.

66) Moran, D.P.J. (1963). Phase behaviour of some palmito-oleo triglyceride systems, Journal of Applied Chemistry, 13(2), 91-100.

67) Motoyama, M., Ando, M., Sasaki, K. and Hamaguchi, H. (2010). Differentiation of animal fats from different origins: Use of polymorphic features detected by Raman spectroscopy, Applied Spectroscopy, 64(11), 1244-1250.

68) Muik, B., Lendl, B., Molina-Diaz, A. and Ayora-Canada, M.J. (2005). Direct monitoring of lipid oxidation in edible oils by Fourier transform Raman spectroscopy, Chemistry and Physics of Lipids, 134(2), 173-182.

69) Mushayakarara, E. and Levin, I.W. (1982). Determination of acyl chain conformation at the lipid interface region: Raman spectroscopic study of the carbonyl stretching mode region of dipalmitoyl phosphatidylcholine and structurally related molecules, Journal of Physical Chemistry, 86(13), 2324-2327.

70) Mykhaylyk, O.O. and Martin, C.M. (2009). Effect of unsaturated acyl chains on structural transformations in triacylglycerols, European Journal of Lipid Science and Technology, 111(3), 227-235.

71) Mykhaylyk, O.O., Smith, K.W., Martin, C.M. and Ryan, A.J. (2007). Structural models of metastable phases occurring during the crystallization process of saturated/unsaturated triacylglycerols, Journal of Applied Crystallography, 40, S297-S302.

72) Oakes, R.E., Beattie, J.R., Moss, B.W. and Bell, S.E.J. (2003). DFT studies of long-chain FAMEs: theoretical justification for determining chain length and unsaturation from experimental Raman spectra, Journal of Molecular Structure: Theochem, 626, 27-45.

73) Okajima, H. and Hamaguchi, H. (2009). Fast low frequency (down to 10 cm^{-1}) multichannel Raman spectroscopy using an iodine vapor filter, Applied Spectroscopy, 63(8), 958-960.

74) Packter, N.M. and Olukoshi, E.R. (1995). Ultrastructural studies of neutral lipid localisation in Streptomyces, Archives of Microbiology, 164(6), 420-427.

75) Peschar, R., Pop, M.M., De Ridder, D.J.A., Van Mechelen, J.B., Driessen, R.A.J. and Schenk, H. (2004). Crystal structures of 1,3-distearoyl-2-oleoylglycerol and cocoa butter in the β(V) phase reveal the driving force behind the occurrence of fat bloom on chocolate, Journal of Physical Chemistry B, 108(40), 15450-15453.

76) Pink, D.A., Green, T.J. and Chapman, D. (1980). Raman-scattering in bilayers of saturated phosphatidyl cholines — experiment and theory, Biochemistry, 19(2), 349-356.

77) Pink D.A., Hanna C.B., Sandt, C., MacDonald, A.J., MacEachern, R., Corkery, R. and Rousseau, D. (2010). Modeling the solid-liquid phase transition in saturated triglycerides, Journal of Chemical Physics, 132(5), 054502.

78) Resouces Council, Science and Technology Agency, Japan (1989). Standard tables of food composition in Japan: Fatty acids, cholesterol and vitamin E (tocopherols), Resources Council, Science and Technology Agency, Japan, Tokyo, 208p.

79) Riiner, Ü. (1970). Investigation of the polymorphism of fats and oils by temperature programmed X-ray diffraction. Lebensmittel-Wissenschaft und

Technologie -Food Science and Technology, 3, 101-106.

80) Sato, K. (1999). Solidification and phase transformation behaviour of food fats - a review. Fett/Lipid, 101(12), 467-474.

81) Sato, K. (2001). Crystallization behaviour of fats and lipids - a review. Chemical Engineering Science, 56(7), 2255-2265.

82) Sato, K., Arishima, T., Wang, Z.H., Ojima, K., Sagi, N. and Mori, H. (1989). Polymorphism of POP and SOS. 1. Occurrence and polymorphic transformation, Journal of the American Oil Chemists' Society, 66(5), 664-674.

83) Sato, K. and Kobayashi, M. (1992). Sisitsu no kouzou to dainamikkusu, Kyouritsu shuppan, Tokyo, 179p.

84) Sato, K. and Kuroda, T. (1987). Kinetics of melt crystallization and transformation of tripalmitin polymorphs, Journal of the American Oil Chemists' Society, 64(1), 124-127.

85) Sato, K., Yano, J., Kawada, I., Kawano, M., Kaneko, F. and Suzuki, M. (1997). Polymorphic behavior of gondoic acid and phase behavior of its binary mixtures with asclepic acid and oleic acid, Journal of the American Oil Chemists' Society, 74(9), 1153-1159.

86) Schachtschneider, J.H. and Snyder, R.G. (1963). Vibrational analysis of the *n*-paraffins - Ⅱ. Normal co-ordinate calculations, Spectrochimica Acta, 19(1), 117-168.

87) Scrimgeour, C.M. and Harwood, J.L. (2007). Fatty acid and lipid structure, In The Lipid Handbook with CD-ROM (Gunstone, F.D., Harwood, J.L. and Dijkstra, A.J., eds.), 3rd edition, 1-36 CRC Press, Boca Raton.

88) Shimanouchi, T. (1977). Sindou bunkougaku. Sono kakuritsu to kagakuteki ouyou (ed. Jigyoukai STskk), Jjigyoukai STskk, Tokyo, 103p.

89) Shindou, H. and Shimizu, T. (2009). Acyl-CoA: Lysophospholipid Acyltransferases, Journal of Biological Chemistry, 284(1), 1-5.

90) Simpson, T.D. (1983). Solid-phase of trimargarin: A comparison to tristearin, Journal of the American Oil Chemists' Society, 60(1), 95-97.

91) Small, D.M. (1986). Appendix Ⅲ. Normal fatty acids: Including data for saturated, unsaturated, and dicarboxylic acids, In The Physical Chemistry of Lipids: From Alkanes to Phospholipids, Handbook of Lipid Research (Small, D.M., ed.), Vol. 4, 587-601, Plenum press, New York.

92) Small, D.M. (1986). Glycerides, In The Physical Chemistry of Lipids: From Alkanes to Phospholipids, Handbook of Lipid Research (Small, D.M., ed.), Vol. 4, 345-394, Plenum press, New York.

93) Small, D.M., ed. (1986). The Physical Chemistry of Lipids: From Alkanes to Phospholipids, Handbook of Lipid Research (Small, D.M., ed.), Vol. 4, 672p, Plenum Press, New York.

94) Smith, A.E. (1953). The crystal structure of the normal paraffin hydrocarbons, Journal of Chemical Physics, 21(12), 2229-2231.

95) Snyder, R.G. (1960). Vibrational spectra of crystalline *n*-paraffins. 1. Methylene rocking and wagging modes, Journal of Molecular Spectroscopy, 4(5), 411-434.

96) Snyder, R.G. (1961). Vibrational spectra of crystalline *n*-paraffins. 2. Intermolecular effects, Journal of Molecular Spectroscopy, 7(2), 116-144.

97) Snyder, R.G. (1967). A revised assignment of B_{2g} methylene methylene wagging fundamental of planar polyethlene chain, Journal of Molecular Spectroscopy, 23(2), 224-228.

98) Snyder, R.G. (1967). Vibrational study of chain conformation of liquid *n*-paraffins and molten polyethylene, Journal of Chemical Physics, 47(4), 1316-1360.

99) Snyder, R.G. (1969). Raman spectrum of polyethylene and the assignment of B_{2g} wag fundamental, Journal of Molecular Spectroscopy, 31(3), 464-465.

100) Snyder, R.G. (1990). Distribution of infrared intensity in the spectra of conformationally disordered chain molecule assemblies, Macromolecules, 23(7), 2081-2087.

101) Snyder, R.G., Aljibury, A.L., Strauss, H.L., Casal, H.L., Gough, K.M. and Murphy, W.F. (1984). Isolated C-H stretching vibrations of *n*-alkanes: Assignments and relation to structure, Journal of Chemical Physics, 81(12), 5352-5361.

102) Snyder, R.G., Hsu, S.L. and Krimm, S. (1978). Vibrational-spectra in C－H stretching region and structure of polymethylene chain, Spectrochimica Acta Part A: Molecular and Biomolecular Spectroscopy, 34(4), 395-406.

103) Snyder, R.G. and Kim, Y. (1991). Conformation and low-frequency isotropic Raman-spectra of the liquid *n*-alkanes C_4-C_9, Journal of Physical Chemistry, 95(2), 602-610.

104) Snyder, R.G. and Schachtschneider, J.H. (1963). Vibrational analysis of the *n*-paraffins. 1. Assignments of infrared bands in the spectra of C_3H_8 through *n*-$C_{19}H_{40}$, Spectrochimica Acta, 19(1), 85-116.

105) Snyder, R.G., Strauss, H.L., Alamo, R. and Mandelkern, L. (1994). Chain-length dependence of interlayer interaction in crystalline *n*-alkanes from Raman longitudinal acoustic mode measurements, Journal of Chemical Physics, 100(8), 5422-5431.

106) Sprunt, J.C., Jayasooriya, U.A. and Wilson, R.H. (2000). A simultaneous FT-Raman-DSC (SRD) study of polymorphism in *sn*-1,3-distearoyl-2-oleoylglycerol (SOS), Physical Chemistry Chemical Physics, 2(19), 4299-4305.

107) Takai, Y., Masuko, T. and Takeuchi, H. (1997). Lipid structure of cytotoxic granules in living human killer T lymphocytes studied by Raman microspectroscopy, Biochimica et Biophysica Acta-General Subjects, 1335(1-2), 199-208.

108) Tasumi, M. and Krimm, S. (1967). Crystal vibrations of polyethylene, Journal of Chemical Physics, 46(2), 755-766.

109) Tasumi, M. and Krimm, S. (1968). Vibrational analysis of chain folding in polyethylene crystals, Journal of Polymer Science Part A-2: Polymer Physics, 6(5), 995-1010.

110) Tasumi, M., Shimanou, T., Kenjo, H. and Ikeda, S. (1966). Molecular vibrations of irregular chains. I. Analysis of indrared spectra and structures of polymethylene chains consisting of CH_2, CHD and CD_2 groups, Journal of Polymer Science Part A-1: Polymer Chemistry, 4(5), 1011-2021.

111) Tasumi, M. and Shimanouchi, T. (1963). A refined treatment of normal vibrations of polymethylene chain, Journal of Molecular Spectroscopy, 11(6), 422-432.

112) Tasumi, M., Shimanouchi, T. and Miyazawa, T. (1962). Normal vibrations and force constants of polymethylene chain, Journal of Molecular Spectroscopy, 9(4), 261-287.

113) Tasumi, M. and Shimanouchi, T. (1965). Crystal vibrations and intermolecular forces of polymethylene crystals, Journal of Chemical Physics, 43(4), 1245-1258.

114) Tasumi, M. and Zerbi, G. (1968). Vibrational analysis of random polymers, Journal of Chemical Physics, 48(8), 3813-3820.

115) Timms, R.E. (1984). Phase-behavior of fats and their mixtures, Progress in Lipid Research, 23(1), 1-38.

116) Timms, R.E. (2003). Confectionary fats handbook: Properties, production and application, 441p, The Oily Press, Bridgewater, UK.

117) Ueno, S. (2010 July 7). Personal communication.

118) Ueno, S., Minato, A., Seto, H., Amemiya, Y. and Sato, K. (1997). Synchrotron radiation X-ray diffraction study of liquid crystal formation and polymorphic crystallization of SOS (*sn*-1,3-distearoyl-2-oleoyl glycerol), Journal of Physical Chemistry B, 101(35), 6847-6854.

119) Ueno, S., Minato, A., Yano, J. and Sato, K. (1999). Synchrotron radiation X-ray diffraction study of polymorphic crystallization of SOS from liquid phase, Journal of Crystal Growth, 198, 1326-1329.

120) Uwaha, M., ed. (2002). Kesshou seichou no shikumi wo saguru ― sono butsuriteki kiso ― . Kesshou seichou no dainamikkusu (Nishinaga, S., Miyazaki, S. and Sato, K., eds.), Vol. 2, Kyoritsu shuppan, Tokyo, 166p.

121) Van Langevelde, A., Van Malssen, K., Hollander, F., Peschar, R. and Schenk, H. (1999). Structure of mono-acid even-numbered β-triacylglycerols, Acta Crystallographica Section B-Structural Science, 55, 114-122.

122) Vogel, H. and Jahnig, F. (1981). Conformational order of the hydrocarbon chains in lipid bilayers. A Raman spectroscopic study, Chemistry and Physics of Lipids, 29(1), 83-101.

123) Wheeler, D.H., Riemenschneider, R.W. and

Sando, C.E. (1940). Preparation, properties, and thiocyanogen absorption of triolein and trilinolein, Journal of Biological Chemistry, 132(2), 687-699.

124) Wood, J.D., Enser, M., Fisher, A.V., Nute, G.R., Sheard, P.R., Richardson, R.I., Hughes, S.I. and Whittington, F.M. (2008). Fat deposition, fatty acid composition and meat quality: A review, Meat Science, 78(4), 343-358.

125) Yano, J., Kaneko, F., Kobayashi, M., Kodali, D.R., Small, D.M. and Sato, K. (1997). Structural analyses and triacylglycerol polymorphs with FT-IR techniques. 2. β'_1-form of 1,2-dipalmitoyl-3-myristoyl-*sn*-glycerol, Journal of Physical Chemistry B, 101(41), 8120-8128.

126) Yano, J., Kaneko, F., Kobayashi, M. and Sato, K. (1997). Structural analyses of triacylglycerol polymorphs with FT-IR techniques. 1. Assignments of CH_2 progression bands of saturated monoacid triacylglycerols, Journal of Physical Chemistry B, 101(41), 8112-8119.

127) Yano, J. and Sato, K. (1999). FT-IR studies on polymorphism of fats: molecular structures and interactions, Food Research International, 32(4), 249-259.

128) Yano, J., Ueno, S., Sato, K., Arishima, T., Sagi, N., Kaneko, F. and Kobayashi, M. (1993). FT-IR study of polymorphic transformation in SOS, POP, and POS, Journal of Physical Chemistry, 97(49), 12967-12973.

129) Zerbi, G., Conti, G., Minoni, G., Pison, S. and Bigotto, A. (1987). Premelting phenomena in fatty acids: An infrared and Raman study, Journal of Physical Chemistry, 91(9), 2386-2393.

130) Zerbi, G., Magni, R., Gussoni, M., Moritz, K.H., Bigotto, A. and Dirlikov, S. (1981). Molecular mechanics for phase-transition and melting of *n*-alkanes: A spectroscopic study of molecular mobility of solid *n*-nonadecane, Journal of Chemical Physics, 75(7), 3175-3194.

131) Zweytick, D., Athenstaedt, K. and Daum, G. (2000). Intracellular lipid particles of eukaryotic cells, Biochimica et Biophysica Acta-Reviews on Biomembranes, 1469(2), 101-120.

Acknowledgements

I would like to take this opportunity to express my sincere gratitude to Professor Hiro-o HAMAGUCHI. He has taught me not only the basics of spectroscopy but also the fundamental philosophy of research. Professor said, "If it is painful, it is not a research" and "Be honest with what has been observed". These are the most precious words for me. His thoughtful words have always encouraged me and will help me enormously in the future as well.

I would also like to mention gratefully Associate-Professor Hideaki KANO, Assistant-Professor Rintaro SHIMADA, Assistant-Professor Hajime OKAJIMA, Professor Koichi IWATA (of Gakushuin University), Assistant-Professor Tomohisa TAKAYA (of Gakushuin University) and Dr. Young-kun MIN for their invaluable advice on my research. Also, Dr. Keisuke SASAKI, Ms. Yumiko ENDO, Dr. Masaru NOMURA and Dr. Katsuhiro AIKAWA (of Institute of Livestock and Grassland Science, National Agriculture and Food Research Organization) are gratefully acknowledged for their constant support to me. I also owe a deep sense of gratitude to the late Dr. Mitsuru MITSUMOTO and Dr. Sayuki NIKKUNI.

The successful completion of this thesis was possible only with the assistance of all the members in Hamaguchi Laboratory, of all the members in Animal Products Research Team and of all the family, friends, well-wishers who have been supporting me throughout the PhD tenure. Finally, my special thanks will go to Mr. Masahiro ANDO for his help with great expertise in Raman instrumentation and to Dr. Shraeddha TIWARI for her cheerful support in writing the manuscript.

ラマン分光法によるトリアシルグリセロールの構造および相挙動解析

本山三知代

農研機構畜産草地研究所　畜産物研究領域，つくば市，305-0901

摘　　要

トリアシルグリセロール（TAG）は生体における主要なエネルギー貯蔵物質である。その多成分系である天然油脂は，食品や医薬品，化粧品などの工業製品に広く用いられる。工業的要請から TAG 多成分系の相挙動については長い間研究が行われてきたが，その全貌は未だ明らかでない。天然油脂の複雑な相挙動について新たな知見を得るために，ラマン分光法を用いて TAG 多成分系の相挙動解析をおこなった。

はじめに，本研究の背景について述べた（第一章）。ラマン分光法は TAG の構造解析に最適の手法であり，多成分系を対象とするときにもその威力を発揮する。次に，TAG の構造と相挙動について最近の知見に重点を置いてまとめた（第二章）。結晶多形現象や“分子性化合物”形成などの TAG の興味深い相挙動について紹介し，それらの現象に影響を及ぼす結晶化条件などの要因についても言及した。また，TAG の各結晶多形より得られたラマンスペクトルについて，各相に特徴的な分子・結晶構造と関係付けながら詳述した（第三章）。長年に渡り蓄積された分光学的知見に基づき，ラマン分光法により TAG 結晶多形の詳細な構造解析が可能である。以上の章において述べた知見に基づき，TAG 多成分系の構造と相挙動に関する二つの研究をおこなった。一つは分子性化合物を形成すると言われている TAG 二成分系について（第四章），もう一つは広く工業的に利用されているいくつかの天然油脂について（第五章）である。

これらの研究の結果，用いた TAG 二成分系における分子性化合物の形成が確かめられ，その構造は過去の報告と異なるものであった（第四章）。このことは，分子性化合物の構造は結晶化条件の影響を決定的に受けていることを示唆し，これまで液相においても存在すると考えられてきた分子性化合物は，おそらく結晶化の過程で動的に生成する構造であるためと考察された。また分子性化合物は，これまでその形成が確認されているモデル二成分系においてだけでなく，天然油脂においても形成されていることを示唆する結果が得られた（第五章）。また，ラマン分光法を用いて相挙動の違いを検出することで，天然油脂の由来を判別できることを明らかにした（第五章）。

最後に，TAG の構造および相挙動についてさらに理解を深めるためのラマン分光法を用いた研究の展望について述べた（第六章）。近年の分光器の発達は TAG 多成分系の研究に明るい可能性をもたらしており，ラマン分光法が天然油脂の相挙動の全貌解明に大いに貢献すると期待される。

キーワード：結晶多形，トリアシルグリセロール多成分系，豚脂，牛脂，判別法